2009

Computational studies of the properties of copper oxide clusters and the reactions of phenol and chlorinated phenols with copper oxide clusters

Gyun-Tack Bae
Louisiana State University and Agricultural and Mechanical College, gbae1@tigers.lsu.edu

COMPUTATIONAL STUDIES OF THE PROPERTIES OF COPPER OXIDE CLUSTERS AND THE REACTIONS OF PHENOL AND CHLORINATED PHENOLS WITH COPPER OXIDE CLUSTERS

A Dissertation
Submitted to the Graduate Faculty of the
Louisiana State University and
Agricultural and Mechanical College
in partial fulfillment of the
requirements for the degree of
Doctor of Philosophy

in

The Department of Chemistry

by
Gyun-Tack Bae
B.S., SoongSil University, 1997
M.S., SoongSil University, 2002
December, 2009

to Kyung Ok Park

ACKNOWLEDGEMENTS

I would like to gratefully and sincerely thank Dr. Hall for his constant support, guidance, understanding, and patience during my graduate studies at Louisiana State University.

I also thank Dr. Dellinger, Dr. Poliakoff, Dr. Chen and Dr. Valsaraj in my thesis committee for valuable suggestions and comments. I thank Dr. McFerrin for her assistance and useful insights.

Finally, I wish to thank my wonderful wife Kyung-Ok whose patience, support and love have made this whole project possible.

TABLE OF CONTENTS

ABSTRACT

We used *ab initio* simulations and calculations to study the structures and stabilities of copper oxide clusters, Cu_nO_n (n=1-8) and CuO_n (n=1-6). The lowest energy structures of neutral and charged copper oxide clusters were determined using primarily the B3LYP/LANL2DZ model chemistry. In Cu_nO_n clusters with n=1-8, a transition from planar to nonplanar geometries occurs at n=4. In CuO_n clusters with n=1-6, all geometries of neutral, positively, and negatively charged clusters are planar or near planar structures. Selected electronic properties, including binding energies, ionization energies, and electronic affinities, were calculated and examined as a function of n. Stabilities were examined by calculating fragmentation channels and Löwdin charge distributions.

We have also analyzed the reactions between neutral copper oxide clusters (Cu_nO_n with n=1-8) and organic compounds (phenol, *ortho*-chlorophenol, and *para*-chlorophenol) using DFT calculations of geometries, thermodynamic properties, reaction pathways, adsorption energies, and Löwdin charge distributions.

CHAPTER 1

INTRODUCTION

The study of clusters is very important to understand the limits of isolated atoms, molecules and bulk matter and to investigate the phenomena of chemical physics such as solvation. One of the most important discoveries is that some clusters show many differences compared to their bulk counterparts for geometries, electronic and chemical properties. Metal clusters are very important in many areas, including catalysis, nanomaterials, and composite materials. Metal oxide clusters are performed for health effects.[1-4] For example, in the World Trade Center disaster, analysis of fine and ultrafine particulates revealed a high concentration of zinc and titanium.[5]

The collision of clusters with solid surfaces at high speeds can give rise to short-lived but particularly extreme conditions of temperature and pressure.[6] It has been shown that these impact-heated clusters provide an environment in which chemical reactions can be induced.[7] Other researchers have studied the formation of surface-bound radicals during the adsorption of organic molecules and aliphatic compounds on metal. Energetic cluster impact also has the potential for technological application in the formation of particularly dense and coherent metal[8,9] and semiconductor thin films.[10]

Metal oxide clusters from combustion react with many organic compounds.[11,12] It is well known that transition metals (iron, vanadium, and copper) are associated with particulate matter (PM). Studies show that PM is a threat to public health in cities.[13] We must understand the characteristics of toxic particles and how they affect the health of the inhabitants of cities. It is well known that PM can be classified as coarse, fine or ultrafine particles. Coarse particles have a diameter greater than 2.5 μm (PM2.5-10). Fine particles

(0.1 to 2.5μm, PM2.5) and ultrafine particles (<0.1 μm in diameter) are predominantly derived from the combustion of fossil fuel.[14] Recently, government and air-quality monitoring agencies determined that both PM10 and PM2.5 particles from vehicle emission are the most dangerous.[15] PM10 exposure has been associated with death from cardiopulmonary disorders and lung cancer in studies of six cities[16] and 151 metropolitan areas[17] in the United States, with a 1% increase in daily mortality for each 10μg/m^3 increase in PM10. Ultrafine particles can penetrate deeper into lung tissue than coarse and fine particles[15] and can increase asthma symptoms.[18] Ultrafine particles also can increase hospitalization rates for respiratory disorders[19-22] and decrease lung function.[23-27] Combustion particles may have a carbon core that is coated with organic compounds, transition metal, nitrates and sulfates. All of these components may play a role in particle toxicity.[28] Chemically, particulate matter pollution is a complex mixture of organic and inorganic compounds, but the properties responsible for its health effects are unknown.

Fine and ultrafine particulate matter is composed predominately of inorganic, organic, and elemental carbon, sulfates and nitrates.[29-31] Table 1.1 shows a long list of transition metals that are present in almost every particulate. The concentration of transition metals in the particulates is determined by the origin; since fine and ultrafine particulates are almost entirely of anthropogenic origin (combustion), the type of fuel generating the particulates determines their definite composition.

Particulate air pollution contains transition metals (iron, vanadium, and copper) which can catalyze the production of reactive oxygen species, such as hydrogen peroxide, superoxide, and hydroxyl radical, which are very stable but are highly reactive.[32] Small organic radicals, such as phenyl, vinyl, or methyl, are somewhat less reactive but are also less stable. Recently, it has been realized that resonance stabilized radicals such as cyclopentadienyl, propargyl and phenoxyl are not highly reactive with molecular species,

including oxygen, and can undergo radical-radical recombination reactions to form polychlorinated dibenzo-p-dioxins and dibenzofurans (PCDD/F), PAH and possibly soot at moderately high temperatures in the post-flame and cool-zone region of combustion and thermal processes.

A contributor to combustion emissions, "fly ash," has been shown to catalyze the production of reactive oxygen species and increase the level of inflammation upon instillation in rat lungs.[33,34]

Table 1.1: Metals in Environmental Nanoparticles and Fuels[35]

	PM 2.5 (μg/g)	Coal		Fuel Oil	
		Fuel (%)	Emission (%)	Fuel (ppmv)	Emission (%)
Metal					
Ni	~0.2		0.015	3-21	12.8
V	13,000-60,000		0.03	3-48	17.6
Fe	$1\text{-}5*10^3$	6-20 (ox)	4-20	27,800	34
Mg	~1	1-4 (ox)	1-5	7,120	6.2
Ca		2-23 (ox)	1-22	41,200	14.8
Co			0.005	2,040	1.2-1.5
Cr	~1		0.02	4,400	5.8-9.0
Cu	~2		0.02	2,780	3.3-3.8
Mn			0.07	1,040	1.2-3.5
Pb	5-10		0.015	2,040	0.7-1.0
Sr			0.1	713	1.7-3
Zn	500-22,000		0.023	5,630	3.3-3.8
Zr			0.015		
Mo			0.001	4,270	5.5-10
Si		35-45 (ox)	22-61	46,000	15-20
K			0.3-4		
Al		15-40 (ox)	13-36	32,000	19.5-28

DNA damage has been observed in cells exposed to radical-containing PM. This damage has been proposed to be due to PFRs formed by the following scheme involving a redox-active metal.[36]

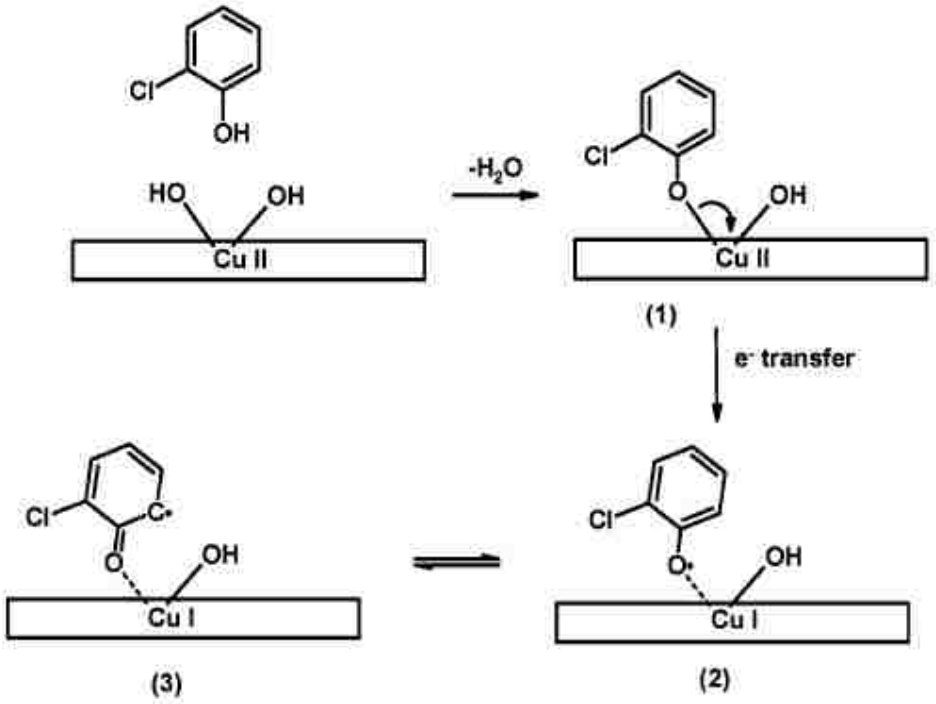

Figure 1.1: Adsorption of 2-MCP on copper (II) oxide[37]

Other researchers have studied the formation of surface-bound radicals during the adsorption of organic molecules on metal oxide.[29,38-41] These reactions may occur by chemisorption of an organic molecule or aliphatic compounds on a surface copper ion. (Figure 1.1)

Figure 1.2 shows nanoparticle formation/growth and mediation of pollutant-forming reactions in combustion systems. Metals are vaporized in the flame zone (Zone 2) and subsequently nucleate to form small metal nanoparticles or condense on the surfaces of other nanoparticles in transit to the postflame (Zone 3). Zones 3 and 4 control formation of gas-phase organic pollutants. Zone 5 is a major source of PCDD/Fs and is increasingly recognized as a source of other pollutants (CHCs, BHCs, and XHCs; polybrominated dibenzo-p-dioxins and dibenzofurans (PBDD/Fs) and PXDD/Fs; partially oxidized hydrocarbons and CHCs; and nitro-PAHs, oxy-PAHs, and oxychloro-PAHs) previously

thought to originate in zones 1-4. Most of the reactions need a transition metal catalysis to form these products.[42]

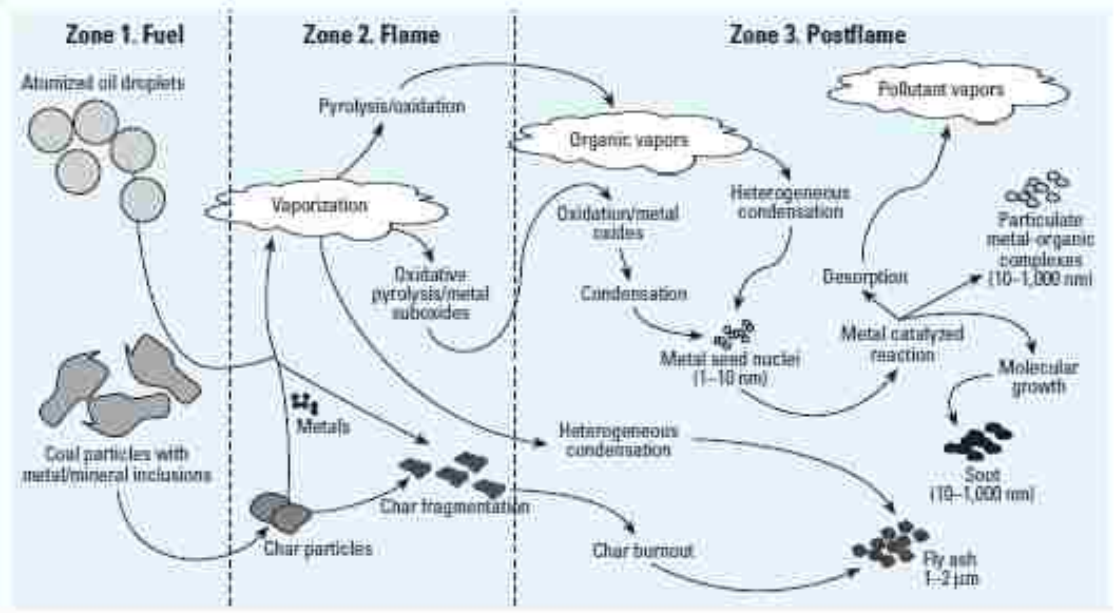

Figure 1.2: Nanoparticle formation/growth and mediation of pollutant-forming reactions in combustion systems.[42]

Figure 1.3 shows the formation of 4,6-dichloro-dibenzofuran (DCDF). The main PCDD/F products detected were the same as under pyrolytic conditions: dibenzo-p-dioxin (DD), 1-monochloro dibenzo-p-dioxin (MCDD), and 6-dichloro-dibenzofuran (DCDF). Molecule 8 can react with gas-phase 2-MCP and there are two possible mechanisms. Scheme (a) is the formation of MCDD and scheme (b) is the formation of DD.

Researchers have studied the formation of PCDD/Fs via a Cu(II)O-mediated reaction of 2-chlorophenol (2-MCP).[43] PCDD/F or dioxins are known as the most environmentally toxic pollutants. We are investigating copper oxide clusters and their reactions because we believe them to be an important part of the metal oxide pathway to the formation of PCDD/Fs. There are some theories about the formation of dioxins.[38,44-46] 1) gas-phase formation from molecular precursors at temperatures $> 600℃$, 2) condensation reactions of precursors

catalyzed by transition metal oxides in “fly ash” at temperatures between 200-600 ℃, and 3) de novo oxidation and chlorination of elemental carbon in soot between 200-600 ℃.[47-50] However, the surface-mediated process can account for the formation of dioxins better than other explanations. It is well known that transition metal (copper or iron) oxides and chlorides play a significant role in dioxin formation.[38]

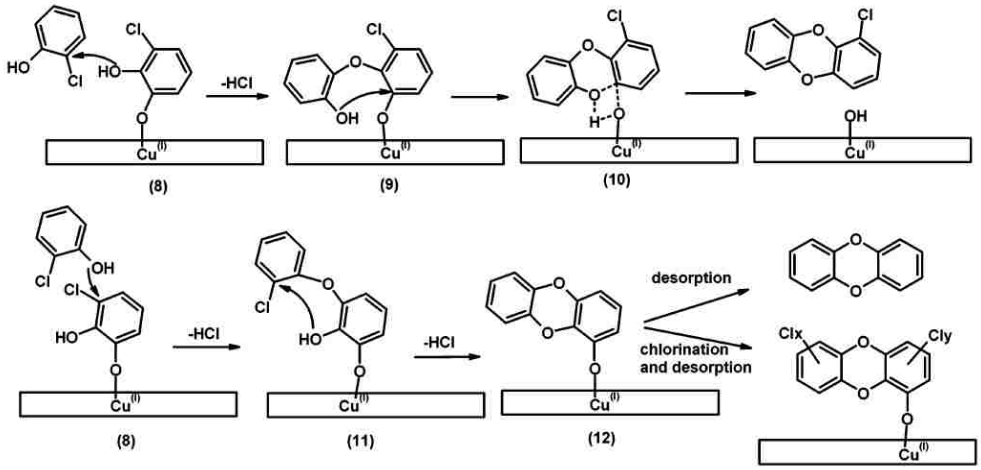

Figure 1.3: Surface-Mediated Formation of MCDD and DD.[37]

Experimental[51-81] and theoretical[68-75,79,82-95] studies of small copper oxide clusters have been made. Steimle and Azuma have reviewed the structure and electronic spectra of copper monoxide (CuO) by using the technique of intermodulated fluorescence.[81] Neutral and anionic CuO molecules have been studied using the laser photoelectron spectroscopy technique.[80] The electron affinity of ground state CuO was determined to be 1.777 eV. CuO^- bond length is 1.670 Å and CuO^- vibrational frequency is 739 cm^{-1}. CuO bond length is 1.704 Å and CuO vibrational frequency is 682 cm^{-1}.

Two geometries of CuO_2 were reported[76]: CuOO (bent, C_s) and CuO_2 (side-on, C_{2v}). Evidence for the bent complex CuOO comes from both experiment[65,67] and theory.[73,74] The linear complex OCuO has been investigated via IR,[79] photoelectron spectra (PES)

measurement,[76] and theoretically.[91] For CuO_3, $OCuO_2^-$, and $Cu(O_3)^-$ clusters, the vibration frequencies[79] have been calculated.[76]

Experiments have been performed on Cu_2O_x clusters with x=1-4 using anion photoelectron spectroscopy (PES).[77] The $Cu_2O_x^-$ species are produced using a laser vaporization cluster beam apparatus, equipped with a magnetic-bottle time-of-flight (TOF) photoelectron analyzer.[76,96,97] Figure 1.4 shows a schematic view of a MTOF-PES apparatus. It consists of a laser vaporization cluster source, a modified Wiley-McLaren time-of-flight (TOF) mass spectrometer, a mass gate, a momentum decelerator, and a MTOF electron analyzer.

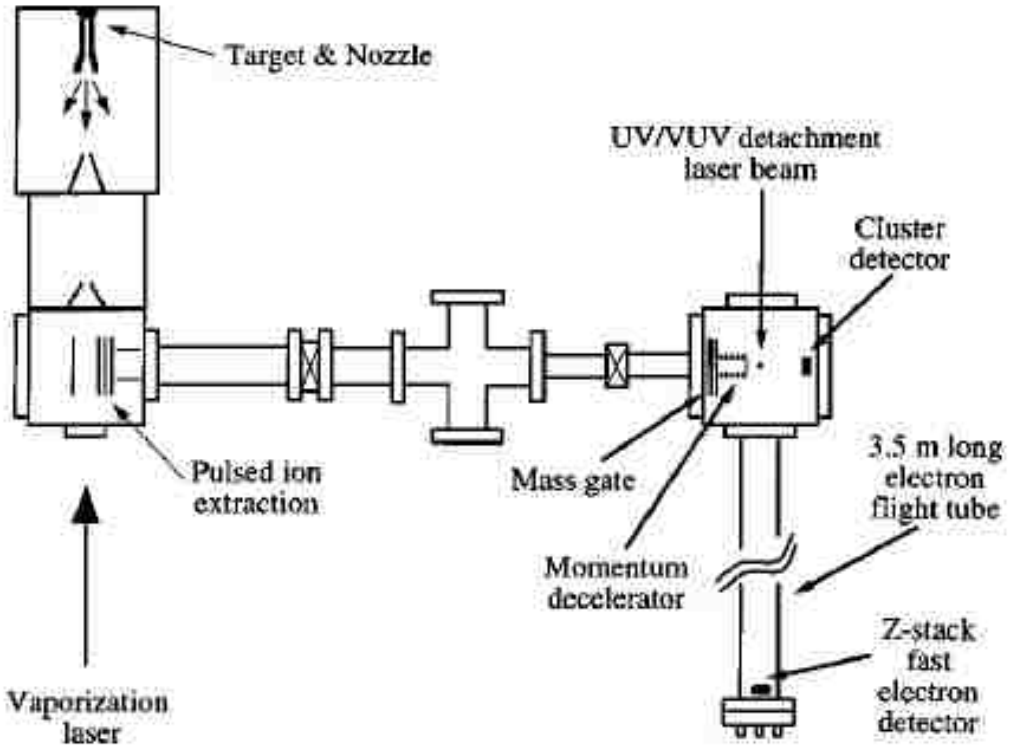

Figure 1.4: Schematic view of the laser-vaporization/magnetic-bottle photoelectron spectroscopy apparatus[97]

Figure 1.5 shows the PES spectra of Cu_2O_x (x=1-4), and the measured energies of all the states are listed in Table 1.2. The ground states of the neutral clusters are labeled “X”

and low-lying excited-state features are labeled A, B, C and so on in ascending order.

Recently, the equilibrium structures of neutral CuO_n clusters with n=1-6 were determined within the framework of density functional theory with a plane-wave basis set and generalized gradient corrections. Figure 1.6 shows the calculated lowest energy structures, bond lengths, and angles of neutral CuO_n clusters with n=1-6.[94]

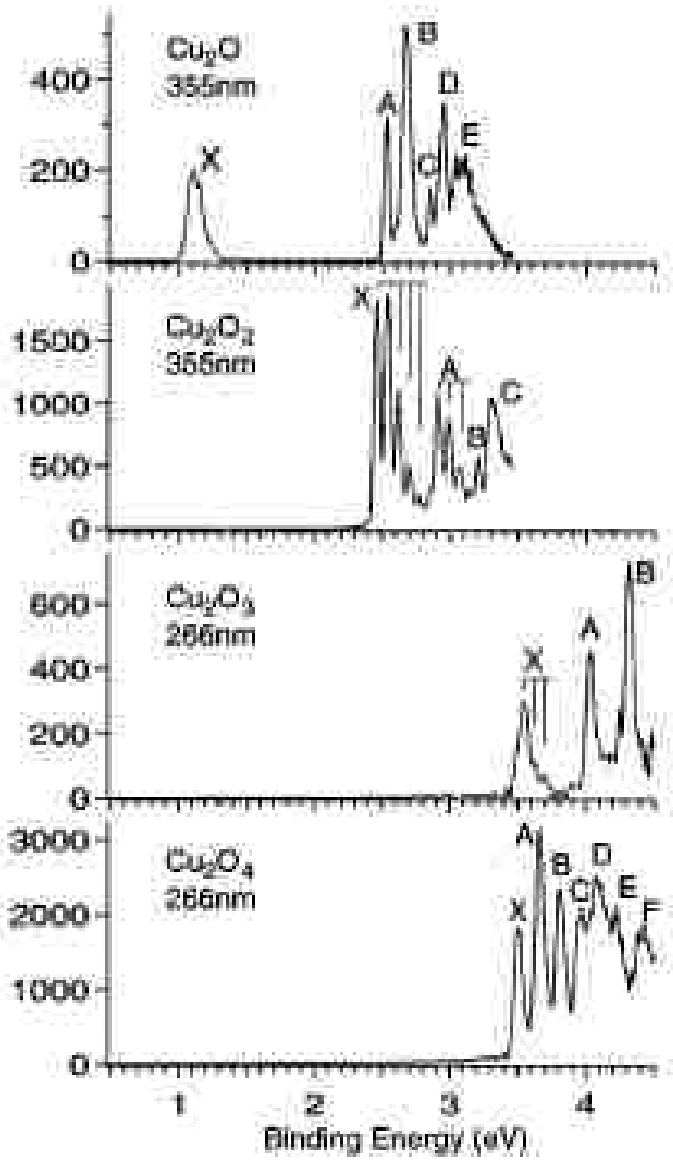

Figure 1.5: Photoelectron spectra of $Cu_2O_x^-$ (x=1-4).[77]

Table 1.2: Observed electronic states and vibrational frequencies of Cu_2O_x (x=1-4) clusters and predicted electron affinities and ground-state vibrational frequencies.[77]

	BE[a] (eV)	ν (exp)[b] (cm^{-1})	EA[c] (eV)	ν (theo)[d] (cm^{-1})
Cu_2O[e]				
X	1.10	<200	1.10	ν_1=681[f]
A	2.53			ν_2=156
B	2.66			ν_3=586
C	2.85			
D	2.95			
Cu_2O_2				
X	2.46	630 (30)	2.12	182 302 466
A	2.91	650 (30)		493 653 718[f]
B	3.12			
C	3.30			
Cu_2O_3				
X	3.54	(640)	3.03	259 259 318
A	4.02			321 321 351
B	4.32			608 608 678[f]
Cu_2O_4[e]				
X	3.50		2.94	119 222 244
A	3.66			267 277 354
B	3.80			533 612 612
C	3.95			647 912 985[f]

[a]Measured electron binding energy (uncertainty: ±0.03 eV). The binding energy (BE) of the X ground state yields the measured adiabatic electron affinity.
[b]Measured sysmmetric stretching vibrational frequencies for the given states. Relative peak positions can be determined more accurately.
[c]Calculated adiabatic electron affinities in eV
[d]Calculated vibrational frequencies for the ground-state cluster structures shown in Fig 1.7.
[e]More highly excited states are not listed due to their broad and overlapping nature.
fTotally symmetric vibrational modes.

One of the results is that the spin of the most stable isomers is quartet state when the number of oxygen atoms is odd, while it is doublet state when this number is even. They have calculated the lowest geometries of CuO_n clusters with n=1-6: linear OCuO for CuO_2, $OCu(O_2)$ for CuO_3, two $Cu(O_2)$ side-on units for CuO_4, one $Cu(O_2)$ side-on unit and $Cu(O_3)$ ozonide for CuO_5, and two $CuO(O_3)$ ozonides for CuO_6.

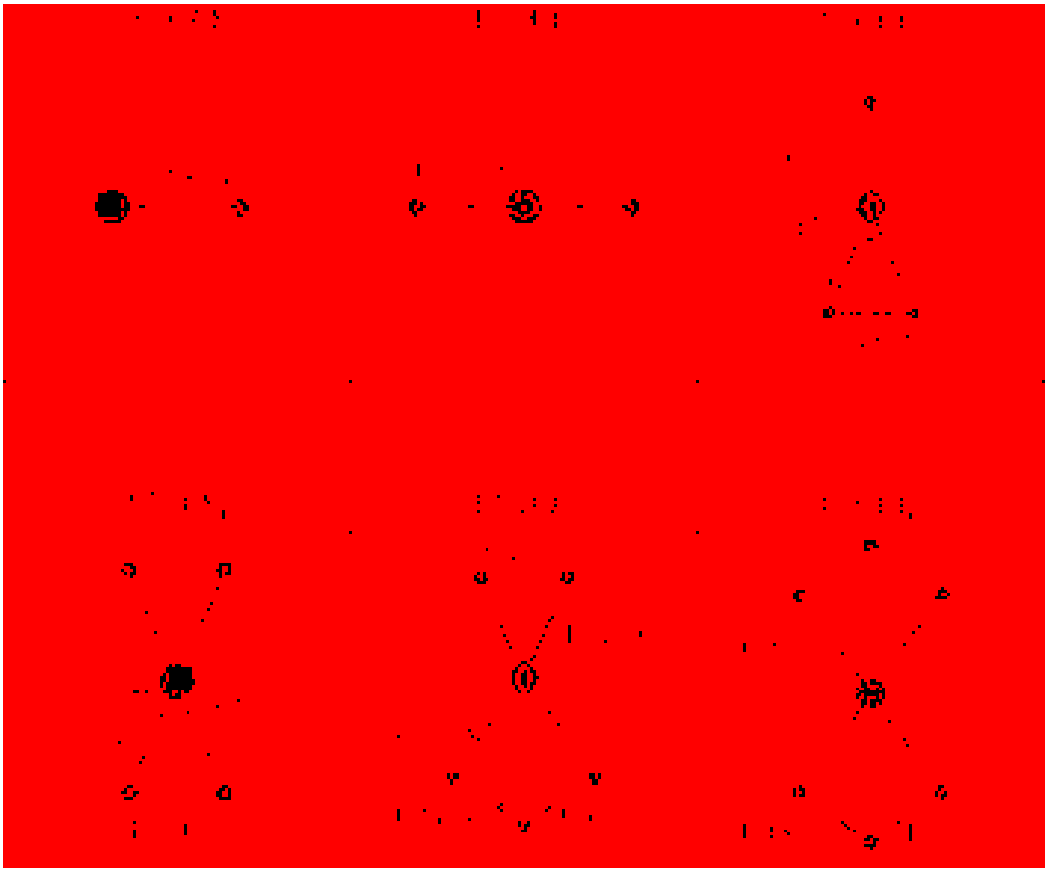

Figure 1.6: Equilibrium geometries of the building blocks identified in the neutral clusters. The bigger circle represents the copper atom, the smaller ones the oxygen atoms. All isomers are composed of one or more of these block sharing the copper atom.[94]

In 1996, Wang et al. investigated the electronic structures of copper oxide clusters, Cu_2O_x (x=1-4), using anion photoelectron spectroscopy and density functional calculations.[77] They found that the ground states of Cu_2O and Cu_2O_2 are a triangle and a rhombus, respectively. For Cu_2O_3, they found two isomers with close energies (bipyramid and bent structure with an O-Cu-O-Cu-O atomic arrangement); the bipyramid structure is in better agreement with the experimental electron affinity (EA). For Cu_2O_4, the hexagonal ring with two O-O bonds is found to be the most stable structure. Figure 1.7 shows the optimized structure and Mulliken charge distributions from density functional theory calculations for Cu_2O_x (x=1-4).

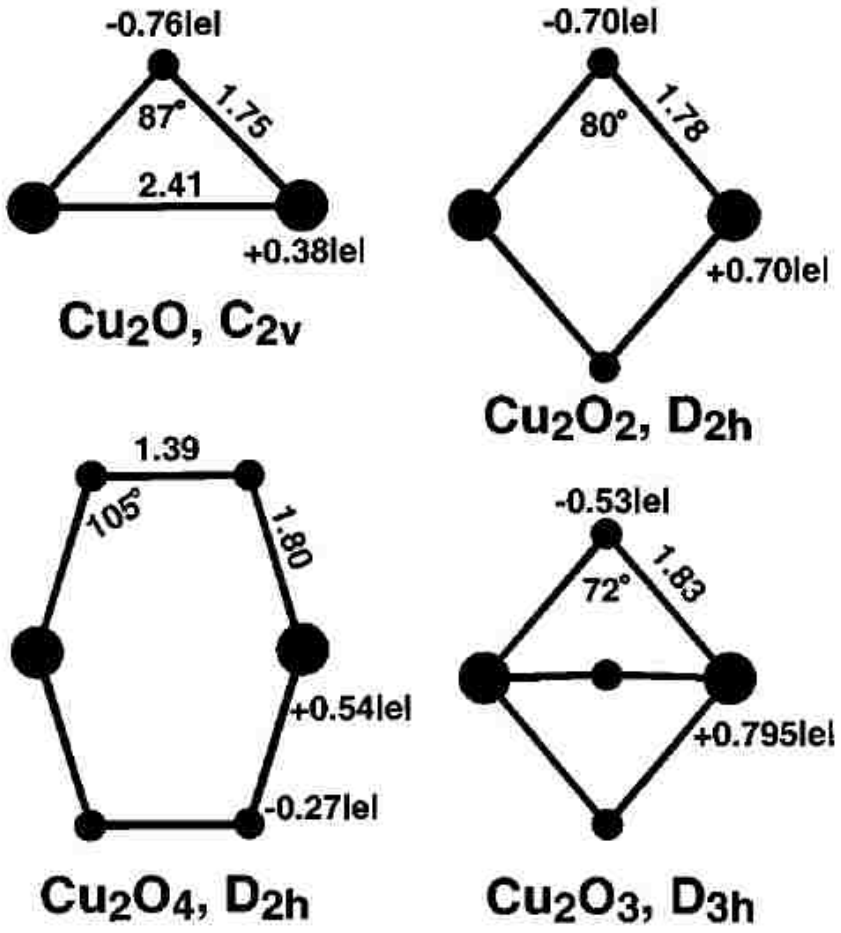

Figure 1.7: The optimized structures, bond lengths, angles and Mulliken charge distributions from density functional theory calculations for Cu_2O_x (x=1-4)[77]

Dai et al. have suggested that the ground state structures of neutral, positively and negatively charged Cu_2O_n clusters with n=1-4 are linear or near linear structures (Figure 1.8). Also, they found that the calculated electron affinities of the clusters with BLYP level are in good agreement with the experimental ones.[77]

There are relatively few experimental and theoretical studies of copper and iron oxide clusters that are presumed present in combustion systems; thus, an understanding of the reaction pathway for PCDD/F is hindered by a lack of knowledge of the structures and energetics of these clusters. Estimates of the relevant cluster sizes range from the micrometer down to just a few metal atoms. This work therefore studies the structures

and energetics of small copper oxide clusters as a first step towards understanding the interactions between metal oxides and free radicals.

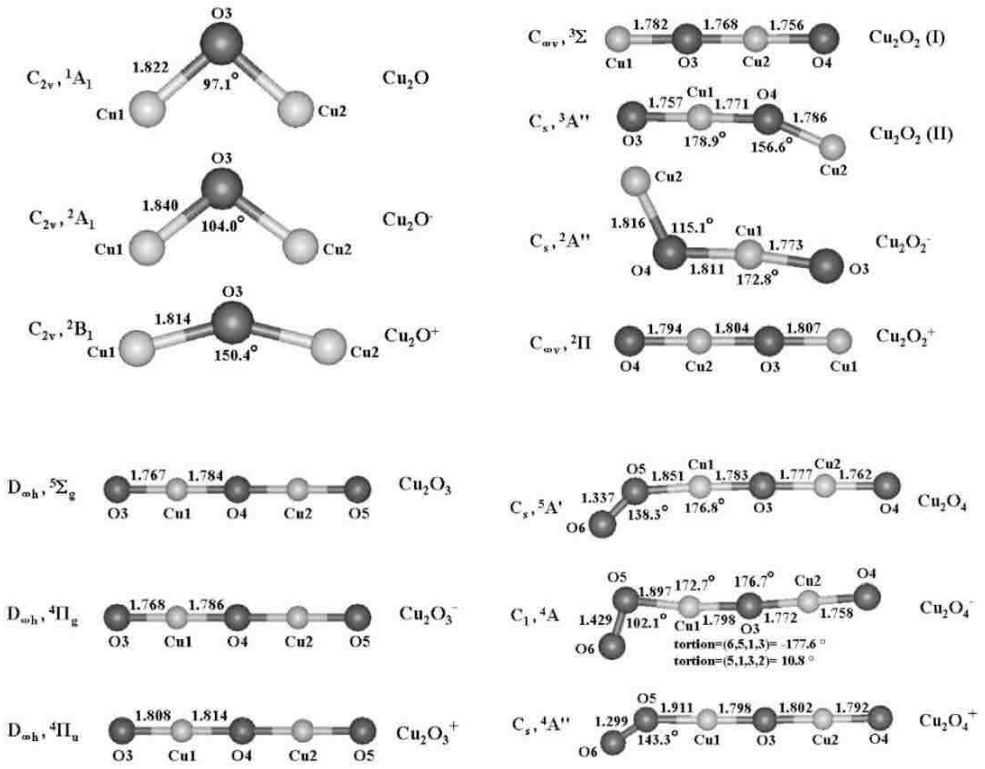

Figure 1.8: The geometries, symmetries, and configurations of the ground states of Cu_2O_n with n=1-4 and its ions. Bond lengths are given in Å.[98]

CHAPTER 2

QUANTUM CHEMISTRY METHODS

2.1 The Hartree-Fock Approximation

Hartree-Fock theory is the fundamental molecular orbital theory and one of the simplest approximate theories for solving the many-body Hamiltonian. Hartree-Fock theory was developed to solve the electronic Schrödinger equation. It assumed that the wavefunction can be approximated by a single Slater determinant made up of one spin orbital per electron.

Given a functional of some trial wavefunction Φ, the expectation value $\mathrm{E}[\Phi]$ of the Hamiltonian operator *H* is a number given by

$$E[\Phi] =< \Phi|H|\Phi > \tag{1}$$

$$|\Phi >= \sum_{i=1}^{N} c_i|\,\Psi_{\mathrm{i}} \tag{2}$$

By equation (1), we see that $\mathrm{E}[\Phi]$, its value depends on the form of the wavefunction, and equation (2) shows a linear variation trail wave function.

We minimize the energy

$$E =< \Phi|H|\Phi \geq \sum_{ij} c_i^* c_j < \Psi_i|H|\Psi_j > \tag{3}$$

subject to the constraint that the trial wave function remains normalized

$$< \Phi|\Phi > -1 = \sum_{ij} c_i^* \, c_j \, < \Psi_i|H|\Psi_j > -1 = 0 \tag{4}$$

using Lagrange's method,

$$\begin{aligned} \mathcal{L} &=< \Phi|H|\Phi > -E(< \Phi|\Phi > -1) \\ &= \sum_{ij} c_i^* \, c_j \, < \Psi_i|H|\Psi_j > -E(\sum_{ij} c_i^* \, c_j \, < \Psi_i|\Psi_j > -1) \end{aligned} \tag{5}$$

where E is the Lagrange multiplier. Therefore, we set the first variation in $\mathcal{L}$ equal to zero.

Taking the differential of $\mathcal{L}$,

$$\begin{aligned} \delta\mathcal{L} &= \sum_{ij} \delta c_i^* \, c_j \, < \Psi_i|H|\Psi_j > -E \sum_{ij} \delta c_i^* \, c_j \, < \Psi_i|\Psi_j > \\ &+ \sum_{ij} c_i^* \delta \, c_j \, < \Psi_i|H|\Psi_j > -E \sum_{ij} c_i^* \delta \, c_j \, < \Psi_i|\Psi_j > = 0 \end{aligned} \tag{6}$$

$$\sum_i \delta c_i^* \left[\sum_j H_{ij} \, c_j - E S_{ij} \, c_j \right] + complex\ conjugate = 0 \tag{7}$$

where $H_{ij} =< \Psi_i|H|\Psi_j >$.

$$< \Psi_i|\Psi_j >= S_{ij} \tag{8}$$

Since δc_i and δc_i^* are arbitrary, the bracketed parts of equation (7) must be zero. Thus

$$\sum_j H_{ij}\, c_j = E \sum_j S_{ij}\, c_j \tag{9}$$

It is clear that this can be written as a matrix product and is in fact an eigenvalue equation in the form

$$\mathbf{Hc} = E\mathbf{Sc} \tag{10}$$

We need to minimize the Hartree-Fock energy expression with respect to changes in the orbitals $\chi_a \rightarrow \chi_a + \delta\chi_a$. We have also been assuming that the orbitals χ are orthonormal,

$$\int dx_1\, \chi_a^*(1)\chi_b(1) = [a|b] = \delta_{ab} \tag{11}$$

That is, the constraints are of the form

$$[a|b] - \delta_{ab} = 0 \tag{12}$$

We can accomplish this by Lagrange's method of undetermined multipliers, where we employ a functional L defined as

$$\mathcal{L}[\{\chi_a\}] = E_0[\{\chi_a\}] - \sum_{a=1}^{N}\sum_{b=1}^{N} \varepsilon_{ba}\,([a|b] - \delta_{ab}) \tag{13}$$

where ε_{ba} are the undetermined Lagrange multipliers, [a|b] is the overlap between spin orbitals a and b and E_0 is the expectation value of the single determinant $|\Psi_0>$.

$$E_0[\{\chi_a\}] = \sum_{a=1}^{N}[a|h|a] + \frac{1}{2}\sum_{a=1}^{N}\sum_{b=1}^{N}[aa|bb] - [ab|ba] \qquad (14)$$

Because *L* is real and $[a|b] = [b|a]^*$, the Lagrange multipliers must be elements of a Hermitian matrix

$$\varepsilon_{ba} = \varepsilon_{ab}^* \qquad (15)$$

Minimization of E_0, subject to the constraints, is thus obtained by minimizing *L*. We therefore vary the spin orbitals an arbitrary infinitesimal amount,

$$\chi_a \rightarrow \chi_a + \delta\chi_a \qquad (16)$$

setting the first variation $\delta\mathcal{L}$=0.

$$\delta\mathcal{L} = \delta E_0 - \sum_{a=1}^{N}\sum_{b=1}^{N}\varepsilon_{ba}\,\delta[a|b] = 0 \qquad (17)$$

This follows directly from equation (13) since the variation in a constant (δ_{ab}) is zero.

$$\delta[a|b] = [\delta\chi_a|\chi_b] + [\chi_a|\delta\chi_b] \qquad (18)$$

and

$$\delta E_0 = \sum_{a=1}^{N} [\delta\chi_a|h|\chi_a] + [\chi_a|h|\delta\chi_a]$$

$$+\frac{1}{2}\sum_{a=1}^{N}\sum_{b=1}^{N}[\delta\chi_a\chi_a|\chi_b\chi_b] + [\chi_a\delta\chi_a|\chi_b\chi_b]$$

$$+ [\chi_a\chi_a|\delta\chi_b\chi_b] + [\chi_a\chi_a|\chi_b\delta\chi_b] \tag{19}$$

$$-\frac{1}{2}\sum_{a=1}^{N}\sum_{b=1}^{N}[\delta\chi_a\chi_b|\chi_b\chi_a] + [\chi_a\delta\chi_b|\chi_b\chi_a]$$

$$+ [\chi_a\chi_b|\delta\chi_b\chi_a] + [\chi_a\chi_b|\chi_b\delta\chi_a]$$

Also

$$\sum_{ab} \varepsilon_{ba}\,([\delta\chi_a|\chi_b] + [\chi_a|\delta\chi_b])$$

$$= \sum_{ab} \varepsilon_{ba}[\delta\chi_a|\chi_b] + \sum_{ab} \varepsilon_{ab}\,[\delta\chi_b|\chi_a]$$

$$= \sum_{ab} \varepsilon_{ba}\,[\delta\chi_a|\chi_b] + \sum_{ab} \varepsilon_{ba}^{*}\,[\delta\chi_a|\chi_b]^{*} \tag{20}$$

$$= \sum_{ab} \varepsilon_{ba}\,[\delta\chi_a|\chi_b] + complex\ conjugate$$

The first variation in $\mathcal{L}$ of equation (17) becomes

$$\delta\mathcal{L} = \sum_{a=1}^{N}[\delta\chi_a|h|\chi_a]$$
$$+\sum_{a=1}^{N}\sum_{b=1}^{N}[\delta\chi_a\chi_a|\chi_b\chi_b] - [\delta\chi_a\chi_b|\chi_b\chi_a] \qquad (21)$$
$$-\sum_{a=1}^{N}\sum_{b=1}^{N}\varepsilon_{ba}[\delta\chi_a|\chi_b] + complex\ conjugate = 0$$

We can use the coulomb and exchange operators. The exchange operator, $\mathcal{K}_b(1)$, can be defined by its effect when operating on a spin orbital $\chi_a(1)$,

$$\mathcal{K}_b(1)\chi_a(1) = \left[\int dx_2\, \chi_b^*(2) r_{12}^{-1} \chi_a(2)\right]\chi_b(1) \qquad (22)$$

and the coulomb operator can be defined as

$$\mathcal{J}_b(1)\chi_a(1) = \left[\int dx_2\, \chi_b^*(2) r_{12}^{-1} \chi_a(2)\right]\chi_b(1) \qquad (23)$$

So

$$\delta\mathcal{L} = \sum_{a=1}^{N}\int dx_1 \delta\,\chi_a^*(1)\Bigg[h(1)\chi_a(1)$$
$$+\sum_{b=1}^{N}\big(\mathcal{J}_b(1) - \mathcal{K}_b(1)\big)\chi_a(1) \qquad (24)$$
$$-\sum_{b=1}^{N}\varepsilon_{ba}\chi_b(1)\Bigg] + \ complex\ conjugate$$
$$= 0$$

Since $\delta\chi_a^*(1)$ is arbitrary, it must be that the quantity in square bracket is zero for all a.

Therefore,

$$\left[h(1) + \sum_{b=1}^{N} \mathcal{J}_b(1) - \mathcal{K}_b(1)\right]\chi_a(1) = \sum_{b=1}^{N} \varepsilon_{ba}\chi_b(1)\, a \qquad (25)$$
$$= 1,2,\ldots,N$$

We can introduce a new operator, the Fock operator, as in the above square bracket. Therefore, the Hartree-Fock equations are just

$$f|\chi_a> = \sum_{b=1}^{N} \varepsilon_{ba}|\chi_b> \qquad (26)$$

The Hartree-Fock equations can be solved numerically, or they can be solved in the space spanned by a set of basis functions. In either case, the solutions depend on the orbitals. Hence, we need to guess some initial orbitals and then refine our guesses iteratively. For this reason, Hartree-Fock is called a self-consistent-filed (SCF) approach.

2.1.1 Unrestricted Hartree-Fock and Restricted Hartree-Fock

We must be more specific about the form of the spin orbitals to consider the actual calculation of Hartree-Fock wave functions. There are two types of spin orbitals: restricted spin orbitals, which are constrained to have the same spatial function for α (spin up) and β (spin down) spin functions; and unrestricted spin orbitals, which have

different spatial functions for α and β spins.

A Hartree-Fock wave function in which electrons whose spins are paired occupy the same spatial orbital is called RHF (restricted Hartree-Fock) wave function. Although the RHF wave function is generally used for closed-shell states, two different approaches are widely used for open-shell states. In the restricted open-shell Hartree-Fock (ROHF) method, electrons that are paired with each other are given the same spatial orbital function.

2.1.2 Basis Sets

In 1951, Roothaan proposed representing the Hartree-Fock orbitals as linear combinations of a complete set of known functions, called basis function. Denoting the atomic orbital basis functions as ψ, we have the expansion for each orbital *i*.

$$\psi_i = \sum_{\mu=1}^{n} C_{\mu i}\, \phi_\mu \qquad (27)$$

where ψ_i is the *i*-th molecular orbital, $C_{\mu i}$ are the coefficients of linear combination, ϕ_μ is the μ-th atomic orbital, and n is the number of atomic orbitals.

Earlier, the Slater Type Orbitals (STO's) were commonly used for atomic Hartree-Fock calculations. They are described as

$$\phi_i(\zeta, n, l, m, r, \theta, \phi) = N r^{n-1} e^{-\zeta r} Y_l^m(\theta, \phi) \qquad (28)$$

where N is a normalization constant and ζ is called the orbital exponent. The *r*, θ, and ϕ are spherical coordinates and Y_l^m is the angular momentum part. The *n*, *l* and *m* are

quantum numbers: principal, angular momentum and magnetic, respectively.

Unfortunately, functions of this kind cannot be evaluated fast enough for efficient molecular integral evaluation. That is why Boys proposed the use of Gaussian-type functions (GTFs) instead of STOs for the atomic orbitals in an LCAO wave function. GTFs are simpler functions and frequently called Gaussian primitives.

The GTFs (also called Cartesian Gaussian) are expressed as

$$g_{ijk} = N x_b^i y_b^j z_b^k e^{-ar_b^2} \tag{29}$$

where N is a normalization constant, i, j, and k are nonnegative integers, α is a positive orbital exponent, and x_b, y_b, z_b are Cartesian coordinates with the origin at nucleus *b*.

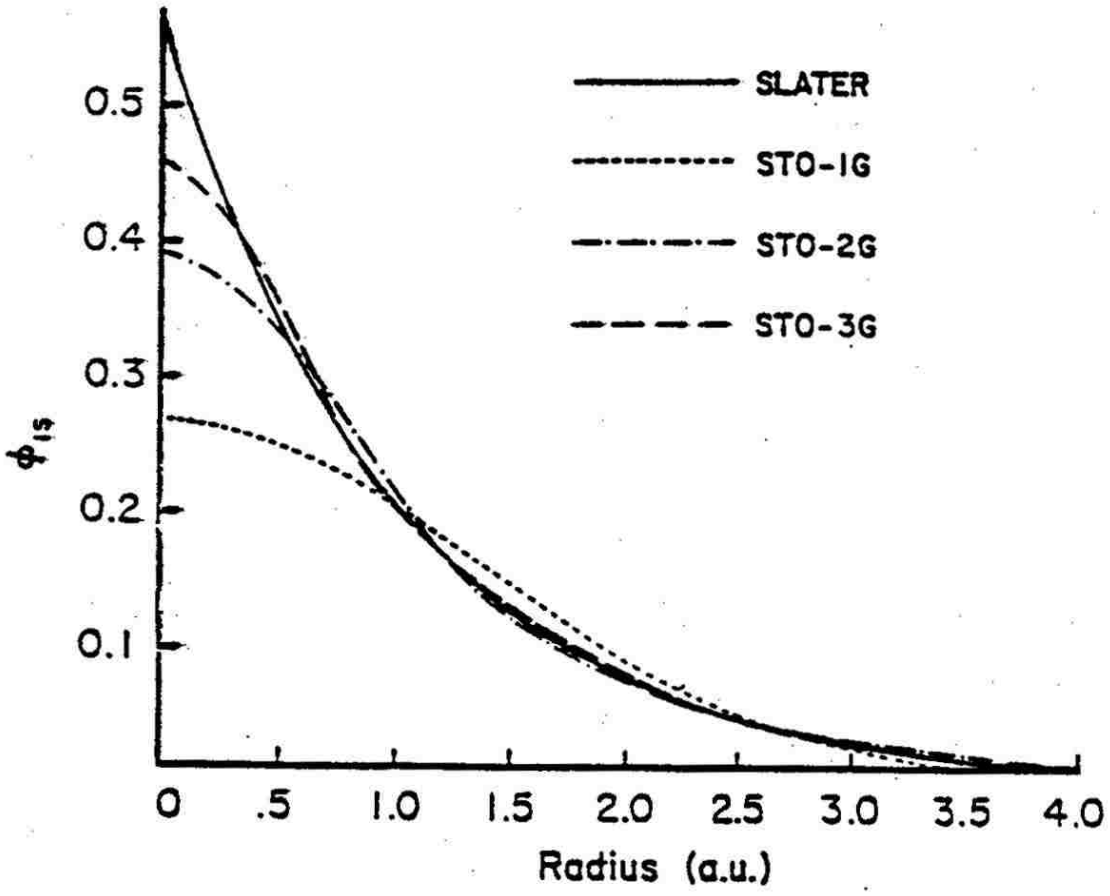

Figure 2.1: Comparison of the quality of the least-square fit of a ls Slater function ($\xi = 1.0$) obtained at the STO-1G, STO-2G, and STO-3G levels.[99]

The Cartesian-Gaussian normalization constant is

$$N = \left(\frac{2\alpha}{\pi}\right)^{3/4} \left[\frac{(8\alpha)^{i+j+k} i!\, j!\, k!}{(2i)!\,(2j)!\,(2k)!}\right]^{1/2} \qquad (30)$$

The sum of exponents at cartesian coordinates, L = $I + j + k$, is used analogously to the angular momentum quantum number for atoms, to mark functions as s-type (L=0), p-type (L=1), d-type (L=2), f-type (L=3), etc.

Gaussian functions are efficient and rapid enough to calculate two-electron integrals; however, Gaussian functions are not optimum basis functions and have functional behavior that is different from the known functional behavior of molecular orbitals. This problem can be solved to fix linear combinations of the primitive Gaussian function. These linear combinations, called contractions, lead to contracted Gaussian-type function (CGTF),

$$\chi_r = \sum_u d_{ur}\, g_u \qquad (31)$$

where the g_u's are normalized Cartesian Gaussian (equation (29)) centered on the same atom and having the same i, j, k values as one another, but different α's. The contraction coefficients d_{ur} are contraction coefficient. In equation 31, χ_r is called a contracted Gaussian-type function (CGTF) and g_u's are called primitive Gaussians.

In the minimal basis set, single zeta (SZ), only one basis function (contraction) per Slater atomic orbital is used. The SZ set consists of one STO for each inner-shell and valence-shell AO of each atom.

A double-zeta (DZ) basis set has two basis functions that differ in their orbital exponents ξ (zeta), and a triple–zeta basis set replaces each STO of a minimal basis set

by three STOs that differ in their orbital exponents.

The split-valence (SV) basis set uses more contractions for each valence AO than core orbitals. Split valence sets are called valence double zeta (VDZ), valence triple zeta (VTZ), and so on, according to the number of STOs used for each valence AO.

The polarization functions are important for reproducing chemical bonding. They are usually added as uncontracted gaussians. Higher angular momentum functions improve the description for anisotropic electron distribution. Normally, p orbitals are added to H and He, d orbitals are added to first-row atoms, f orbitals are added to second-row atoms, and so on. The basis sets are also frequently augmented with the so-called diffuse functions. These gaussians have very small exponents and decay slowly with distance from the nucleus. Anions, compounds with lone pairs, and hydrogen-bonded dimers have significant electron density at a great distance from the nucleus. To improve the accuracy for such compounds, diffuse functions are used.

Symbols of Pople's basis set are like n-ijG or n-ijkG, where n is a number of primitives for the inner shells and ij or ijk is a number of primitives for contractions in the valence shell. The ij notations describe sets of valence double zeta.

.

2.2 Density Functional Theory (DFT)

2.2.1 The Hohenberg-Kohn Theorem

In 1964, Pierre Hohenberg and Walter Kohn proved that the ground state electron density ρ_0 of a many-electron system in the presence of an external potential $V(\mathbf{r}_i)$ uniquely determines the external potential.[100] Therefore, density functional theory (DFT)

attempts to calculate ground state electronic energy E_0 which is function of ρ_0 and other ground state molecular properties from the ground state electron density ρ_0.

We define the purely electronic Hamiltonian as

$$H = -\frac{1}{2}\sum_{i=1}^{n}\nabla_i^2 + \sum_{i=1}^{n} v(r_i) + \sum_{j}\sum_{i>j}\frac{1}{r_{ij}} \tag{32}$$

$$v(r_i) = -\sum_{\alpha}\frac{Z_\alpha}{r_{i\alpha}} \tag{33}$$

In DFT, $v(r_i)$ is called the external potential. The potential energy of interaction between electron i and the nuclei depends on the coordinates x_i, y_i, z_i of electron i and on the nuclear coordinates.

Let us assume that two different external potentials (v_a and v_b) can each be consistent with the same nondegenerate ground state density ρ_0. Let H_a and H_b be the n-electron Hamiltonians (equation 32) corresponding to $v_a(r_i)$ and $v_b(r_i)$, where v_a and v_b are not necessarily given by equation (33). With each Hamiltonian will be associated a ground state wave function Ψ_0 and its associated eigenvalue E_0. The variational theorem of molecular orbital theory dictates that the expectation value of the Hamiltonian a over the wave function b must be higher than the ground state energy of a,

$$E_{0,a} < \langle \Psi_{0,b} | H_a | \Psi_{0,b} \rangle \tag{34}$$

We may rewrite this expression as

$$
\begin{aligned}
E_{0,a} &< \langle \Psi_{0,b} | H_a - H_b + H_b | \Psi_{0,b} \rangle \\
&< \langle \Psi_{0,b} | H_a - H_b | \Psi_{0,b} \rangle + \langle \Psi_{0,b} | H_b | \Psi_{0,b} \rangle \\
&< \langle \Psi_{0,b} | v_a - v_b | \Psi_{0,b} \rangle + E_{0,b}
\end{aligned} \tag{35}
$$

Since the potentials v are one-electron operators, the integral in the last line of equation (35) can be written in terms of the ground state density

$$
E_{0,a} < \int [v_a(r) - v_b(r)] \rho_0(r) dr + E_{0,b} \tag{36}
$$

As we have made no distinction between a and b, we get the electron density $\rho_{0,b}$ corresponding to $\Psi_{0,b}$. If we go through the same reasoning with a and b interchanged, we get

$$
E_{0,b} < \int [v_b(r) - v_a(r)] \rho_0(r) dr + E_{0,a} \tag{37}
$$

Now, when we add inequalities equation (36) and equation (37), we have

$$
\begin{aligned}
E_{0,a} + E_{0,b} &< \int [v_b(r) - v_a(r)] \rho_0(r) dr \\
&\quad + \int [v_a(r) - v_b(r)] \rho_0(r) dr + E_{0,b} \\
&\quad + E_{0,a} \\
&< \int [v_b(r) - v_a(r) + v_a(r) - v_b(r)] \, \rho_0(r) dr + E_{0,b} \\
&\quad + E_{0,a}
\end{aligned} \tag{38}
$$

$$< E_{0,b} + E_{0,a}$$

This result, that the sum of the two energies is less than itself, is false. So our initial assumption, that two different external potentials could produce the same ground-state electron density, must be false.

The ground-state electronic energy E_0 is thus a functional of the function $\rho_0(r)$ and so must be its individual parts. One can write

$$E_0[\rho_0] = \bar{T}[\rho_0] + \bar{V}_{Ne}[\rho_0] + \bar{V}_{ee}[\rho_0] \tag{39}$$

This ground state energy is the sum of electronic kinetic-energy terms, electron-nuclear attractions, and electron-electron repulsions. This expression can be classified by the known term and unknown terms. $\bar{V}_{Ne}[\rho_0]$ is known as

$$\bar{V}_{Ne} = \langle \Psi_0 | \sum_{i=1}^{n} v(r_i) | \Psi_0 \rangle = \int \rho_0(r) v(r) dr \tag{40}$$

where v(r) is the nuclear attracting potential energy function for an electron located at point r.

However, the functionals $\bar{T}[\rho_0]$ and $\bar{V}_{ee}[\rho_0]$ are unknown. We have

$$E_0[\rho_0] = \int \rho_0(r) v(r) dr + F[\rho_0] \tag{41}$$

where the functional $F[\rho_0]$ is called Hohenberg-Kohn functional, is defined $\bar{T}[\rho_0] + \bar{V}_{ee}[\rho_0]$ and is independent of the external potential. Therefore, equation (41) is

unhelpful in providing any indication of how to predict the density of a system, because the functional $F[\rho_0]$ is unknown.

2.2.2 The Hohenberg-Kohn Variation Theorem

The proof of the Hohenberg-Kohn variation theorem is as follows. First, we have some well-behaved candidate density that integrates the proper number of electrons, N. In that case, the first theorem indicates that this density determines a candidate wave function and Hamiltonian. Therefore we can evaluate the energy expectation value

$$\langle \Psi_{\text{cand}} | \mathrm{H}_{\text{cand}} | \Psi_{\text{cand}} \rangle = E_{cand} \geq E_0 \qquad (42)$$

which must be greater than or equal to the true ground state energy.

In principle, we can keep choosing different densities and those that provide lower energies, as calculated by equation (42), are closer to correct.

2.2.3 The Kohn-Sham Method

We know that the density determines the external potential, which determines the Hamiltonian, which determines the wave functions. However, the Hohenberg-Kohn theorem cannot calculate the correct Hamiltonian for the electron-electron interaction term. In a key breakthrough, Kohn and Sham discovered a practical method for finding ρ_0 and for finding E_0 from ρ_0.[101]

The Kohn-Sham method started as a fictitious system (denoted by the subscript s and often called the noninteracting system) of non electrons that have the same external potential-energy functions, $v_s(\mathrm{r_i})$.

Next, Kohn-Sham rewrote the energy functional from equation (39) as

$$E_v[\rho] = \int \rho(r)v(r)dr + \bar{T}_s[\rho] + \frac{1}{2}\iint \frac{\rho(r_1)\rho(r_2)}{r_{12}} dr_1 dr_2 + \Delta\bar{T}[\rho] + \Delta\bar{V}_{ee}[\rho] \quad (43)$$

because $\Delta\bar{T}[\rho]$ and $\Delta\bar{V}_{ee}[\rho]$ are defined by

$$\Delta\bar{T}[\rho] \equiv \bar{T}[\rho] - \bar{T}_s[\rho] \quad (44)$$

and

$$\Delta\bar{V}_{ee}[\rho] \equiv \Delta\bar{V}_{ee}[\rho] - \frac{1}{2}\iint \frac{\rho(r_1)\rho(r_2)}{r_{12}} dr_1 dr_2 \quad (45)$$

where $\frac{1}{2}\iint \frac{\rho(r_1)\rho(r_2)}{r_{12}} dr_1 dr_2$ is the classical expression for the electrostatic interelectronic repulsion energy.

The difficult terms $\Delta\bar{T}[\rho]$ and $\Delta\bar{V}_{ee}[\rho]$ have been defined as the exchange-correlation energy functional.

$$E_{xc}[\rho] \equiv \Delta\bar{T}[\rho] + \Delta\bar{V}_{ee}[\rho] \quad (46)$$

It is very important to get a good approximation to E_{xc} for evaluating exact energy. The local density approximation (LDA) and generalized gradient approximations (GGA)

are introduced.

This is the Hamiltonian of the reference system

$$H_s = \sum_{i=1}^{n}\left[-\frac{1}{2}\nabla_i^2 + v_s(r_i)\right] \equiv \sum_{i=1}^{n} h_i^{KS} \quad where\ h_i^{KS} \equiv -\frac{1}{2}\nabla_i^2 + v_s(r_i) \tag{47}$$

where h_i^{KS} is the one-electron Kohn-Sham Hamiltonian.

2.2.4 Local Density Approximation (LDA)

Local density approximation can be used where charge density is slowly varying and the exchange-correlation energy of an electronic system is constructed by assuming the exchange-correlation energy per electron at a point r in the electron gas.

In this case, we can write E_{xc} as

$$E_{xc}^{LDA}[\rho] = \int \rho(r)\varepsilon_{xc}(\rho)dr \tag{48}$$

where $\varepsilon_{xc}(\rho)$ is the exchange plus correlation energy per electron in a homogeneous electron gas with electron density ρ.

2.2.5 Generalized Gradient Approximation (GGA)

The LDA approach will have limitations if the electron density is typically rather far from spatially uniform. The function of E_{xc} of LDA is only ρ, and LSDA (local-spin-density-approximation) deals separately with the electron density $\rho^{\alpha}(r)$, and the density $\rho^{\beta}(r)$ and the functional, E_{xc}, become $E_{xc} = E_{xc}[\rho^{\alpha}, \rho^{\beta}]$.

GGA is also included in the gradients of the electron density $\rho^{\alpha}(r)$ and the density $\rho^{\beta}(r)$ in the integrand as

$$E_{xc}^{GGA}[\rho^{\alpha},\rho^{\alpha}] = \int f(\rho^{\alpha}(r),\rho^{\beta}(r),\nabla\rho^{\alpha}(r),\nabla\rho^{\beta}(r))dr \qquad (49)$$

where f is some function of the spin densities and their gradients.

Commonly used exchange functionals, E_x, are B86[102], P[103], LG[104] and PBE[105,106].

The most popular GGA correlation functionals, E_c, are the Lee-Yang-Parr (LYP) functional,[107] P86 or Pc86 (Perdew 1986),[103] PW91 or PWc91 (Perdew and Wang 1992),[108] and the Becke correlation functional called Bc95 or B96.[109]

A B3LYP calculation combines Becke's GGA exchange with the GGA correlation functional of Lee, Yang, and Parr. This functional is defined by

$$\begin{aligned} E_{xc}^{B3LYP} = (1-a_0-a_x)E_x^{LSDA} + a_0E_x^{exact} + a_xE_x^{B88} \\ + (1-a_c)E_c^{VWN} + a_cE_c^{LYP} \end{aligned} \qquad (50)$$

2.3 Monte Carlo Simulation

The Monte Carlo simulations use random numbers and probability theory for solving problems. Von Neumann, Ulam and Metropolis developed the Monte Carlo simulation method at the end of the Second World War to study the diffusion of neutrons in fissionable materials.[110]

The name of Monte Carlo simulation was coined by S. Ulam and Nicholas Metropolis in reference to games of chance, a popular attraction in Monte Carlo, Monaco.

2.3.1 The Metropolis Method

The Metropolis algorithm is based on the notion of detailed balance that describes equilibrium for systems whose configurations have probability proportional to the Boltzmann factor. The Boltzmann factor, $e^{-E/T}$, is proportional to the probability that the system will be found in a particular configuration at energy E when the temperature of the environment is T. Therefore,

$$P \propto e^{-E/T} \tag{51}$$

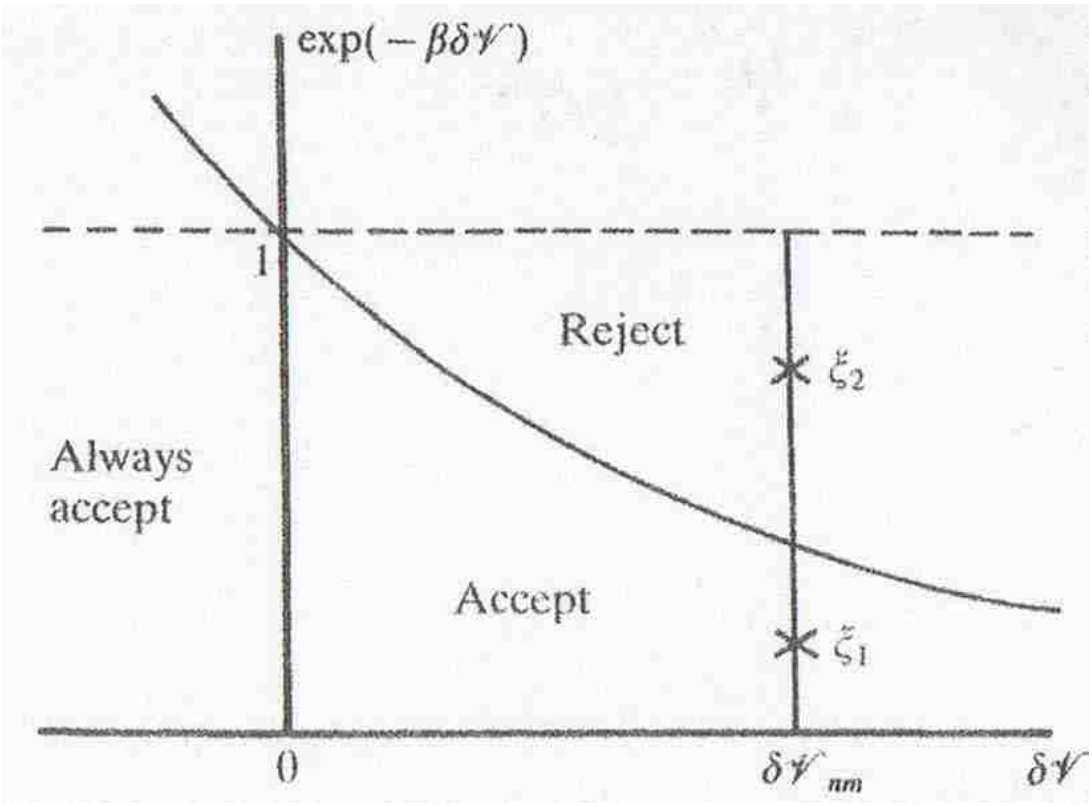

Figure 2.3: Accepting uphill moves in the MC simulation.[110]

Consider two configurations A and B, each of which occurs with probability proportional to the Boltzmann factor. The nice thing about forming the ratio is that it converts relative

probabilities involving an unknown proportionality constant (called the inverse of the partition function) into a pure number. In a seminal paper of 1953, Metropolis et al. noted that we can achieve the relative probability of equation (51) in a simulation by proceeding as follows:

1. Starting from a configuration A, with known energy E_A, make a change in the configuration to obtain a new (nearby) configuration B.

2. Compute E_B (typically as a small change from E_A).

3. If $E_B < E_A$, assume the new configuration, since it has lower energy (a desirable thing, according to the Boltzmann factor).

4. If $E_B > E_A$, accept the new (higher energy) configuration with probability *p*.

If we follow these rules, then we will sample points in space of all possible configurations with probability proportional to the Boltzmann factor, consistent with the theory of equilibrium statistical mechanics. We can compute average properties by adding them along the path we follow through possible configurations. The hardest part about implementing the Metropolis algorithm is the first step: how to generate useful new configurations.

If the random number, ξ, is less than a probability of $\exp^{(-\beta\delta Vnm)}$, the move is accepted. Figure 2.3 shows this procedure. Suppose that a particular uphill move is attempted in running the procedure. There are two points at random numbers, ξ_1 and ξ_2. If the random number ξ_1 is chosen, the move is accepted, but if ξ_2 is chosen, the move is rejected.

The Monte Carlo simulations need to compare only potential energy (*V*). First of all, we calculate the initial potential energy (V_1) at the initial state (R_1), moving coordinate directions using a random number generator to get the new state (R_2) and to calculate new potential energy (V_2).

In our MC simulations, we generate the initial structure by attaching CuO molecule to an optimized and smaller copper oxide clusters. The simulations repeated the

following steps: (1) Given the initial configuration R_1, new configuration R_2 is generated by random number generator of one randomly chosen atom. (2) Once the total energies (V_1 and V_2) of these two configurations are calculated, the acceptance probability of the new configuration R_2 is then determined as

$$P(R_2|R_1) = min[1, \exp(\beta(V_2 - V_1)] \quad (52)$$

where $\beta = -1/k_B T$, T is the temperature and k_B is Boltzmann's constant. (3) If the configuration R_2 is accepted, it will be the configuration of the next MC step, and V_1 is set equal to V_2. If the configuration R_2 is not accepted, the configuration R_1 and its energy V_1 are retained and used to start the next step. In this way, the simulations will eventually reach equilibrium. This procedure is the Metropolis method.[111] About 500 MC steps were needed to reach the equilibrium state. We performed our MC simulations at temperature from 2000K to 300K.

CHAPTER 3

Cu_nO_n (n=1-8) CLUSTERS

We used *ab initio* simulations and calculations to study the structures and stabilities of copper oxide clusters, Cu_nO_n (n=1-8). The lowest energy structures of neutral and charged copper oxide clusters were determined using primarily the B3LYP/LANL2DZ model chemistry. A transition from planar to nonplanar geometries occurs at n=4. Selected electronic properties including binding energies, ionization energies, and electronic affinities were calculated and examined as a function of n. Stabilities were examined by calculating fragmentation channels and Löwdin charge distributions.

3.1 Method

3.1.1 Monte Carlo Simulations

We performed *ab initio* Monte Carlo simulation (using Gaussian 03[112] and homegrown scripts) to locate stable geometric structures for Cu_nO_n clusters with n=1-8. The simulations used multiple starting geometries for each cluster size. To calculate the total energy at each MC step, we used Gaussian 03[112] program with B3LYP (Becke's 3-parameter exchange functional with Lee-Yang-Parr correlation energy functional)[107,113,114] and 6-31G** basis set.[115,116] About 500 MC steps were needed to reach the equilibrium state. We performed our MC simulations at temperatures from 2000K to 300K.

The Monte Carlo simulations of Cu_3O_3 cluster are shown in Figure 3.1. We generate the initial structure: Cu-O molecule is attached on optimized copper oxide clusters. We

performed 160 MC steps to find the local energy of Cu_3O_3 cluster.

These geometries were then optimized using standard *ab* initio methods using the GAMESS[117] quantum chemistry package. The smaller clusters were then used as starting points to look for the global minimum geometries for larger clusters where the Monte Carlo procedure was not practical. We used the B3LYP (Becke's 3-parameter exchange functional with Lee-Yang-Parr correlation energy functional)[107,113,114] version of DFT with LANL2DZ basis set.

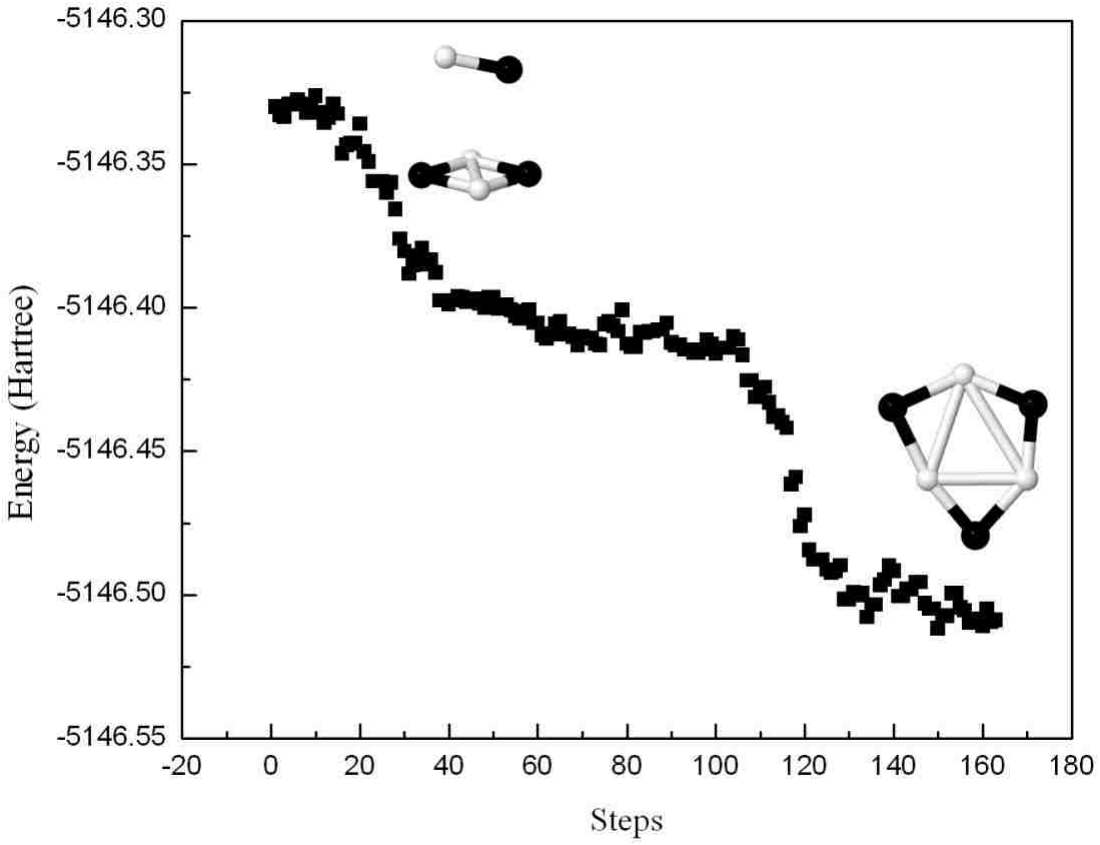

Figure 3.1: Monte Carlo simulation of Cu_3O_3 cluster. Copper/oxygen atoms are colored white/black.

3.1.2 Basis Sets

We used 6-31G*[118-120], 6-31++G**,[118,121-125] 6-311G**[124,126-128], 6-311++G**[123,124], LANL2DZ[129-131] and DGDZVP[132,133] basis set to choose the best basis set for copper oxide clusters. 6-31G* basis set is described by six 3d functions per atom:$3d_{xx}$, $3d_{yy}$, $3d_{zz}$, $3d_{xy}$, $3d_{yz}$, and $3d_{zx}$. These six, the Cartesian Gaussian, are linear combinations of the usual five 3d functions: $3d_{xy}$, $3d_{x^2-y^2}$, $3d_{yz}$, $3d_{zx}$, and $3d_{z^2}$ and 3s function ($x^2 + y^2 + z^2$), including polarization functions. The polarization functions are denoted by an asterisk, *. Two asterisks, **, indicate that polarization functions are also added to light atoms (hydrogen and helium). The diffuse functions are denoted by a plus sign, +. Two plus signs, ++, indicate that diffuse functions are also added to light atoms (hydrogen and helium).

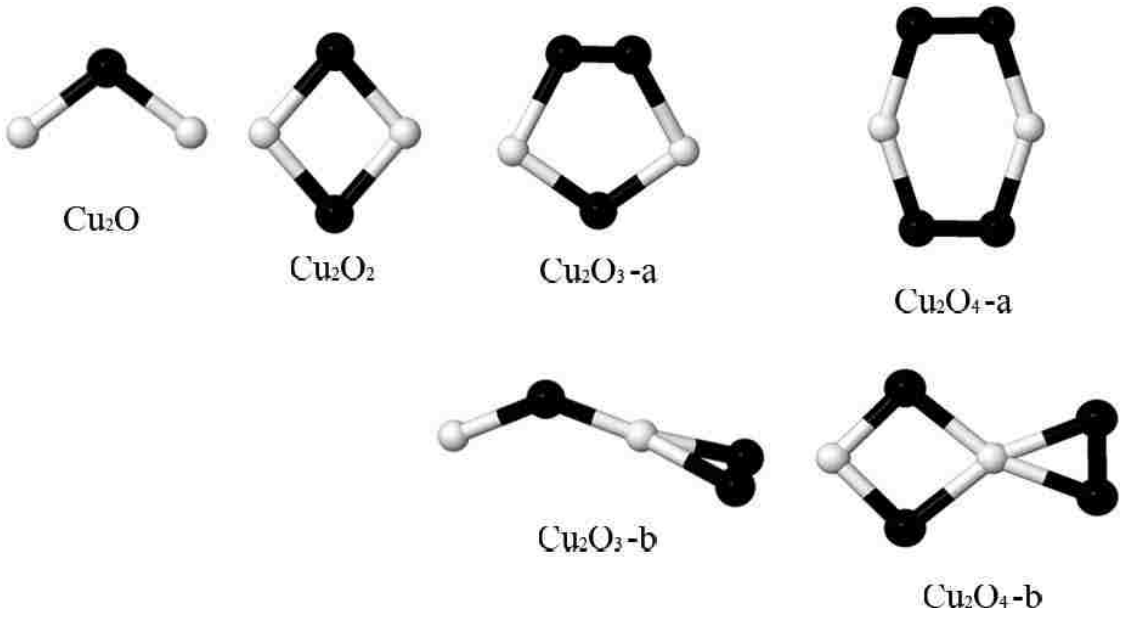

Figure 3.2: Lowest energy clusters for Cu_2O_n, n=1-4. Different basis sets give different lowest isomers for n=3 and 4 (Cu_2O_3-a:6-31G**; Cu_2O_3-b: 6-31++G**, 6-311G**, 6-311++G**, LANL2DZ and DGDZVP; Cu_2O_4-a: 6-31++G**, 6-311++G**, LANL2DZ and DGDZVP; Cu_2O_4-b: 6-31G** and 6-311G**) (See Table 2.1 for details.) Copper/oxygen atoms are colored white/black.

Effective core potential (ECP) or Effective Potential (EP) approaches are developed to treat inner shell electrons as if they were some averaged potential rather than actual particles. An effective core potential (ECP) is a linear combination of specially designed Gaussian functions that model the core electrons; the core electrons are represented by an effective potential, and one treats only the valence electrons explicitly. LANL2DZ basis set is known as Los Alamos National Laboratory basis set and was developed by Hay and Wadt.[129-131] LANL2DZ basis set has been widely used in quantum chemistry in the study of compounds or clusters containing heavy elements. The functions of this basis set have been obtained by fitting the procedure of pseudo-orbitals with Gaussian functions. DGDZVP basis sets are denoted by double-zeta valence plus polarization (DZVP) in DGauss.[132-134]

Table 2.1: Electronic affinities comparing basis sets with experimental data

	Electron Affinities (eV)						
	6-31G**	6-31++G**	6-311G**	6-311++G**	LANL2DZ	DGDZVP	EXP[77]
Cu_2O	0.94	1.27	0.14	1.24	1.15	1.15	1.10
Cu_2O_2	1.41	2.33	0.89	1.76	2.41	2.24	2.46
Cu_2O_3	2.35	2.65	1.67	3.09	3.25	3.08	3.54
Cu_2O_4	3.26	3.34	2.75	3.35	3.54	3.31	3.50

Calculations found the lowest energy clusters for Cu_2O_n (n=1-4), shown in Figure 2.2. For Cu_2O_3 and Cu_2O_4, different isomers were found depending on the basis set (Cu_2O_3-a: 6-31G**; Cu_2O_3-b: 6-31++G**, 6-311G**, 6-311++G**, LANL2DZ and DGDZVP; Cu_2O_4-a: 6-31++G**, 6-311++G**, LANL2DZ and DGDZVP; Cu_2O_4-b: 6-31G** and 6-311G**). Experimental data of electron affinities of Cu_2O to Cu_2O_4 clusters are available.[77] A comparison of calculated and measured electron affinities are shown in Table 2.1. The best agreement with experimental data is found with the LANL2DZ basis set, which is therefore used in the remainder of this work.

3.2 Results

3.2.1 Geometric Structures

The optimized structures of neutral and charged $(CuO)_n$ clusters with n=1-8 are shown in Figure 3.2 and the corresponding bond lengths in Table 3.1. Spin states, adiabatic ionization energies, adiabatic electron affinities, and binding energies per copper atoms are given in Table 3.2. The lowest spin state (i.e., singlet, doublet, triplet and quartet) of a given cluster was used in these calculations. Every neutral copper oxide cluster, $(CuO)_n$, can be formed from a $Cu_{n-1}O_{n-1}$ cluster by attaching a Cu-O molecule to the side of a $Cu_{n-1}O_{n-1}$ cluster.

The calculated bond lengths for CuO^- and CuO are 1.74Å and 1.81Å and are in acceptable agreement with the measured values of 1.67Å and 1.72Å.[80] Based on the present simulations and calculations, the structure of the lowest energy Cu_2O_2 cluster is a rhombus. The spin states of optimized structures are singlet, doublet, and doublet for the neutral, cation, and anion clusters, respectively. Wang et al.[77] and Dai et al.[98] have suggested minimum energy structures for Cu_2O_2 based on ab initio calculations and/or experimental measurements. Wang et al. suggest the structure is a rhombus, while Dai et al. suggest the structure is linear or near linear. The rhombic structure of Wang et al. has a Cu-O bond length of 1.78Å and a Cu-O-Cu bond angle of 80°. Our calculations give a Cu-O bond length of ≈1.86Å and a Cu-O-Cu bond angle of ≈82°. The present work supports the rhombic structure as the lowest energy structure for Cu_2O_2.

Our calculations find Cu_3O_3 clusters to be nearly planar. The neutral cluster is a quartet, while the charged clusters have triplet ground states. The average Cu-O-Cu bond angles are 121.8° (cation), 98.1° (neutral), and 94.2° (anion). The calculated Cu- O bond lengths are 1.89Å (cation), 1.90Å (neutral), and 1.85 (anion).

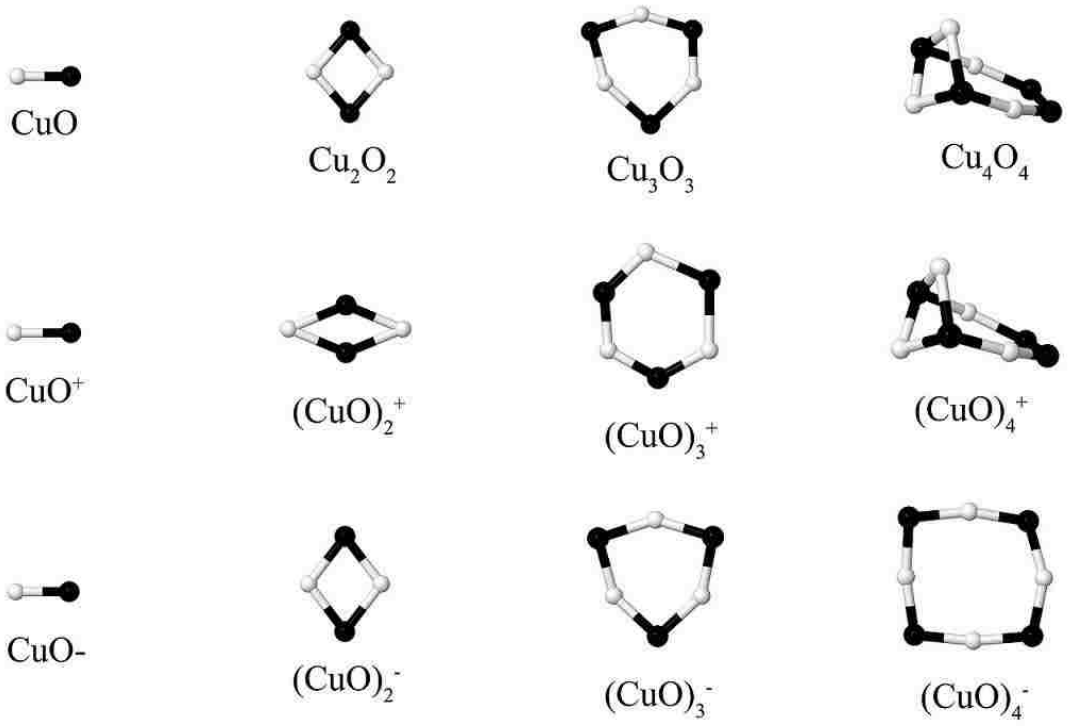

Figure 3.3: Optimized structures of neutral, positively, and negatively charged $(CuO)_n$ clusters with n=1-4. Copper/oxygen atoms are colored white/black.

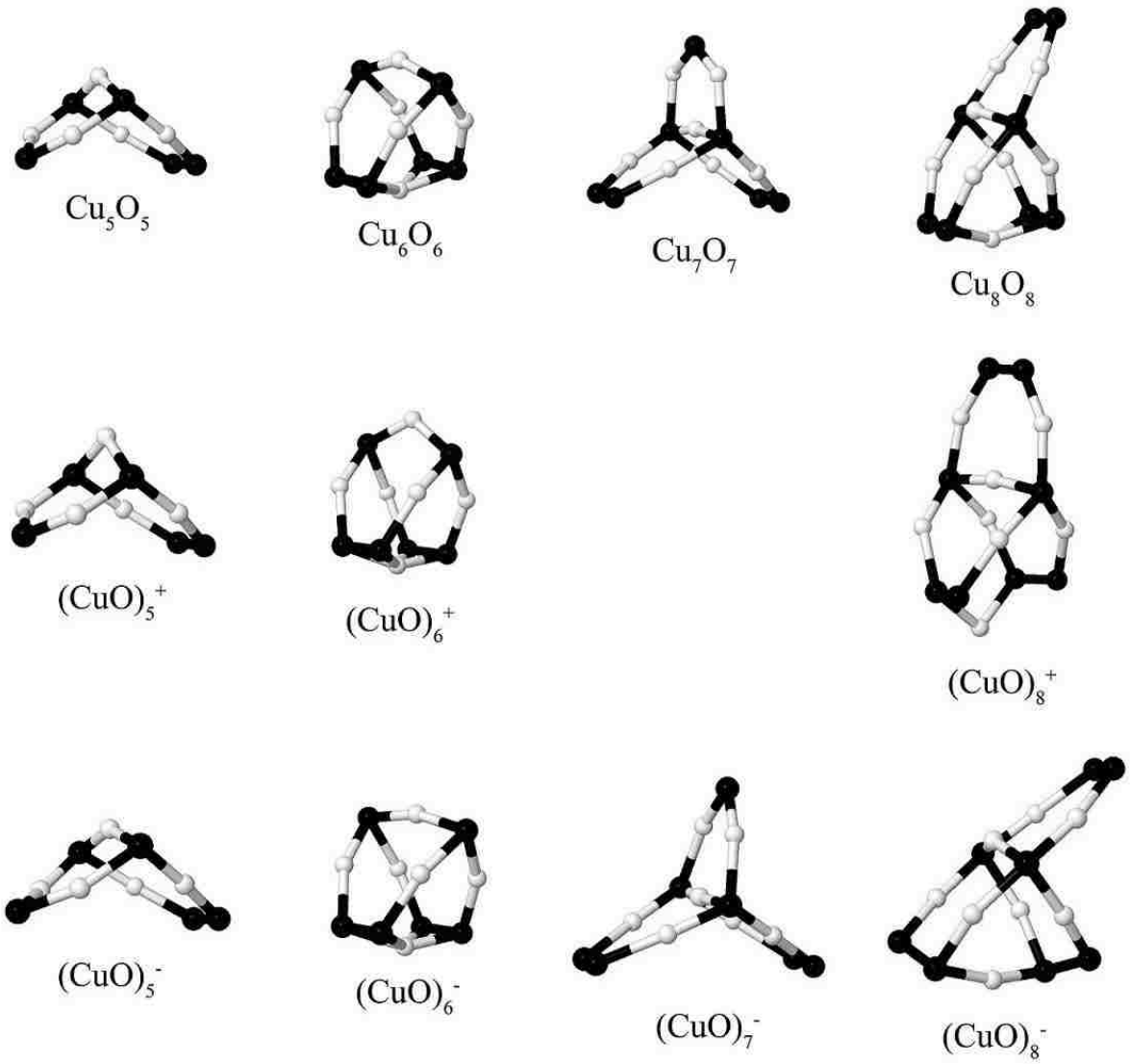

Figure 3.4: Optimized structures of neutral, positively, and negatively charged $(CuO)_n$ clusters with n=5-8. Copper/oxygen atoms are colored white/black.

Table 3.1: Bond lengths (Å) of Cu-O-Cu in $(CuO)_n$ (n=1-8) clusters

Clusters		*d*			
CuO	CuO	d_{1-2}=1.81			
	CuO^+	d_{1-2}=1.76			
	CuO^-	d_{1-2}=1.74			
Cu_2O_2	Cu_2O_2	d_{1-3}=1.86	d_{1-4}=1.86	d_{2-3}=1.86	d_{2-4}=1.86
	$Cu_2O_2^+$	d_{1-3}=2.01	d_{1-4}=2.01	d_{2-3}=2.01	d_{2-4}=2.01
	$Cu_2O_2^-$	d_{1-3}=1.92	d_{1-4}=1.92	d_{2-3}=1.92	d_{2-4}=1.92
Cu_3O_3	Cu_3O_3	d_{1-4}=1.83	d_{1-6}=2.06	d_{2-4}=1.81	
		d_{2-5}=1.83	d_{3-5}=1.83	d_{3-6}=2.03	
	$Cu_3O_3^+$	d_{1-4}=1.75	d_{1-6}=1.77	d_{2-4}=1.78	
		d_{2-5}=2.13	d_{3-5}=2.12	d_{3-6}=1.79	
	$Cu_3O_3^-$	d_{1-4}=1.84	d_{1-6}=1.85	d_{2-4}=1.85	
		d_{2-5}=1.85	d_{3-5}=1.85	d_{3-6}=1.85	
Cu_4O_4	Cu_4O_4	d_{1-5}=1.96	d_{1-6}=1.97	d_{2-6}=1.88	d_{2-7}=1.93
		d_{3-5}=1.88	d_{3-8}=1.93	d_{4-5}=1.97	d_{4-6}=1.96
	$Cu_4O_4^+$	d_{1-5}=1.94	d_{1-6}=1.93	d_{2-6}=1.88	d_{2-7}=1.94
		d_{3-5}=1.87	d_{3-8}=1.93	d_{4-5}=1.92	d_{4-6}=1.95
	$Cu_4O_4^-$	d_{1-5}=1.81	d_{1-6}=1.81	d_{2-6}=1.80	d_{2-7}=1.79
		d_{3-5}=1.81	d_{3-8}=1.83	d_{4-5}=1.80	d_{4-6}=1.80
Cu_5O_5	Cu_5O_5	d_{1-6}=1.83	d_{1-10}=1.87	d_{2-6}=1.83	d_{2-7}=1.88
		d_{3-7}=1.88	d_{3-8}=1.92	d_{4-9}=1.92	d_{4-10}=1.87
		d_{5-7}=1.90	d_{5-10}=1.90	d_{8-9}=1.40	
	$Cu_5O_5^+$	d_{1-6}=1.87	d_{1-10}=1.87	d_{2-6}=1.80	d_{2-7}=1.88
		d_{3-7}=1.88	d_{3-8}=1.87	d_{4-9}=1.87	d_{4-10}=1.88
		d_{5-7}=1.96	d_{5-10}=1.96	d_{8-9}=1.37	
	$Cu_5O_5^-$	d_{1-6}=1.87	d_{1-10}=1.91	d_{2-6}=1.87	d_{2-7}=1.90
		d_{3-7}=1.87	d_{3-8}=1.92	d_{4-9}=1.92	d_{4-10}=1.87
		d_{5-7}=1.96	d_{5-10}=1.96	d_{8-9}=1.41	
Cu_6O_6	Cu_6O_6	d_{1-7}=1.94	d_{1-12}=1.90	d_{2-8}=1.94	d_{2-9}=1.90
		d_{3-9}=1.90	d_{3-10}=1.94	d_{4-11}=1.94	d_{4-12}=1.90
		d_{5-9}=1.88	d_{5-12}=1.89	d_{6-7}=2.02	d_{6-8}=2.10
		d_{6-10}=2.02	d_{6-11}=2.10	d_{7-8}=1.52	d_{10-11}=1.52
	$Cu_6O_6^+$	d_{1-7}=1.99	d_{1-12}=1.90	d_{2-8}=1.99	d_{2-9}=1.93
		d_{3-9}=1.93	d_{3-10}=1.99	d_{4-11}=1.99	d_{4-12}=1.90
		d_{5-9}=1.86	d_{5-12}=1.85	d_{6-7}=1.98	d_{6-8}=1.98
		d_{6-10}=1.98	d_{6-11}=1.98	d_{7-8}=1.49	d_{10-11}=1.49
	$Cu_6O_6^-$	d_{1-7}=1.96	d_{1-12}=1.92	d_{2-8}=1.96	d_{2-9}=1.94
		d_{3-9}=1.94	d_{3-10}=1.96	d_{4-11}=1.96	d_{4-12}=1.92
		d_{5-9}=1.91	d_{5-12}=1.92	d_{6-7}=2.01	d_{6-8}=2.05
		d_{6-10}=2.06	d_{6-11}=2.00	d_{7-8}=1.56	d_{10-11}=1.56

Table 3.1: Bond lengths (Å) of Cu-O-Cu in $(CuO)_n$ (n=7-8) clusters

Clusters		*d*			
Cu_7O_7	Cu_7O_7	$d_{1\text{-}8}$=1.94	$d_{1\text{-}14}$=1.92	$d_{2\text{-}9}$=1.94	$d_{2\text{-}10}$=1.92
		$d_{3\text{-}10}$=1.92	$d_{3\text{-}12}$=1.94	$d_{4\text{-}13}$=1.94	$d_{4\text{-}14}$=1.92
		$d_{5\text{-}10}$=1.92	$d_{5\text{-}14}$=1.92	$d_{6\text{-}10}$=1.98	$d_{6\text{-}11}$=1.88
		$d_{7\text{-}11}$=1.88	$d_{7\text{-}14}$=1.98	$d_{8\text{-}9}$=1.40	$d_{12\text{-}13}$=1.40
	$Cu_7O_7^-$	$d_{1\text{-}8}$=2.19	$d_{1\text{-}14}$=1.89	$d_{2\text{-}9}$=2.18	$d_{2\text{-}10}$=1.90
		$d_{3\text{-}10}$=1.90	$d_{3\text{-}12}$=2.15	$d_{4\text{-}13}$=2.15	$d_{4\text{-}14}$=1.90
		$d_{5\text{-}10}$=2.05	$d_{5\text{-}14}$=2.06	$d_{6\text{-}10}$=2.14	$d_{6\text{-}11}$=1.71
		$d_{7\text{-}11}$=1.73	$d_{7\text{-}14}$=2.07	$d_{8\text{-}9}$=1.39	$d_{12\text{-}13}$=1.40
Cu_8O_8	Cu_8O_8	$d_{1\text{-}9}$=1.94	$d_{1\text{-}14}$=1.97	$d_{2\text{-}10}$=1.95	$d_{2\text{-}11}$=1.97
		$d_{3\text{-}11}$=1.98	$d_{3\text{-}15}$=1.93	$d_{4\text{-}14}$=1.96	$d_{4\text{-}16}$=1.93
		$d_{5\text{-}9}$=1.99	$d_{5\text{-}10}$=2.06	$d_{5\text{-}15}$=2.06	$d_{5\text{-}16}$=2.02
		$d_{6\text{-}11}$=1.96	$d_{6\text{-}14}$=1.96	$d_{7\text{-}11}$=1.91	$d_{7\text{-}12}$=1.94
		$d_{8\text{-}13}$=1.94	$d_{8\text{-}14}$=1.92	$d_{9\text{-}10}$=1.55	$d_{12\text{-}13}$=1.40
		$d_{15\text{-}16}$=1.55			
	$Cu_8O_8^+$	$d_{1\text{-}9}$=2.08	$d_{1\text{-}14}$=1.93	$d_{2\text{-}10}$=2.07	$d_{2\text{-}11}$=1.94
		$d_{3\text{-}11}$=2.07	$d_{3\text{-}15}$=1.93	$d_{4\text{-}14}$=2.08	$d_{4\text{-}16}$=2.12
		$d_{5\text{-}10}$=2.12	$d_{5\text{-}15}$=2.13	$d_{6\text{-}11}$=1.92	$d_{6\text{-}14}$=1.93
		$d_{7\text{-}11}$=1.95	$d_{7\text{-}12}$=1.82	$d_{8\text{-}13}$=1.83	$d_{8\text{-}14}$=1.95
		$d_{9\text{-}10}$=1.42	$d_{12\text{-}13}$=1.38	$d_{15\text{-}16}$=1.42	
	$Cu_8O_8^-$	$d_{1\text{-}9}$=1.92	$d_{1\text{-}14}$=1.95	$d_{2\text{-}10}$=1.84	$d_{2\text{-}11}$=1.97
		$d_{3\text{-}11}$=1.95	$d_{3\text{-}15}$=1.92	$d_{4\text{-}14}$=1.98	$d_{4\text{-}16}$=1.84
		$d_{5\text{-}9}$=1.90	$d_{5\text{-}15}$=1.92	$d_{6\text{-}11}$=1.98	$d_{6\text{-}14}$=1.95
		$d_{7\text{-}11}$=1.91	$d_{7\text{-}12}$=2.13	$d_{8\text{-}13}$=2.15	$d_{8\text{-}14}$=1.93
		$d_{9\text{-}10}$=1.58	$d_{12\text{-}13}$=1.39	$d_{15\text{-}16}$=1.58	

The Cu_4O_4 cluster is the first nonplanar structure found for Cu_nO_n and consists of 2 copper atoms above and below the plane of a Cu_2O_4 unit. A similar structure is found for the cation cluster, while the anion cluster is planar. The spin states of the optimized structures are triplet (neutral) and doublet (cation and anion). The Cu-O bond lengths are 1.92Å (cation), 1.94Å (neutral), and 1.81Å (anion).

The Cu_5O_5 clusters consist of fused 6-membered (Cu_3O_3) and 7-membered (Cu_3O_4) rings sharing a O-Cu-O edge. The angle between the rings is 131.5°. In these clusters, there is one O-O bond. The spin states of optimized structures are quartet (neutral) and triplet (cation and anion).

Cu_6O_6 clusters have cage structures. The spin states of optimized structures are triplet (neutral) and doublet (cation and anion). Cu_7O_7 clusters exhibit another fused structure with three rings sharing a common edge. Similar to the Cu_5O_5 clusters, the rings are 6- and 7-membered. There are two O-O bonds in these structures. We were unable to optimize the Cu_7O_7 due to severe spin-contamination issues. The spin states of optimized structures are quartet (neutral) and triplet (anion). Cu_8O_8 can be constructed from Cu_6O_6 by addition of a Cu_2O_2 group to an an edge of the Cu_6O_6 cluster. The spin states of optimized structures are triplet (neutral), quartet (cation) and doublet (anion).

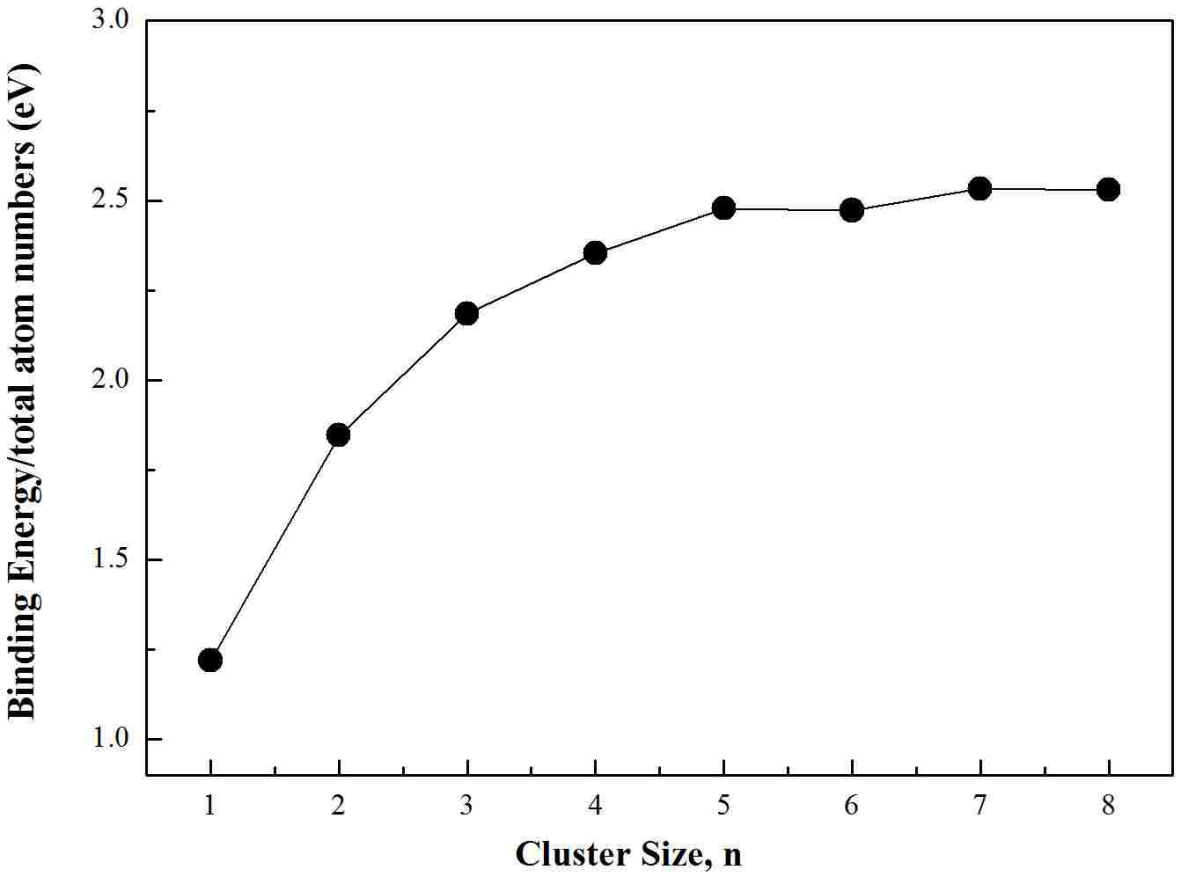

Figure 3.5: Atomization energies of neutral $(CuO)_n$ clusters with n=1-8

3.2.2 Atomization Energies and Second Difference Energies

The atomization energies per atom have been calculated from

$$E_b = [n\,E(Cu) + n\,E(O) - E(Cu_nO_n)]/2n \qquad (1)$$

Table 3.2: Spin states, ionization energies (IE), electron affinities (EA), and binding energies (Eb) for Cu_nO_n, n=1-8. Energies are in electron volts and are calculated using the B3LYP/LANL2DZ model chemistry.

Clusters	Spin State	IE	EA	E_b
CuO	doublet			
CuO^+	singlet	12.25	1.35	1.22
CuO^-	singlet			
Cu_2O_2	singlet			
$Cu_2O_2^+$	doublet	8.24	2.35	1.85
$Cu_2O_2^-$	doublet			
Cu_3O_3	quartet			
$Cu_3O_3^+$	triplet	9.36	3.65	2.19
$Cu_3O_3^-$	triplet			
Cu_4O_4	triplet			
$Cu_4O_4^+$	doublet	8.37	3.40	2.35
$Cu_4O_4^-$	doublet			
Cu_5O_5	quartet			
$Cu_5O_5^+$	triplet	8.78	3.64	2.48
$Cu_5O_5^-$	Triplet			
Cu_6O_6	triplet			
$Cu_6O_6^+$	doublet	8.46	3.61	2.47
$Cu_6O_6^-$	doublet			
Cu_7O_7	quartet			
			2.00	2.53
$Cu_7O_7^-$	triplet			
Cu_8O_8	triplet			
$Cu_8O_8^+$	quartet	8.26	3.13	2.53
$Cu_8O_8^-$	doublet			

Figure 3.2 shows the atomization energy per atom, E_a, as a function of the number of copper atoms in the cluster. This energy rises rapidly from n=1 to n=5 and appears to be converging to about 2.5eV. The second difference in energies is defined by

$$\Delta^2 E(n) = [E(n+1) - E(n)] - [E(n) - E(n-1)] \qquad (2)$$

and is often used to identify so-called "magic clusters," which are clusters with particular stability. The second difference is plotted in Figure 3.4. There is an odd-even alteration in the values of $\Delta^2 E(n)$ with Cu_5O_5 (and possibly Cu_3O_3) appearing to be particularly stable.

The geometric structures Cu_5O_5 and Cu_3O_3 are characterized by rings with at least 6 atoms. We have investigated whether ring strain plays an important role in the stability of these clusters by calculating the RMS deviations of Cu-O-Cu and O-Cu-O angles from "ideal" values. For a planar, completely symmetric ring, the angle would be 120°. The Cu-O-Cu angles in Cu_5O_5 and Cu_3O_3 are nearly tetrahedral (≈ 109.5). We thus choose the tetrahedral angle as the "ideal" Cu-O-Cu bond angle and 130.5° as the "ideal" O-Cu-O bond angle. Table 3.3 shows these root-mean-square (rms) deviations. There is a slight correlation between the second energy difference and the Cu-O-Cu bond angles, so there is a possibility that ring strain due to Cu-O-Cu deviating from perfect tetrahedral angles plays a role in the stability of the clusters. We have investigated that the stability of copper oxide clusters is discussed in term of the ring size effect. The even numbered clusters have small rings (3- and 4-membered). These small rings lead to ring strain and a loss of stability. On the contrary, the odd numbered clusters have large rings (6- and 7-membered).

Table 3.3: Root-mean-square deviations of Cu-O-Cu and O-Cu-O angles

Cu_nO_n (n=2-8)	Cu_2O_2	Cu_3O_3	Cu_4O_4	Cu_5O_5	Cu_6O_6	Cu_7O_7	Cu_8O_8
RMS deviations (Cu-O-Cu angles)	27.5	13.0	21.7	10.9	16.2	20.6	26.5
RMS deviations (O-Cu-O angles)	32.5	11.6	29.7	21.9	16.4	29.8	39.8

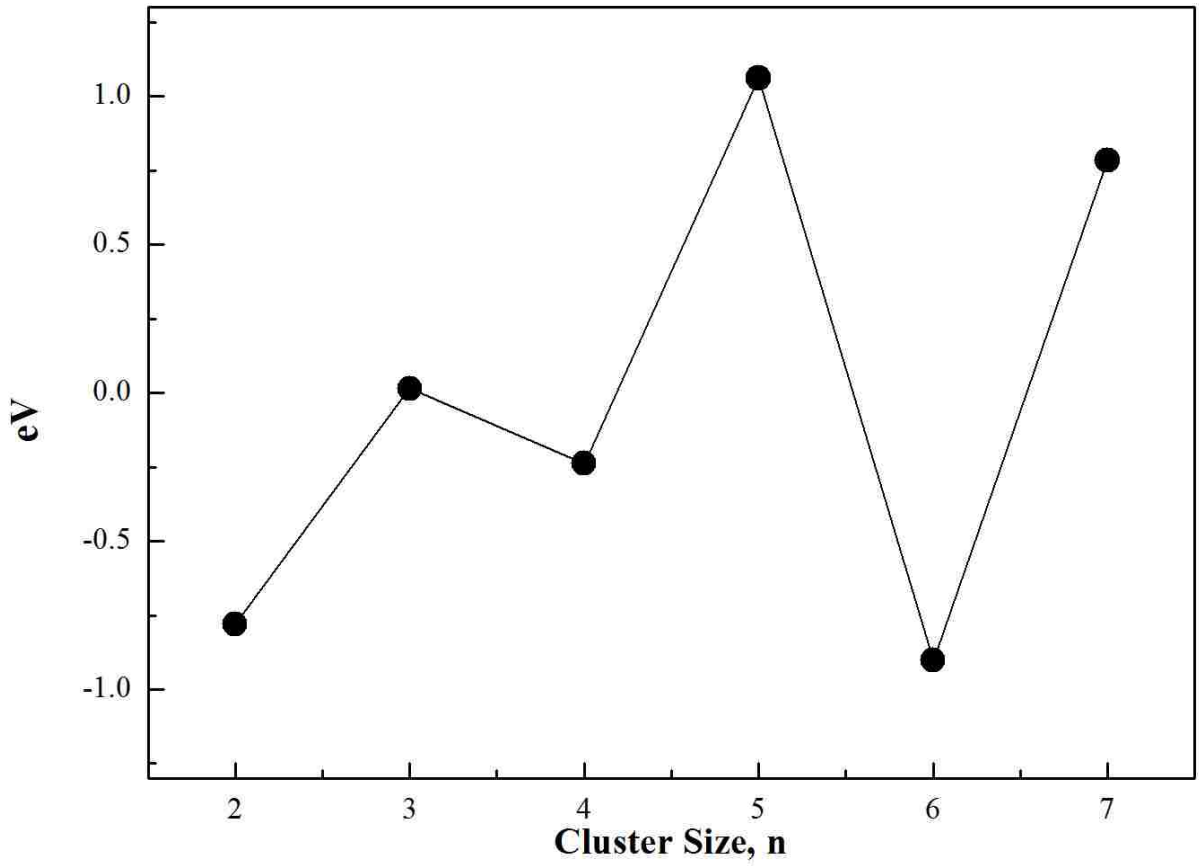

Figure 3.6: Second difference of the energy of $(CuO)_n$ clusters with n=1-7

3.2.3 Ionization Potential, Electron Affinities and HOMO-LUMO Gaps

Figure 3.5 represents the ionization potentials ($IP(X_n) = E(X_n^+) - E(X_n)$) and electron affinities ($EA(X_n) = E(X_n) - E(X_n^-)$). Ionization potentials and electron affinities have been calculated taking the lowest structural energies, which are adiabatic energies. The even-odd oscillation in IP can be explained based on the electronic clusters

structures. In the case of clusters with an even number of copper atoms, all electrons are paired, giving a closed shell electronic structure and spin pairing. In contrast, all odd numbered clusters have a single unpaired electron. Therefore, it is much more difficult to ionize the even numbered clusters than odd ones. It is seen that the copper oxide clusters with n=1, 3, and 5 have higher IPs.

However, it should be much easier to attach an electron to copper oxide clusters with an odd number of copper atoms than the even ones. In figure 3.5, the electron affinities energies are increasing for n=1-3 and showing a stabilization for n=3-6.

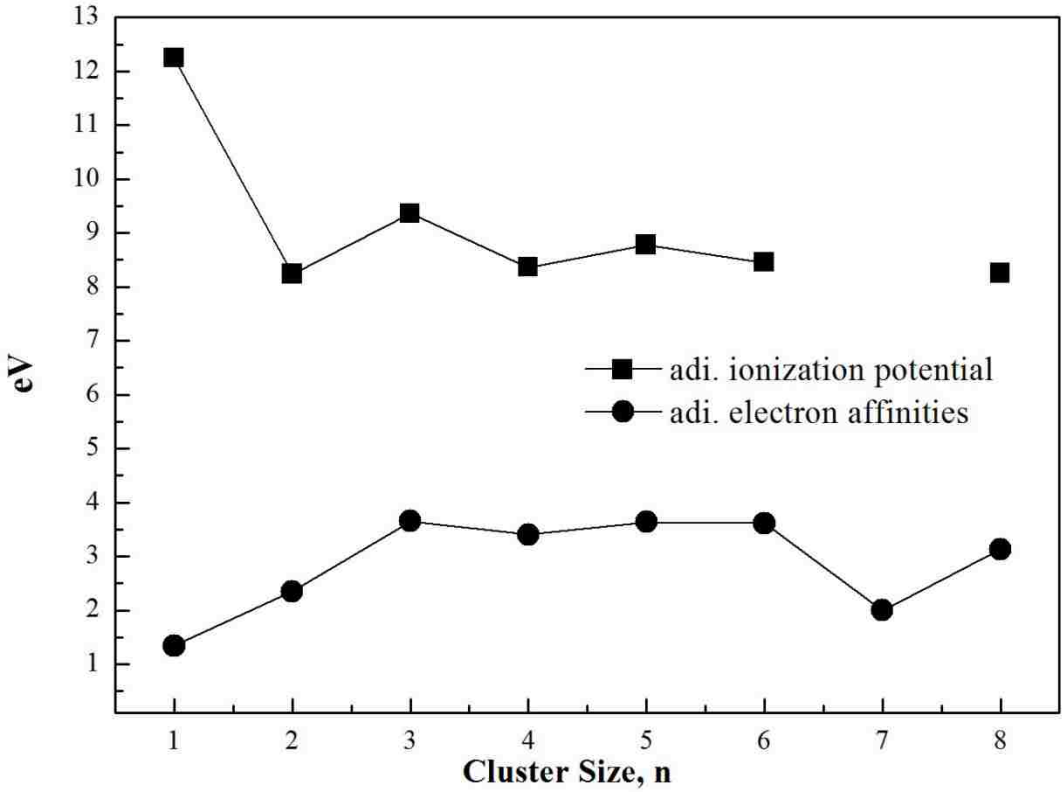

Figure 3.7: Calculated adiabatic ionization potential and electron affinities of $(CuO)_n$ clusters with n=1-8

The calculated HOMO-LUMO gaps of the lowest-energy structures for neutral $(CuO)_n$ (n=1-8) clusters are shown in Figure 3.6. The magnitude of the gaps varies from 2.24 eV to 3.67 eV. Usually the clusters with larger HOMO-LUMO gaps are more stable and chemically

inert. Interestingly, we note that the Cu_3O_3 cluster has largest HOMO-LUMO gap among the clusters we studied.

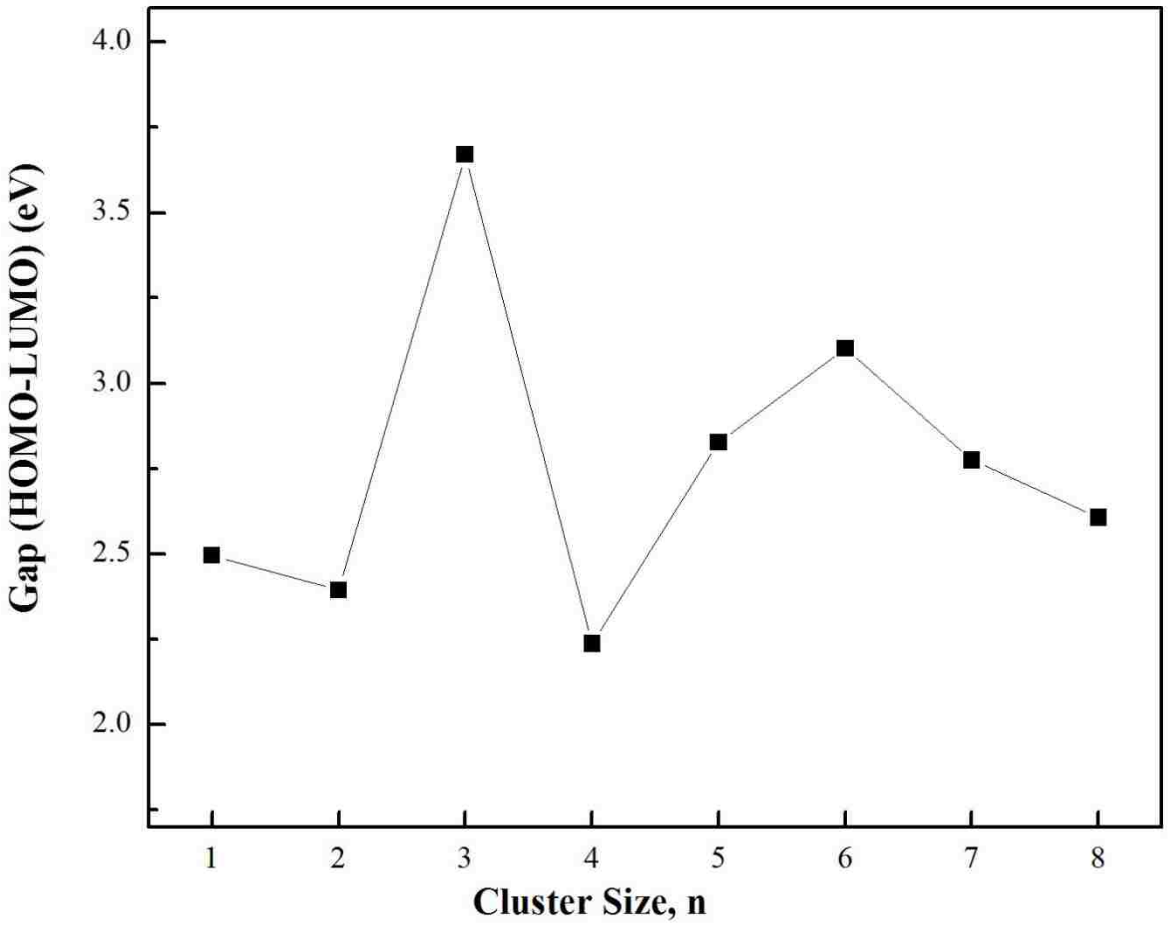

Figure 3.8: Calculated HOMO-LUMO gap of neutral $(CuO)_n$ clusters with n=1-8

3.2.4 Fragmentation Channels

We have also calculated the fragmentation energies of $(CuO)_n$ (n=1-8) clusters for various dissociation pathways. The fragmentation channels of $(CuO)_n$, n=1-8 clusters are shown in Table 3.4. The fragmentation energy of Cu_6O_6 cluster (dissociation to Cu_5O_5 + CuO) is the lowest value (56.59 kcal/mol), which we would like to emphasize as the most favorable pathway to break the cluster. The fragmentation products of all copper oxide

clusters contain a CuO cluster, except those of Cu_7O_7, which fragments into Cu_5O_5 $+Cu_2O_2$.

Table 3.4: Fragmentation channels of $(CuO)_n$ clusters with n=1-8

$E_{n+m} \rightarrow E_n + E_m$	kcal/mol
$(CuO)_2 \rightarrow CuO+CuO$	57.91
$(CuO)_3 \rightarrow Cu_2O_2+CuO$	75.90
$(CuO)_4 \rightarrow Cu_3O_3+CuO$	75.56
$\rightarrow Cu_2O_2+Cu_2O_2$	93.55
$(CuO)_5 \rightarrow Cu_4O_4+CuO$	81.07
$\rightarrow Cu_3O_3+Cu_2O_2$	98.72
$(CuO)_6 \rightarrow Cu_5O_5+CuO$	56.59
$\rightarrow Cu_4O_4+Cu_2O_2$	79.74
$\rightarrow Cu_3O_3+Cu_3O_3$	79.41
$(CuO)_7 \rightarrow Cu_6O_6+CuO$	77.40
$\rightarrow Cu_5O_5+Cu_2O_2$	76.07
$\rightarrow Cu_4O_4+Cu_3O_3$	81.25
$(CuO)_8 \rightarrow Cu_7O_7+CuO$	59.27
$\rightarrow Cu_6O_6+Cu_2O_2$	78.76
$\rightarrow Cu_5O_5+Cu_3O_3$	59.45
$\rightarrow Cu_4O_4+Cu_4O_4$	64.96

3.2.5 Löwdin Charge Distributions

The calculations of Löwdin charge distributions[99] of copper oxide clusters are shown in Table 3.5.

From Löwdin charges one gets useful information about the amount of charge transfer between Cu and O in an oxide. Average Löwdin charges of the Cu atoms are 0.24 |e| for CuO, 0.26 |e| for Cu_2O_2, 0.23 |e| for Cu_3O_3, 0.17 |e| for Cu_4O_4, 0.18 |e| for Cu_5O_5, 0.20 |e| for Cu_6O_6, 0.15 |e| for Cu_7O_7, and 0.15 |e| for Cu_8O_8 in neutral clusters. Average Löwdin charges of the O atoms are -0.24 |e| for CuO, -0.26 |e| for Cu_2O_2, -0.23 |e| for Cu_3O_3, -0.17 |e| for Cu_4O_4, -0.19 |e| for Cu_5O_5, -0.17 |e| for Cu_6O_6, -0.14 |e| for Cu_7O_7, and -0.15 |e| for Cu_8O_8 in neutral clusters.

Table 3.5: Löwdin charges of copper and oxygen atoms in $(CuO)_n$ (n=1-8)

Clusters		qCu (atom number)			qO (atom number)		
CuO	CuO	0.24(1)			-0.24(2)		
	CuO^+	0.95(1)			0.05(2)		
	CuO^-	-0.53(1)			-0.47(2)		
Cu_2O_2	Cu_2O_2	0.26(1)	0.25(2)		-0.26(3)	-0.26(4)	
	$Cu_2O_2^+$	0.60(1)	0.60(2)		-0.10(3)	-0.10(4)	
	$Cu_2O_2^-$	-0.10(1)	-0.10(2)		-0.40(3)	-0.40(4)	
Cu_3O_3	Cu_3O_3	0.19(1)	0.30(2)	0.19(3)	-0.23(4)	-0.23(5)	-0.22(6)
	$Cu_3O_3^+$	0.46(1)	0.46(2)	0.51(3)	-0.14(4)	-0.20(5)	-0.10(6)
	$Cu_3O_3^-$	0.04(1)	0.03(2)	-0.03(3)	-0.35(4)	-0.36(5)	-0.34(6)
Cu_4O_4	Cu_4O_4	0.23(1)	0.12(2)		-0.27(5)	-0.27(6)	
		0.08(3)	0.24(4)		-0.07(7)	-0.05(8)	
	$Cu_4O_4^+$	0.42(1)	0.29(2)		-0.18(5)	-0.20(6)	
		0.25(3)	0.40(4)		0.01(7)	0.004(8)	
	$Cu_4O_4^-$	0.06(1)	0.07(2)		-0.28(5)	-0.36(6)	
		0.09(3)	0.10(4)		-0.32(7)	-0.36(8)	
Cu_5O_5	Cu_5O_5	0.24(1)	0.23(2)	0.12(3)	-0.28(6)	-0.26(7)	-0.07(8)
		0.12(4)	0.20(5)		-0.07(9)	-0.26(10)	
	$Cu_5O_5^+$	0.39(1)	0.39(2)	0.25(3)	-0.16(6)	-0.25(7)	0.008(8)
		0.25(4)	0.37(5)		0.009(9)	-0.25(10)	
	$Cu_5O_5^-$	0.05(1)	0.05(2)	0.02(3)	-0.27(6)	-0.34(7)	-0.10(8)
		0.02(4)	0.02(5)		-0.10(9)	-0.34(10)	
Cu_6O_6	Cu_6O_6	0.14(1)	0.15(2)	0.15(3)	-0.12(7)	-0.13(8)	-0.25(9)
		0.14(4)	0.15(5)	0.27(6)	-0.13(10)	-0.12(11)	-0.25(12)
	$Cu_6O_6^+$	0.25(1)	0.23(2)	0.23(3)	-0.05(7)	-0.04(8)	-0.24(9)
		0.25(4)	0.40(5)	0.32(6)	-0.05(10)	-0.05(11)	-0.24(12)
	$Cu_6O_6^-$	0.03(1)	0.03(2)	0.03(3)	-0.17(7)	-0.17(8)	-0.33(9)
		0.03(4)	0.007(5)	0.20(6)	-0.17(10)	-0.17(11)	-0.32(12)
Cu_7O_7	Cu_7O_7	0.15(1)	0.15(2)	0.16(3)	-0.06(8)	-0.06(9)	-0.26(10)
		0.16(4)	-0.07(5)		-0.24(11)	-0.06(12)	
		0.24(6)	0.24(7)		-0.06(13)	-0.26(14)	
	$Cu_7O_7^-$	0.12(1)	0.12(2)	0.15(3)	-0.13(8)	-0.13(9)	-0.27(10)
		0.14(4)	-0.16(5)		-0.31(11)	-0.14(12)	
		0.006(6)	0.009(7)		-0.13(13)	-0.27(14)	
Cu_8O_8	Cu_8O_8	0.16(1)	0.16(2)	0.13(3)	-0.13(9)	-0.14(10)	-0.26(11)
		0.13(4)	0.27(5)	0.013(6)	-0.06(12)	-0.06(13)	-0.26(14)
		0.15(7)	0.15(8)		-0.13(15)	-0.13(16)	
	$Cu_8O_8^+$	0.24(1)	0.24(2)	0.24(3)	-0.05(9)	-0.07(10)	-0.25(11)
		0.23(4)	0.44(5)	-0.04(6)	-0.03(12)	-0.03(13)	-0.25(14)
		0.22(7)	0.22(8)		-0.07(15)	-0.05(16)	
	$Cu_8O_8^-$	0.09(1)	0.04(2)	0.05(3)	-0.16(9)	-0.22(10)	-0.26(11)
		0.002(4)	0.06(5)	0.01(6)	-0.12(12)	-0.12(13)	-0.26(14)
		0.14(7)	0.13(8)		-0.16(15)	-0.16(16)	

3.3 Conclusions

The electronic and structural properties of small copper oxide clusters have been studied using density functional theory and several basis sets. Comparison with existing experimental work demonstrated that the LANL2DZ basis set is in best agreement and therefore was used to study Cu_nO_n with n=1-8 clusters. A transition from planar to nonplanar geometries occurs at n=4, though the negatively charged Cu_4O_4 cluster is planar. Atomization energies and second difference energies demonstrate that Cu_5O_5 cluster has the highest stability. We find that odd numbered copper oxide clusters have higher stabilities than even numbered copper oxide clusters, which can be explained in two ways. First, the Cu-O-Cu angles are relatively close to tetrahedral values and correlate reasonably well with second difference energy.

Second, we have investigated that the stability of copper oxide clusters is discussed in term of the ring size effect. The even numbered clusters have small rings (3- and 4-membered). These small rings lead to ring strain and a loss of stability. On the contrary, the odd numbered clusters have large rings (6- and 7-membered). Therefore, we expect that odd numbered copper oxide clusters (Cu_9O_9, $Cu_{11}O_{11}$…) will be most stable.

Ionization potentials have some oscillations with cluster size, as these are typical for clusters. The lowest fragmentation energy of Cu_6O_6 cluster (dissociation to Cu_5O_5 + CuO) is, we would like to emphasize, the most favorable pathway to break the cluster. We also expect that bigger copper oxide clusters than Cu_8O_8 cluster would dissociate to contain a CuO cluster as small copper oxide clusters. (From CuO to Cu_8O_8 clusters)

CHAPTER 4

COMPUTATIONAL STUDIES OF REACTIONS OF PHENOL AND CHLORINATED PHENOLS WITH COPPER OXIDE CLUSTERS

We already performed *ab initio* Monte Carlo simulated annealing simulations and density functional theory calculations to study the structures and stabilities of copper oxide clusters, Cu_nO_n (n=1-8). We determined the lowest energy structures of neutral, positively and negatively charged copper oxide clusters using the GAMESS[117] quantum chemistry package. We used the B3LYP (Becke's 3-parameter exchange functional with Lee-Yang-Parr correlation energy functional)[107,113,114] version of DFT with LANL2DZ basis set. The geometries were found to undergo a structural change from two dimensional to three dimensional when n = 4 in neutral copper oxide clusters. In this chapter, we have analyzed the interactions between neutral copper oxide clusters and organic compounds (phenol, *ortho*-chlorophenol and *para*-chlorophenol) for geometric parameters, thermodynamic properties, reaction pathway, adsorption energies and Löwdin charge distributions.

4.1 Method

4.1.1 DFT Calculations

It is known that phenols adsorb on the copper oxide surfaces through H_2O elimination at surface oxide and hydroxyl sites resulting in surface phenolate formation.[135-139]

Therefore, our calculations include two types of reactions. First, each copper oxide cluster is reacted with a water molecule. Second, the hydrogenated clusters are reacted with the organic compounds phenol, *ortho*-chlorophenol and *para*-chlorphenol.

The reaction enthalpies were calculated according to the following procedure: (1) the total electronic energies for the reactants and the products were calculated, (2) these were corrected for zero-point energies to obtain a theoretical enthalpy at 0K, and (3) thermal corrections were applied to get the reaction enthalpy at 298.15K. The enthalpies, H, is the calculated sum of H_{elec}, H_{trans}, H_{rot}, and H_{vib} and the Gibbs free energies are the calculated sum of G_{elec}, Gt_{rans}, G_{rot}, and G_{vib}. In water molecule reactions, we need to consider possible reaction sites to find the lowest energy structures. From CuO to Cu_3O_3 clusters, we have found just one possible reaction site. However, from Cu_4O_4 to Cu_7O_7 clusters, we need to consider three or four possible reaction sites. Actually, we have checked all energies and structures after reaction with water molecule following possible reaction sites. Fig 4.1-7 show the lowest structures [(2), (7), (12), (17), (22), (27), (32) clusters] of each cluster with water molecule reaction.

In phenol and *para*-chlorophenol reactions, we have started two possible initial geometries to change dihedral angle (Cu-O*-C-C, the asterisk denotes the atom of the adsorption site on the copper oxide clusters) 0 and 90 degrees. In *ortho*-chlorophenol reaction, we have started four possible initial geometries to change dihedral angle (Cu-O*-C-C) 0, 90, 180 and 270 degrees. Therefore we can find the global energy structure of each molecule with organic compound reactions. Then we confirm the lowest energy using PES with single point energy calculation. Figure 4.1 shows this PES calculation with Cu_7O_7-Phenol cluster reaction. Thus we confirm that the dihedral angle of the lowest energy structure of Cu_7O_7-phenol cluster is 0 degree or 180 degrees.

Figure 4.2-8 show the lowest structures [(3), (4), (5), (8), (9), (10), (13), (14), (15),

(18), (19), (20), (23), (24), (25), (28), (29), (30), (33), (34), (35) clusters] of each cluster with organic compound reactions.

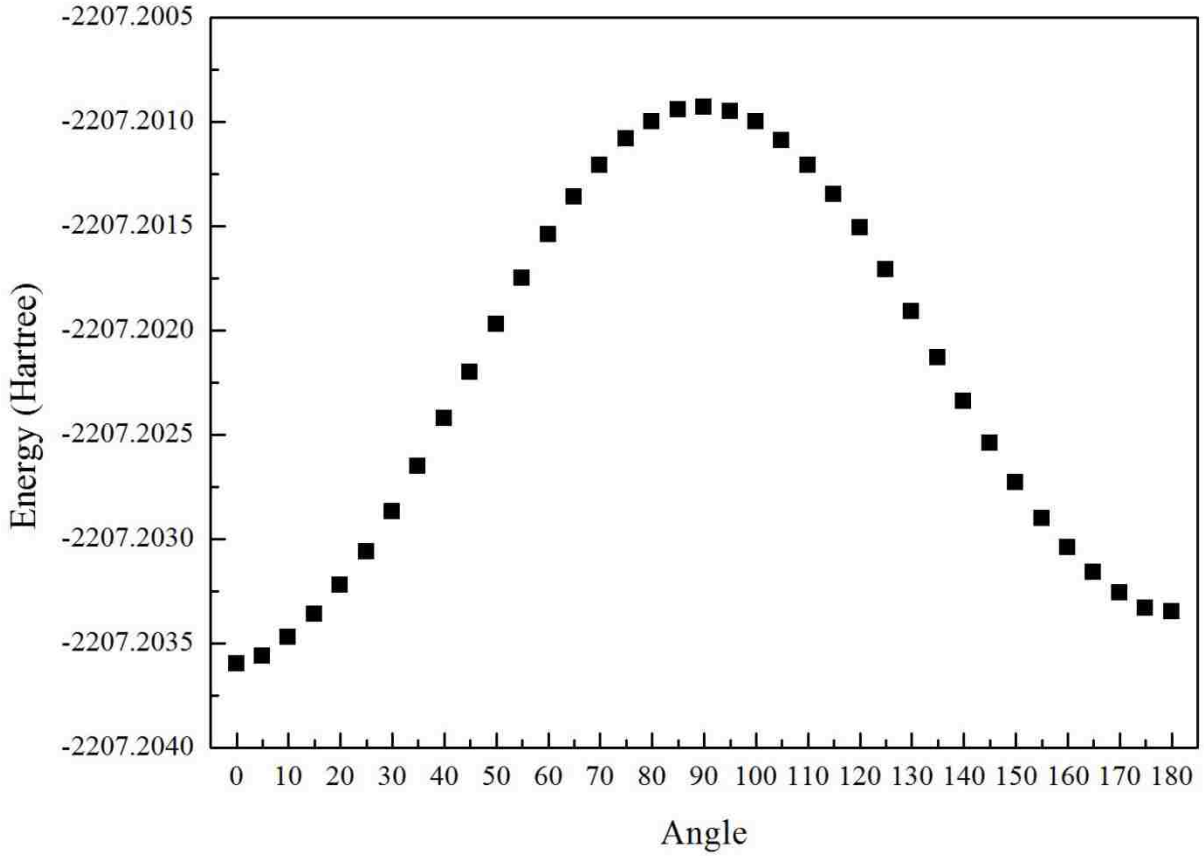

Figure 4.1: PES calculation with Cu_7O_7-phenol reaction

4.2 Results

4.2.1 Geometric Structures

We already studied neutral, positively and negatively charged copper oxide clusters. Figure 3.2 shows the lowest energy structures of neutral copper oxide clusters from CuO to Cu_8O_8.

Table 4.1: Average bond lengths of water, organic compounds and copper oxide-organic compounds clusters

Clusters		Avg. Bond lengths						
		Cu-O	O-H	O-O	C-C	C-O	C-H	C-Cl
H_2O			0.98					
Phenol			0.98		1.41	1.40	1.09	
ortho-chlorophenol			0.98		1.41	1.39	1.09	1.81
para-chlorophenol			0.98		1.41	1.40	1.09	1.82
	(1)	1.81						
	(2)	1.77	0.98					
CuO	(3)	1.79	0.98		1.41	1.35	1.09	
	(4)	1.79	0.97		1.41	1.34	1.09	1.80
	(5)	1.79	0.97		1.41	1.35	1.09	1.81
	(6)	1.86						
	(7)	1.77	0.98					
Cu_2O_2	(8)	1.78	0.99		1.41	1.35	1.09	
	(9)	1.78	0.99		1.41	1.34	1.09	1.80
	(10)	1.79	0.97		1.41	1.34	1.08	1.81
	(11)	1.90						
	(12)	1.75	0.98					
Cu_3O_3	(13)	1.77	0.98		1.42	1.34	1.09	
	(14)	1.77	0.98		1.41	1.33	1.09	1.80
	(15)	1.77	0.98		1.41	1.34	1.08	1.81
	(16)	1.94		1.40				
	(17)	1.86	0.98	1.40				
Cu_4O_4	(18)	1.86	0.97	1.40	1.41	1.35	1.09	
	(19)	1.86	0.97	1.40	1.41	1.34	1.09	1.81
	(20)	1.86	0.97	1.40	1.41	1.35	1.09	1.81
	(21)	1.88		1.40				
	(22)	1.89	0.98	1.40				
Cu_5O_5	(23)	1.93	0.97	1.40	1.41	1.35	1.09	
	(24)	1.92	0.97	1.40	1.41	1.35	1.08	1.83
	(25)	1.92	0.97	1.40	1.41	1.35	1.08	1.81
	(26)	1.96		1.52				
	(27)	1.94	0.98	1.56				
Cu_6O_6	(28)	1.95	0.98	1.57	1.41	1.39	1.09	
	(29)	1.96	0.98	1.57	1.41	1.37	1.09	1.84
	(30)	1.95	0.98	1.57	1.41	1.39	1.09	1.82
	(31)	1.93		1.40				
	(32)	1.94	1.13	1.40				
Cu_7O_7	(33)	1.95	1.21	1.40	1.40	1.40	1.08	
	(34)	1.95	1.07	1.40	1.40	1.38	1.08	1.82
	(35)	1.94	1.22	1.40	1.40	1.39	1.08	1.81
	(36)	1.97		1.50				
	(37)	1.95	1.13	1.50				
Cu_8O_8	(38)	1.95	1.07	1.50	1.41	1.39	1.09	
	(39)	1.95	1.05	1.50	1.41	1.37	1.09	1.83
	(40)	1.95	1.06	1.50	1.41	1.39	1.09	1.82

The geometries of copper oxide clusters are found to undergo a structure change from two dimensional to three dimensional when n=4 in neutral copper oxide clusters. After the water reaction, the geometries of copper oxide clusters for CuO, Cu_2O_2 and Cu_3O_3 clusters are changed to linear or near linear clusters and three dimensional structure Cu_4O_4 cluster is changed to near planar structure. From Cu_5O_5 to Cu_8O_8 clusters still have three dimensional structures after the water reaction.

The calculation results of average bond lengths (O-H, O-O, C-C, C-O, C-H and C-Cl) are for copper oxide clusters, copper oxide-water clusters and copper oxide-organic compounds clusters shown Table 4.1. Average Cu-O bond lengths of copper oxide clusters, CuO, Cu_2O_2, Cu_3O_3, Cu_4O_4 and Cu_6O_6, are decreased after the water reaction. Average Cu-O bond lengths of Cu_5O_5 and Cu_6O_6 clusters are slightly increased from 1.88 to 1.89 and 1.93 to 1.94, respectively. It is interesting that Cu_3O_3 cluster has the biggest gap of average Cu-O bond length, from 1.90 to 1.75 after the water reaction. After organic compounds reactions, average Cu-O bond lengths of all copper oxide cluster-organic compounds clusters are slightly longer than those of copper oxide-water clusters.

Table 4.2 shows the energy, H, and G. With careful analysis of the table, the obvious correlation of energy and the position of chlorine substitute in copper oxide cluster reveal that *para* position copper oxide chlorophenols are more stable from CuO to Cu_4O_4 and Cu_7O_7 clusters than *ortho* position copper oxide chlorophenols.

The correlation of H^0 can be the same with energy. *Para* position copper oxide chlorophenol clusters have smaller values (from CuO to Cu_4O_4 and Cu_7O_7 clusters).

Gibbs energies are a little bit different than energies and enthalpies. The Gibbs energy value of *ortho* position Cu_3O_3 chlorophenol cluster is smaller than that of *para* postion.

Table 4.2: The spin states, energies, enthalpies and Gibbs free energies of copper oxide-organic compounds complexes

Clusters		Spin State	Energy(eV)	H^0 (eV)	G^0 (eV)
	(1)	doublet	-7382.21	-7382.11	-7382.83
	(2)	doublet	-9463.41	-9463.25	-9464.16
CuO	(3)	doublet	-15747.71	-15747.45	-15748.69
	(4)	doublet	-16138.01	-16137.72	-16139.01
	(5)	doublet	-16138.09	-16137.81	-16139.08
	(6)	singlet	-14766.92	-14766.76	-14767.73
	(7)	triplet	-16848.28	-16848.04	-16849.20
Cu_2O_2	(8)	triplet	-23132.54	-23132.20	-23133.67
	(9)	triplet	-23522.84	-23522.45	-23524.02
	(10)	triplet	-23522.94	-23522.55	-23524.13
	(11)	quartet	-22152.42	-22152.16	-22153.43
	(12)	quartet	-24233.03	-24232.71	-24234.15
Cu_3O_3	(13)	quartet	-30517.33	-30516.89	-30518.66
	(14)	quartet	-30907.63	-30907.15	-30909.08
	(15)	quartet	-30907.72	-30907.27	-30909.05
	(16)	triplet	-29537.90	-29537.58	-29538.99
	(17)	triplet	-31618.96	-31618.57	-31620.14
Cu_4O_4	(18)	triplet	-37903.41	-37902.91	-37904.76
	(19)	triplet	-38293.70	-38293.17	-38295.12
	(20)	triplet	-38293.80	-38293.27	-38295.22
	(21)	quartet	-36923.62	-36923.22	-36924.84
	(22)	quartet	-39003.95	-39003.49	-39005.21
Cu_5O_5	(23)	quartet	-45288.03	-45287.46	-45289.46
	(24)	quartet	-45678.52	-45677.90	-45680.00
	(25)	quartet	-45678.44	-45677.82	-45679.93
	(26)	triplet	-44308.28	-44307.84	-44309.48
	(27)	triplet	-46388.64	-46388.14	-46389.90
Cu_6O_6	(28)	triplet	-52672.57	-52671.94	-52674.04
	(29)	triplet	-53063.14	-53062.48	-53064.60
	(30)	triplet	-53062.95	-53062.28	-53064.44
	(31)	quartet	-51693.84	-51693.29	-51695.22
	(32)	quartet	-53773.83	-53773.23	-53775.28
Cu_7O_7	(33)	quartet	-60057.68	-60056.95	-60059.33
	(34)	quartet	-60447.96	-60447.19	-60449.65
	(35)	quartet	-60448.09	-60447.32	-60449.7
	(36)	triplet	-59078.62	-59078.02	-59079.99
	(37)	triplet	-61159.04	-61158.39	-61160.49
Cu_8O_8	(38)	triplet	-67442.83	-67442.05	-67444.48
	(39)	triplet	-67833.30	-67832.47	-67835.01
	(40)	triplet	-67833.22	-67832.39	-67834.93

4.2.2 Energetic Properties and Löwdin Charge Distributions

The changes of energies, enthalpies, and Gibbs energies of reactions between copper oxide clusters and water are shown in Figure 4.2-4.9. The changes of energies, enthalpies, and Gibbs energies of reactions between copper oxide-water clusters and phenol and chlorinated phenols are also shown in Figure 4.2-4.9. Copper oxide clusters (CuO, Cu_2O_2, Cu_3O_3, Cu_4O_4, and Cu_7O_7) with *para*-chlorophenol are more stable than those with *ortho*-chlorophenol.

We have investigated the adsorption energies (AEs) to display the characteristics of the energetic interactions among copper oxide clusters and organic compounds (phenol, *ortho*-chlorophenol and *para*-chlorophenol). The calculation formula is as follows:

$$E_b = E(Cu_nO_n - Organic\ Compounds) - (E(Cu_nO_n) + E(Organic\ Compounds)) \quad (1)$$

Table 4.3 shows that adsorption energies of copper oxide clusters (from CuO to Cu_4O_4 and Cu_7O_7) with *ortho*-chlorophenol are higher than phenol and *para*-chlorophenol. Adsorption energies of Cu_5O_5 and Cu_8O_8 clusters are almost same comparing phenol and chlorinated phenols. Cu_6O_6 cluster with *para*-chlorophenol has higher adsorption energy than phenol and *ortho*-chlorophenol. It is well known *ortho*-chlorophenol is more stable than *para*-chlorophenol because hydrogen bonding stabilization plays an important role. As well as inductive, electrostatic repulsion, and steric effect can explain why *ortho*-chlorophenol is more stable.

Therefore, we can explain why adsorption energies of copper oxide clusters with *ortho* -chlorophenol are higher than phenol and *para*-chlorophenol because H atom of OH group of *ortho*-chlorophenol is displaced to copper oxide cluster. Cu_5O_5 cluster can be explained that there is hydrogen bonding between Cl atom of *ortho*-chlorophenol and hydrogen. It is

interesting that Cu_6O_6 and Cu_8O_8 clusters have weak Cu-Cl bond (2.72Å and 2.93Å). These bonds can make stabilization of copper oxide clusters with *ortho*-chlorophenol.

From these results, we can conclude that the Cu_7O_7 cluster has energetically preferred adsorption with *ortho*-chlorophenol. Cu_7O_7 cluster-phenol has the highest adsorption energy (-23.06eV).

Table 4.3: Adsorption energies (kcal/mol) in copper oxide-organic compounds clusters

Clusters	Adsorption Energies(kcal/mol)
CuO – Phenol	-64.94
CuO - *ortho*-chlorophenol	-61.79
CuO - *para*-chlorophenol	-64.75
Cu_2O_2 – Phenol	-67.54
Cu_2O_2 - *ortho*-chlorophenol	-64.42
Cu_2O_2 - *para*-chlorophenol	-67.72
Cu_3O_3 – Phenol	-51.14
Cu_3O_3 - *ortho*-chlorophenol	-48.26
Cu_3O_3 - *para*-chlorophenol	-51.37
Cu_4O_4 – Phenol	-64.85
Cu_4O_4 - *ortho*-chlorophenol	-61.81
Cu_4O_4 - *para*-chlorophenol	-65.16
Cu_5O_5 – Phenol	-39.58
Cu_5O_5 - *ortho*-chlorophenol	-40.89
Cu_5O_5 - *para*-chlorophenol	-40.07
Cu_6O_6 – Phenol	-36.93
Cu_6O_6 - *ortho*-chlorophenol	-40.02
Cu_6O_6 - *para*-chlorophenol	-36.63
Cu_7O_7 – Phenol	-26.52
Cu_7O_7 - *ortho*-chlorophenol	-23.06
Cu_7O_7 - *para*-chlorophenol	-27.03
Cu_8O_8 – Phenol	-35.17
Cu_8O_8 - *ortho*-chlorophenol	-35.92
Cu_8O_8 - *para*-chlorophenol	-35.10

The results of this study have some implications of formation of PCDD/Fs from chlorinated phenols. First, small copper oxide clusters (from CuO-Cu_4O_4) show clearly a significant role for an adsorption between *ortho*-chlorophenol and copper oxide clusters from adsorption energies. Second, big copper oxide clusters (from Cu_5O_5 and Cu_8O_8) are more

complicate to explain the correlations between copper oxide clusters and chlorides. However, it is clearly found that phenol and chlorinated phenols can easily make adsorption as increasing clusters size.

We have displayed the Löwdin charge, q(given in units of |e|) distributions[99] of copper oxide clusters, copper oxide-water clusters and copper oxide-organic compound clusters. Table 4.4 shows the charges of average copper, oxygen, hydrogen, carbon, chlorine, adsorption site oxygen and carbon. We also calculated the charges of neutral copper oxide clusters. (Table 3.5).

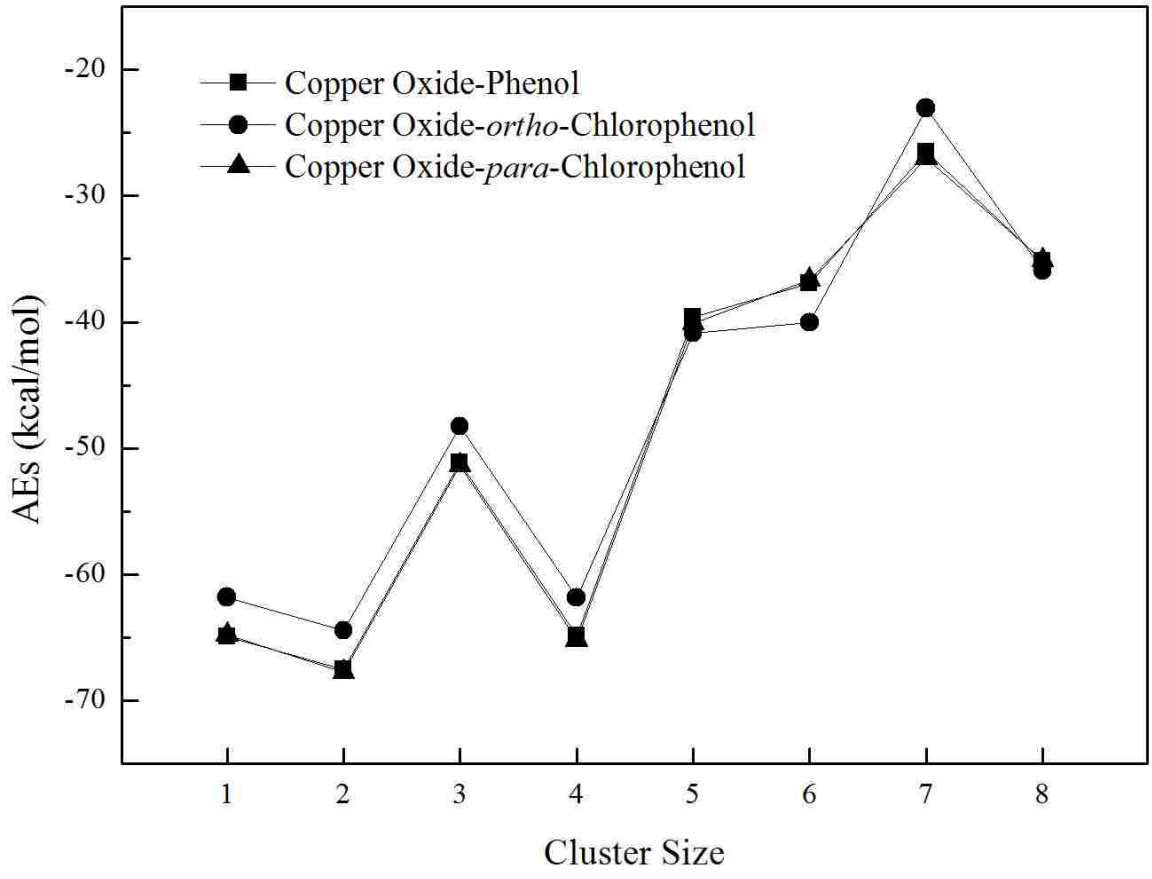

Figure 4.2: Adsorption energies (kcal/mol) in copper oxide-organic compounds clusters

Table 4.4: Average Lowdin charge distributions of copper oxide clusters, copper oxide-water clusters and copper oxide-organic compounds clusters

Clusters		Avg. Charge Distribution						
		qCu	qO	qH	qC	qCl	qO*	qC*
H_2O			-0.58	0.29				
Phenol			-0.36	0.17	-0.11			
ortho-Chlorophenol			-0.34	0.18	-0.12	0.12		
para-Chlorophenol			-0.35	0.19	-0.11	0.088		
	(1)	0.24	-0.24					
	(2)	0.23	-0.43	0.31				
CuO	(3)	0.13	-0.34	0.18	-0.086		-0.235	0.122
	(4)	0.16	-0.34	0.19	-0.093	0.16	-0.244	0.133
	(5)	0.16	-0.35	0.19	-0.090	0.12	-0.249	0.123
	(6)	0.26	-0.26					
	(7)	0.25	-0.37	0.31				
Cu_2O_2	(8)	0.19	-0.32	0.18	-0.084		-0.231	0.125
	(9)	0.20	-0.31	0.19	-0.092	0.16	-0.232	0.113
	(10)	0.20	-0.32	0.19	-0.089	0.12	-0.237	0.125
	(11)	0.23	-0.23					
	(12)	0.25	-0.34	0.31				
Cu_3O_3	(13)	0.21	-0.31	0.18	-0.083		-0.241	0.129
	(14)	0.22	-0.30	0.19	-0.091	0.16	-0.243	0.118
	(15)	0.22	-0.30	0.19	-0.088	0.12	-0.247	0.129
	(16)	0.17	-0.17					
	(17)	0.10	-0.25	0.32				
Cu_4O_4	(18)	0.12	-0.21	0.19	-0.085		-0.235	0.122
	(19)	0.13	-0.21	0.19	-0.093	0.15	-0.239	0.114
	(20)	0.12	-0.21	0.20	-0.090	0.12	-0.240	0.123
	(21)	0.18	-0.19					
	(22)	0.18	-0.26	0.32				
Cu_5O_5	(23)	0.16	-0.23	0.18	-0.091		-0.260	0.118
	(24)	0.17	-0.23	0.19	-0.099	0.22	-0.283	0.104
	(25)	0.18	-0.23	0.19	-0.096	0.10	-0.272	0.123
	(26)	0.17	-0.17					
	(27)	0.17	-0.24	0.32				
Cu_6O_6	(28)	0.16	-0.21	0.18	-0.089		-0.268	0.138
	(29)	0.14	-0.21	0.19	-0.090	0.26	-0.282	0.130
	(30)	0.16	-0.21	0.20	-0.092	0.10	-0.274	0.140
	(31)	0.15	-0.14					
	(32)	0.11	-0.19	0.37				
Cu_7O_7	(33)	0.12	-0.18	0.20	-0.095		-0.348	0.128
	(34)	0.12	-0.17	0.20	-0.10	0.15	-0.358	0.115
	(35)	0.12	-0.20	0.21	-0.099	0.097	-0.354	0.128
	(36)	0.15	-0.15					
	(37)	0.13	-0.20	0.37				
Cu_8O_8	(38)	0.13	-0.18	0.19	-0.10		-0.366	0.094
	(39)	0.12	-0.18	0.20	-0.10	0.22	-0.369	0.114
	(40)	0.13	-0.18	0.21	-0.10	0.087	-0.367	0.099

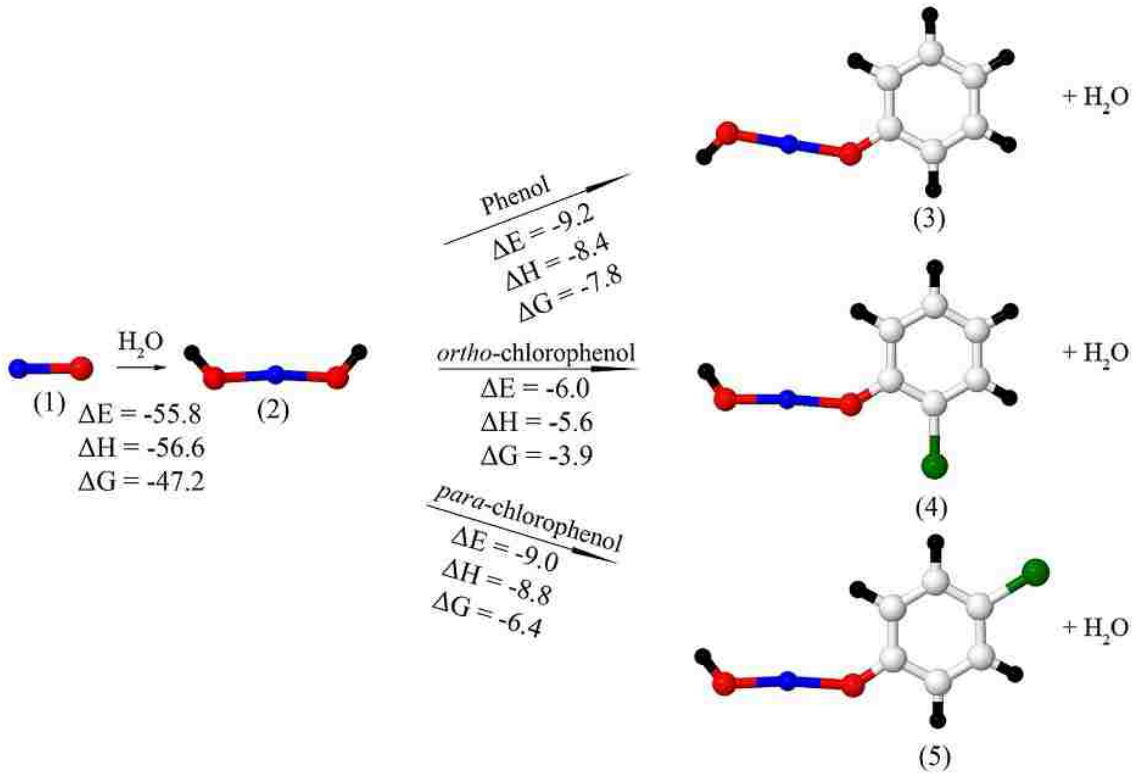

Figure 4.3: Reaction pathway of CuO cluster. Copper/oxygen/carbon/hydrogen/chlorine atoms are colored blue/red/white/black/green.

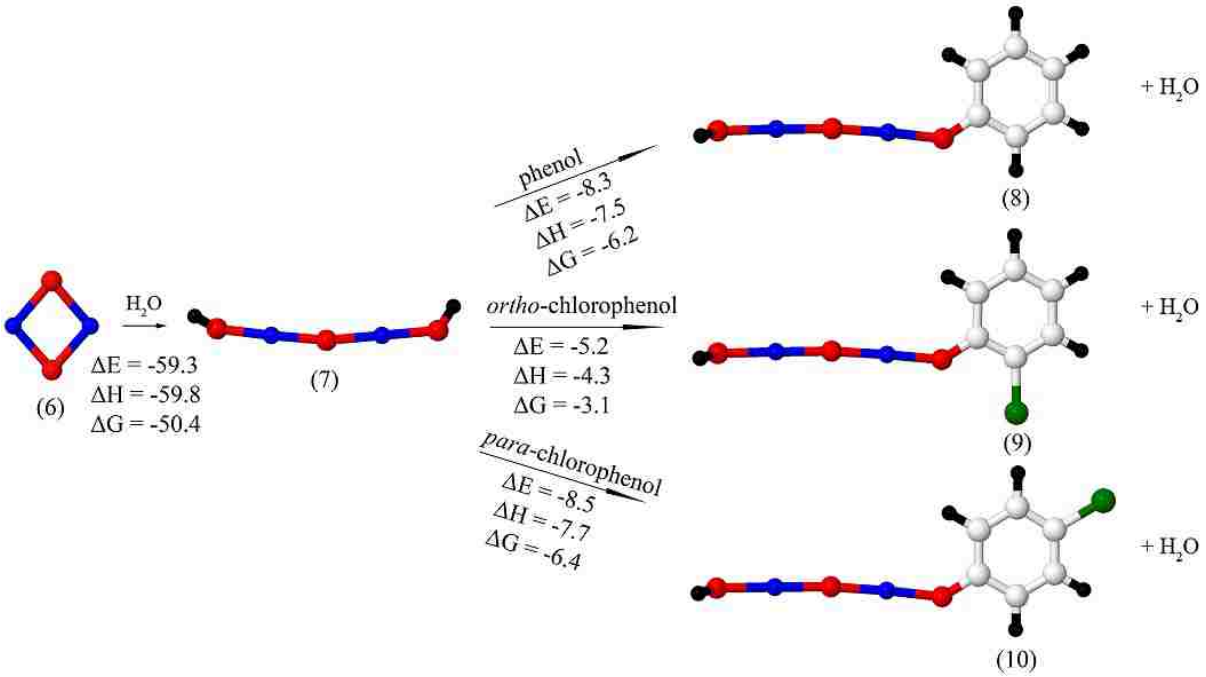

Figure 4.4: Reaction pathway of Cu_2O_2 cluster. Copper/oxygen/carbon/hydrogen/chlorine atoms are colored blue/red/white/black/green.

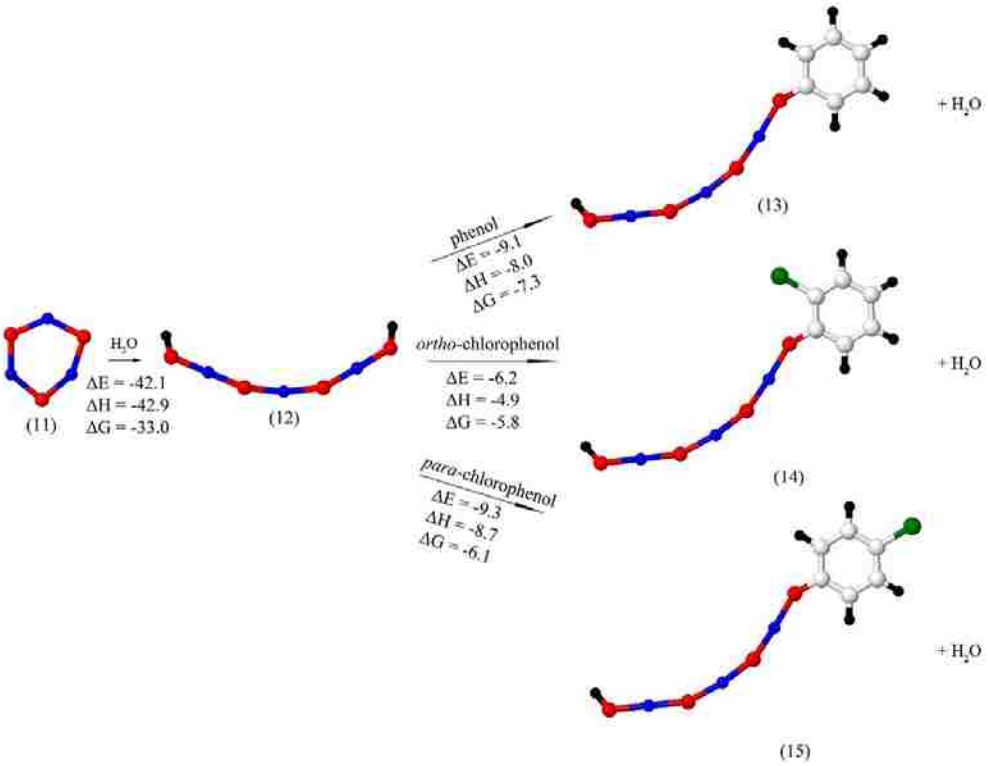

Figure 4.5 Reaction pathway of Cu_3O_3 cluster. Copper/oxygen/carbon/hydrogen/chlorine atoms are colored blue/red/white/black/green.

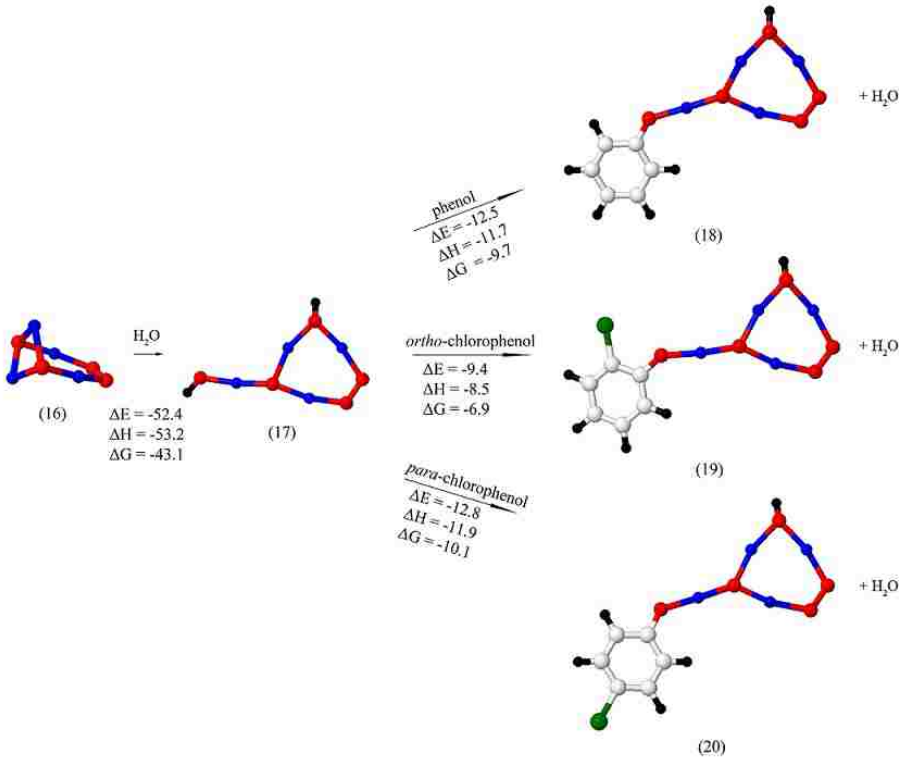

Figure 4.6: Reaction pathway of Cu_4O_4 cluster. Copper/oxygen/carbon/hydrogen/chlorine atoms are colored blue/red/white/black/green.

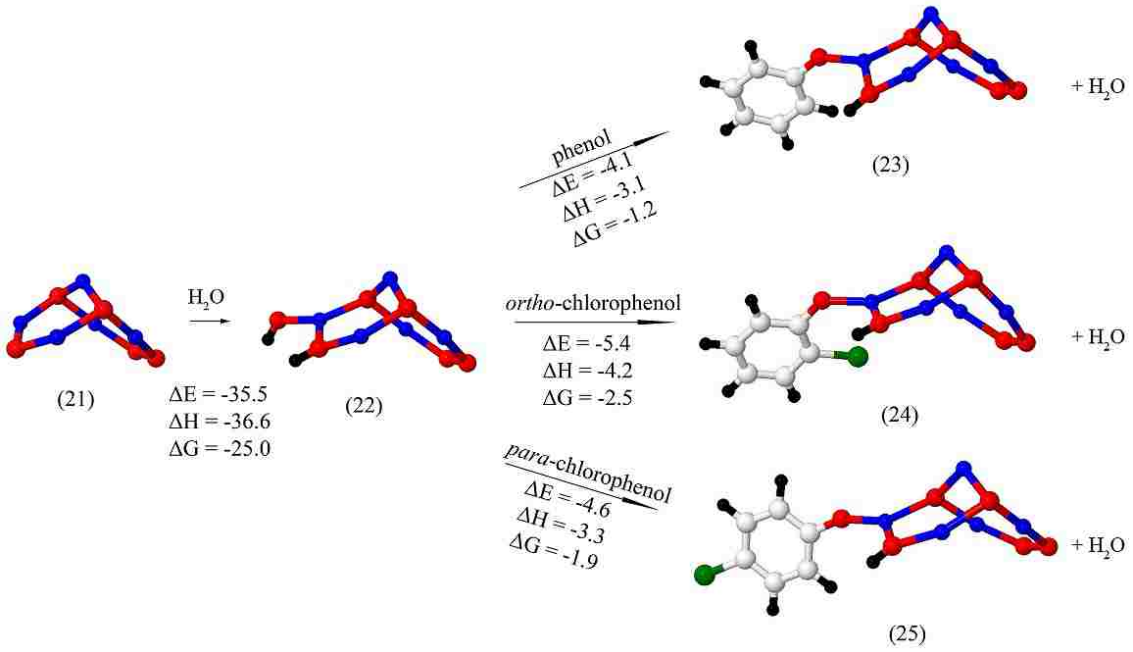

Figure 4.7: Reaction pathway of Cu_5O_5 cluster. Copper/oxygen/carbon/hydrogen/chlorine atoms are colored blue/red/white/black/green.

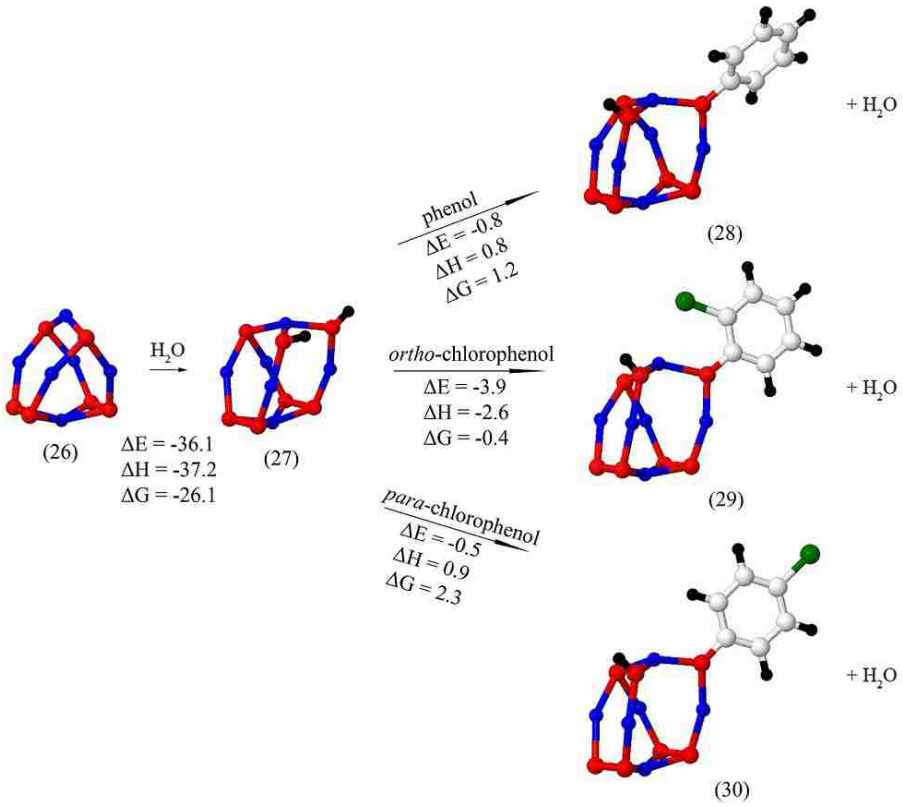

Figure 4.8: Reaction pathway of Cu_6O_6 cluster. Copper/oxygen/carbon/hydrogen/chlorine atoms are colored blue/red/white/black/green.

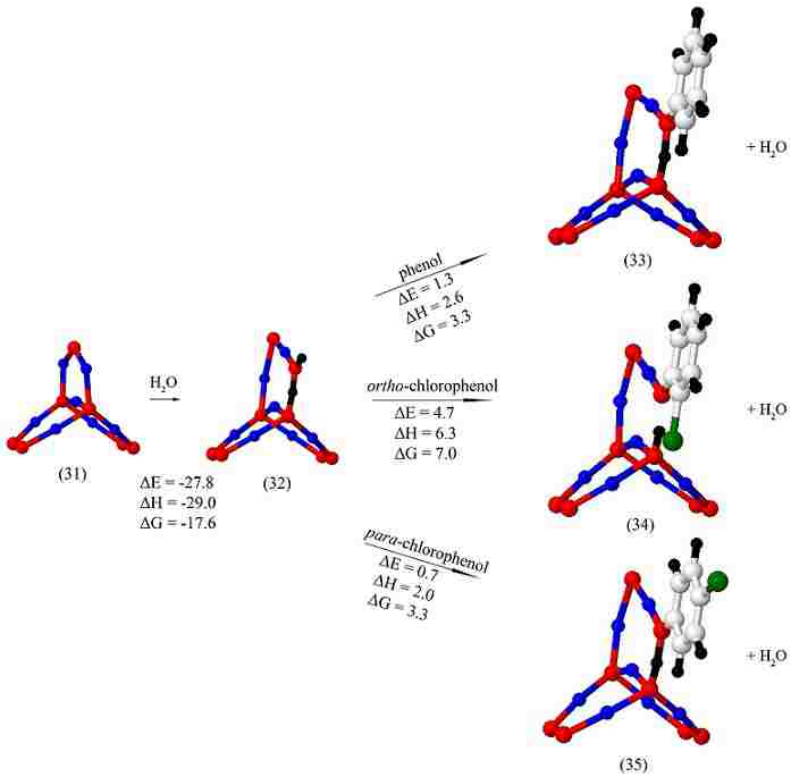

Figure 4.9: Reaction pathway of Cu_7O_7 cluster. Copper/oxygen/carbon/hydrogen/chlorine atoms are colored blue/red/white/black/green.

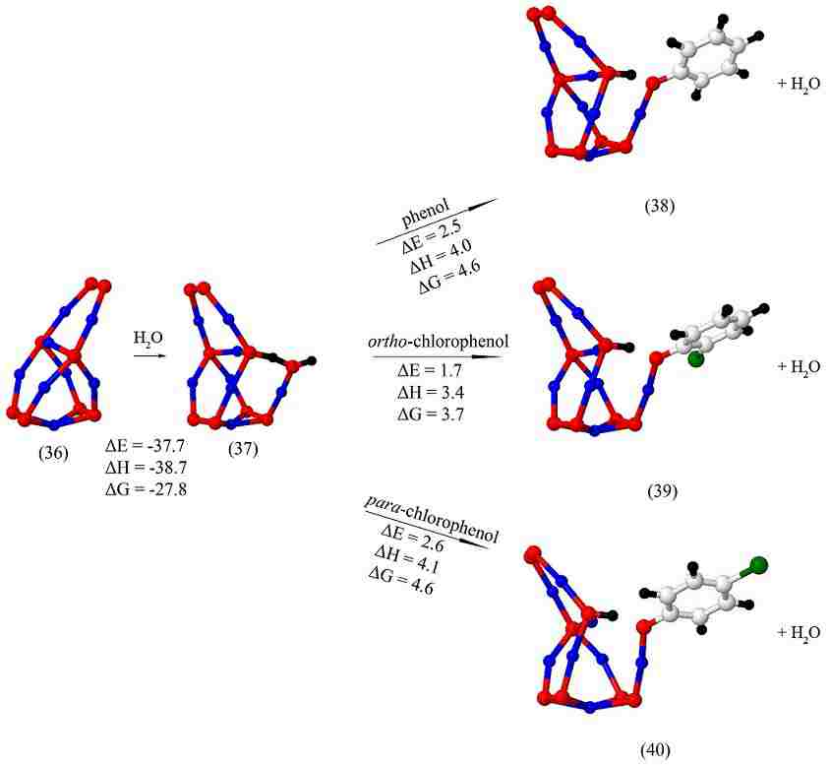

Figure 4.10: Reaction pathway of Cu_8O_8 cluster. Copper/oxygen/carbon/hydrogen/chlorine atoms are colored blue/red/white/black/green.

From these charge transfers of adsorption site oxygen, we investigated the correlation between the reaction site and the charge distribution. We found that organic compounds are likely to bind to the copper atom with the largest charge. For example, largest positive charge copper atom (0.30) of three copper atoms in Cu_3O_3 cluster was reacted the water molecule and would be structure (12).

Therefore, the charge transfer of the oxygen atom from the water molecule is explanation that the copper atoms (Cu_4O_4, Cu_5O_5, and Cu_7O_7 clusters) of reaction sites with the water molecule have large positive charges (0.24, 0.24, and 0.24).

The reaction sites of Cu_6O_6 and Cu_8O_8 clusters are not the copper atoms with the largest positive charge because they have a very stable square structure at the bottom of clusters. From these charge transfer of adsorption site oxygen, we investigated the correlation between the charge distribution and the adsorption energies. For instance, the Löwdin charge distributions of the adsorption site oxygens of copper oxide with phenol are -0.235, -0.231, -0.241, -0.235, -0.260, -0.268, -0.348 and -0.366 |e| and the adsorption energies of copper oxide with phenol are -64.94, -67.54, -51.14, -64.85, -39.58, -36.93, -26.52 and -35.17 kcal/mol that the charge distributions of adsorption site oxygen decrease which means there is negative charge transfer away from that site as adsorption energies decrease.

4.3 Conclusions

We have investigated the stabilities and reactivities of copper oxide clusters. Reactions of the previously optimized neutral Cu_nO_n clusters with water and organic compounds (phenol, *ortho*-chlorophenol and *para*-chlorophenol) were studied using *ab initio* methods.

The energies, enthalpies, Gibbs free energies of copper oxide, copper oxide-water

and copper oxide-organic compounds clusters were calculated to investigate their reaction energetics. We also calculated bond lengths, adsorption energies and Löwdin charge distributions.

It is known that chlorinated phenols are structurally closely related to PCDD/Fs and thought as important for PCDD/Fs formation. We find that organic compounds (phenol and chlorinated phenols) are likely to bind to the copper atom with the largest charge. For Cu_4O_4 to Cu_8O_8 clusters, we can predict the reaction site from charge distributions of copper oxide clusters.

Our calculations of reaction energies indicate that generally *ortho*-chlorophenol binds less stronglyto the surface of copper oxide clusters than phenol and *para*-chlorophenol, which can be explained in two ways. First, H atom of OH group of *ortho*-chlorophenol is displaced to copper oxide cluster. Second, weak Cu-Cl bonds can make stabilization of copper oxide clusters with *ortho*-chlorophenol. The results can help an understanding the mechanisms of the formation of PCDD/Fs from chlorinated phenols in the copper oxide clusters.

CHAPTER 5

CuO_n (n=1-6) CLUSTERS

Chemical reactions and bonding of metal oxide clusters have been researched over the past thirty years due to their importance in the studies of combustion and health hazards. Especially, copper atoms and oxygen atoms are studied because of bioinorganic chemistry for dioxygen metabolism.[140]

Small clusters consisting of one copper atom and one oxygen atom atoms have been studied experimentally[55-80] and theoretically.[68-75,79,86-94] Recently, a theoretical study of CuO_m (m=1-6) clusters was conducted using DFT calculation.[94] The purpose of our research is to understand the structural, energetic and electronic properties of neutral, positively and negatively charged copper oxide clusters. In neutral copper oxide clusters, we found similar geometries with Massobrio et al.[94] and the differences of total spin states of the most stable isomers. For instance, they concluded that the spin of the most stable isomers is quartet state when the number of oxygen atoms is odd, while it is doublet state when this number is even. They used DFT calculation with a plane-wave basis set and generalized gradient corrections. However, we found that CuO, CuO_2, CuO_4 and CuO_6 clusters are most stable at doublet, quartet, quartet and quartet spin states, respectively.

In this chapter, we used *ab initio* simulations and calculations to study the structures and stabilities of copper oxide clusters, CuO_n (n=1-6). The lowest energy structures of neutral and charged copper oxide clusters were determined using primarily the B3LYP/LANL2DZ model chemistry. All geometries of neutral, positively, and negatively charged CuO_n clusters with n=1-6 are planar or near planar structures. Selected electronic

properties, including binding energies, ionization energies, and electron affinities, were calculated and examined as a function of n. Stabilities were examined by calculating fragmentation channels and Löwdin charge distributions.

5.1 Method

5.1.1 MC Simulation and DFT Calculation

We performed *ab initio* Monte Carlo simulation (using Gaussian 03[112] and homegrownscripts) to locate stable geometric structures for CuO_n clusters with n=1-6. The simulations used multiple starting geometries for each cluster size. The temperature was decreased from 2000K to 300K for up to 300MC steps.

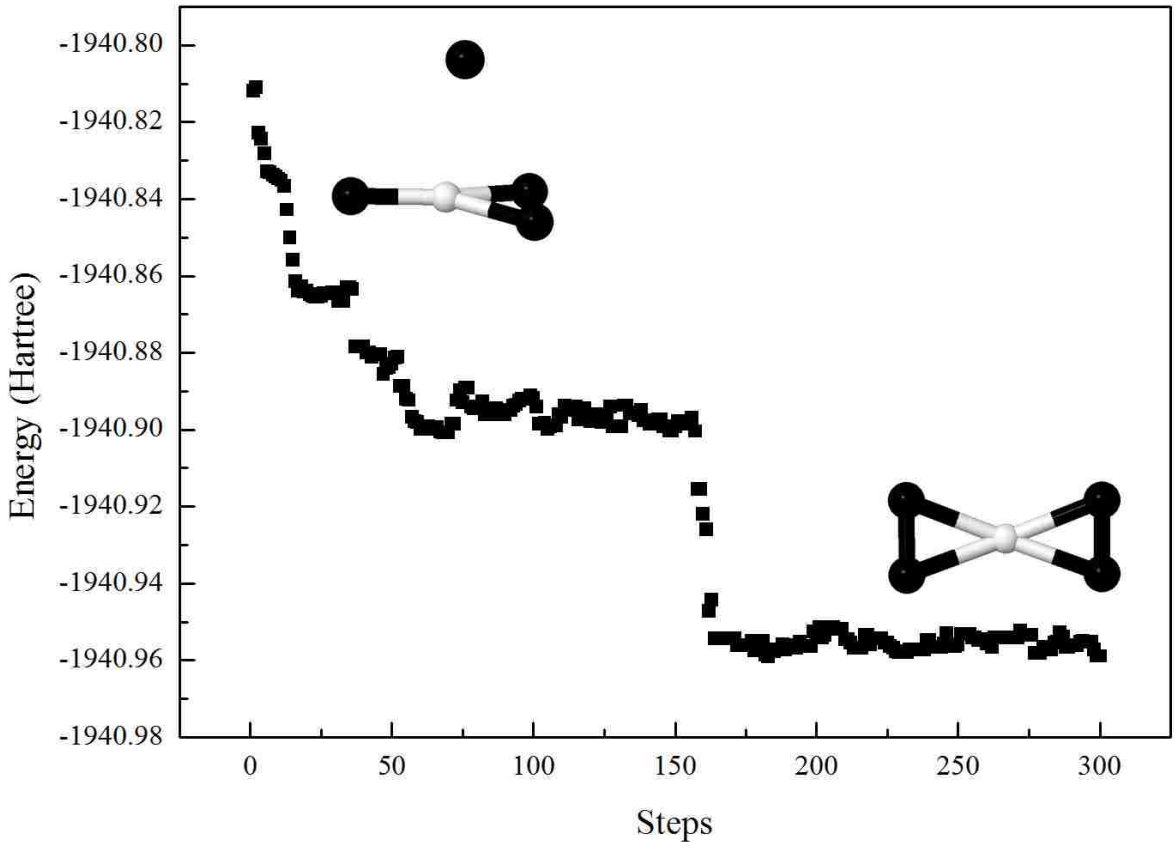

Figure 5.1: Monte Carlo simulation of CuO_4 cluster. Copper/oxygen atoms are colored white/black.

To calculate the total energy at each MC step, we used Gaussian 03 program[112] with B3LYP (Becke's 3-parameter exchange functional with Lee-Yang-Parr correlation energy functional)[107,113,114] and 6-31G** basis set[115,116] but all configurations of each MC step were not optimized. About 300 MC steps were needed to reach the equilibrium state. The Monte Carlo simulations of CuO_4 cluster are shown in Figure 5.1. We generate initial structure: O atom is attached optimized CuO_3 cluster. We performed 300 MC steps to find the local energy of CuO_4 cluster.

These geometries were optimized using standard *ab initio* methods using the GAMESS[117] quantum chemistry package. The smaller clusters were then used as starting points to look for the global minimum geometries for larger clusters where the Monte Carlo procedure was not practical. We used the B3LYP (Becke's 3-parameter exchange functional with Lee-Yang-Parr correlation energy functional)[107,113,114] version of DFT with LANL2DZ basis set.

5.2 Results

5.2.1 Geometric Structures

The optimized structures, bond lengths, angles and Löwdin charge distributions of neutral, positively and negatively charged CuO_n clusters with n=1-6 are shown in Figure 5.1-3. The low-lying spin states (i.e., singlet, doublet, triplet, and quartet) of a given cluster were considered in the calculations.

In single copper oxides clusters, all neutral, positively and negatively charged optimized structures are planar or near planar. Theoretical values of Cu-O calculated with different methods, along with the experimental values, are also included for comparison in Table 5.2. Our calculated values of bond length (1.81Å), dissociation energy (2.44eV)

and electron affinity (1.35 eV) are in agreement with experimental data (1.72 Å, 2.79 eV and 1.78eV).[80] Massobrio et al.[94] found the most stable CuO cluster at quartet spin state; however, our result is that the doublet spin state CuO cluster is more stable than the quartet spin state CuO cluster.

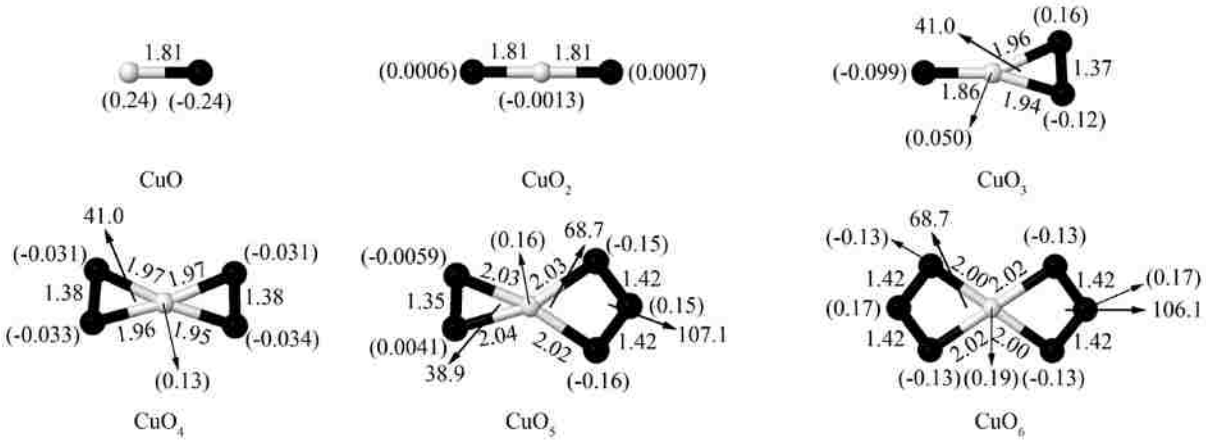

Figure 5.1: Optimized structures, bond lengths, angles and Löwdin charge distributions (parenthesis) of neutral CuO_n clusters with n=1-6. Copper/oxygen atoms are colored white/black.

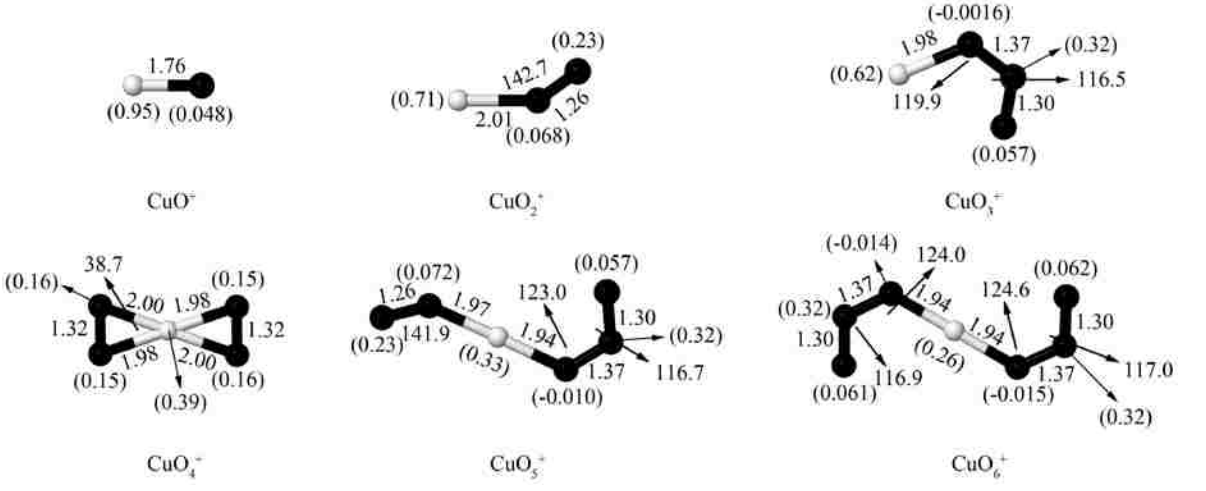

Figure 5.2: Optimized structures, bond lengths, angles and Löwdin charge distributions (parenthesis) of positive charged CuO_n clusters with n=1-6. Copper/oxygen atoms are colored white/black.

The bond length (1.81Å) of neutral Cu-O in CuO cluster is longer than that of charged clusters (1.76Å and 1.74Å). Charged CuO cluster is formed by removing or entering an electron from an oxygen 2pπ orbital which is weakly antibonding. The spin

states of optimized structures are doublet, singlet and singlet at neutral, positively and negatively charged clusters, respectively. The experimental bond length of CuO^- (singlet state)[80] is 1.67 Å, which is shorter than ours (1.74 Å).

Three isomers of CuO_2 clusters have been proposed[94]: OCuO, CuOO bent, and CuO_2 side-on in doublet and quartet spin states. They found OCuO linear cluster is most stable at doublet spin state. According to our results, the lowest structure of CuO_2 is similar to the Massobrio et al. calculation, but quartet spin state neutral CuO_2 cluster is more stable than doublet spin state cluster. Bond lengths are also different: our calculation is 1.81Å and that of Massobrio et al.[94] is 1.73Å. The lowest structure of positive charge CuO_2 cluster is CuO_2 side-on at triplet spin state. The lowest structure of negatively charged CuO_2 cluster is OCuO linear cluster at triplet state. The bond length of positively charged CuO_2 cluster (2.01Å) is longer than neutral (1.81Å) and negatively charged clusters (1.79Å).

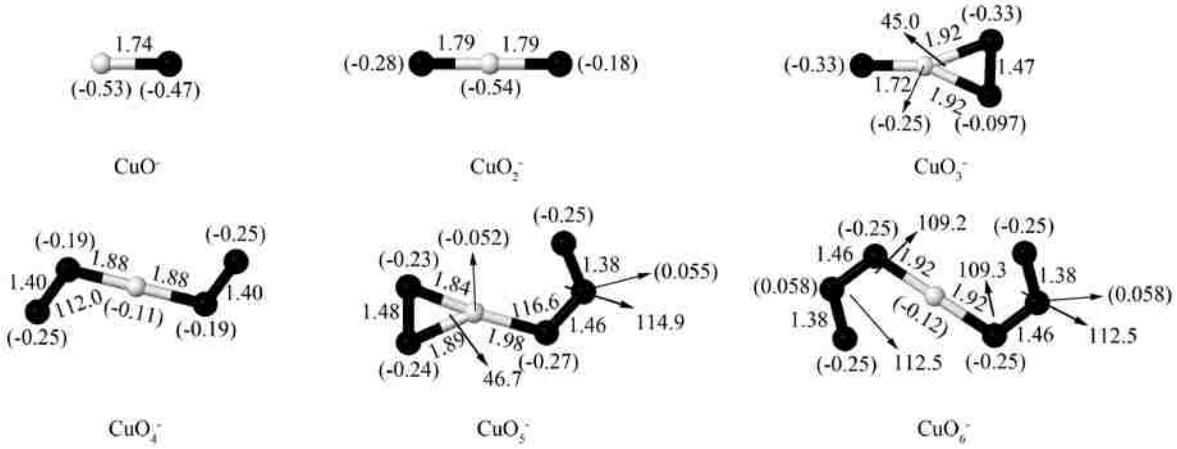

Figure 5.3 Optimized structures, bond lengths, angels and Löwdin charge distributions (parenthesis) of negative charged CuO_n clusters with n=1-6. Copper/oxygen atoms are colored white/black.

Two isomers of CuO_3 clusters have been proposed[94]: CuO_3, ozonide and $OCuO_2$ in their quartet and doublet spin states. $OCuO_2$ cluster is found to be most stable at quartet spin state, which is in good agreement with our results. Our calculated bond lengths

(average 1.92Å) of Cu-O of neutral CuO_3 clusters are longer than those of our negatively charged cluster (average 1.82Å) and the Massobrio et al. neutral result (average 1.83Å). The lowest structure of positively charged CuO_3 clusters is not $OCuO_2$ but CuO_3 ozonide at singlet spin state. The lowest structure of negatively charged CuO_3 cluster is $OCuO_2$ at single spin state. The angle of O-Cu-O of negatively charged CuO_3 cluster (45°) is larger than our neutral CuO_3 cluster (41°) and that of Massobrio et al. (42°).

Table 5.1: Spin states, ionization potential (eV), electron affinities (eV) and binding energy of CuO_n (n=1-6) clusters.

		Spin state	IP	EA	E_b
CuO	CuO	doublet	12.25	1.35	1.22
	CuO^+	singlet			
	CuO^-	singlet			
CuO_2	CuO_2	quartet	7.56	3.38	1.45
	CuO_2^+	triplet			
	CuO_2^-	triplet			
CuO_3	CuO_3	quartet	9.85	2.47	1.78
	CuO_3^+	singlet			
	CuO_3^-	singlet			
CuO_4	CuO_4	quartet	10.32	3.07	2.00
	CuO_4^+	triplet			
	CuO_4^-	triplet			
CuO_5	CuO_5	quartet	9.89	2.60	1.98
	CuO_5^+	triplet			
	CuO_5^-	triplet			
CuO_6	CuO_6	quartet	10.89	3.70	1.91
	CuO_6^+	singlet			
	CuO_6^-	triplet			

We have proposed optimized neutral, positively and negatively charged CuO_4 clusters; the geometry corresponds to two CuO_2 side-on units sharing a common Cu atom. Massobrio et al. have proposed five CuO_4 clusters (doublet and quartet spin states), of which the most stable CuO_4 cluster has the same geometry as ours. However, spin state is different from ours. Our calculation is quartet spin state of lowest CuO_4 cluster and the

Massobrio et al. calculation is doublet state of lowest CuO_4 cluster. The lowest structure of positively charged CuO_4 cluster is similar to neutral CuO_4 cluster. Two Cu-O bonds of four Cu-O bonds in negatively charged CuO_4 cluster are broken. The Cu-O bond length of positively charged CuO_4 cluster (average 1.99Å) is longer than the bond lengths of our neutral (average 1.96Å) and negatively charged (average 1.88Å) clusters and Massobrio *et al.* CuO_4 calculations (average 1.87Å).

Table 5.2: The calculated values of bond length (*Re* in angstrom), dissociation energy (*De* in eV), the frequency (ω in cm-1) and electron affinity (EA in eV) of CuO are compared with experimental values.

Re(Å)	*De*(eV)	ω(cm^{-1})	EA(eV)	Method
1.72	2.79	640	1.78	Exp[80]
1.76		587		DFT[79]
1.74				DFT[94]
1.81	2.44	571	1.35	Ours

Neutral CuO_5 cluster is highly symmetrical and yields similar compact planar arrangements for quartet spin state. This structure consists of one ozonide $Cu(O_3)$ and one $Cu(O_2)$ side-on unit. Bond Cu-O bond lengths of our neutral CuO_5 calculation are 2.03Å and 2.04Å at $Cu(O_3)$ and $Cu(O_2)$ side-on unit, respectively. Massobrio et al. suggested the same geometry: bond lengths of Cu-O are 1.97Å and 1.98Å at $Cu(O_3)$ and $Cu(O_2)$ side-on units.[94] We found that the Cu-O bond lengths of the neutral CuO_5 cluster (average 2.03Å) are longer than those of our charged clusters (CuO_5^+: average 1.96Å, CuO_5^-: average 1.90) and of the Massobrio et al. CuO_5 clusters calculations (average 1.98Å). At the lowest structures of positively charged CuO_5 cluster, one of the Cu-O bonds at $Cu(O_3)$ side-on unit is broken. At the lowest structures of negatively charged CuO_5 cluster, one of the Cu-O bonds at $Cu(O_3)$ and $Cu(O_2)$ side-on unit is broken.

Neutral CuO_6 cluster is planar and consists of two $Cu(O_3)$ units. We have suggested that the lowest energy of neutral, positively and negatively charged CuO_6 clusters at

quartet, singlet and triplet spin states are more stable. However, Massobrio et al. suggested that the doublet spin state of neutral CuO_6 cluster is more stable. In the lowest structures of charged CuO_6 clusters, two CuO bonds are broken, each in a $Cu(O_3)$ unit. The positively and negatively charged CuO_6 clusters have lowest energy at singlet and triplet spin states. The Cu-O bond lengths of our neutral CuO_6 cluster (average 2.01Å) are longer than those of our charged clusters (CuO_6^+: average 1.94Å, CuO_6^-: average 1.92Å) and the Massobrio et al. calculations (average 1.97Å).

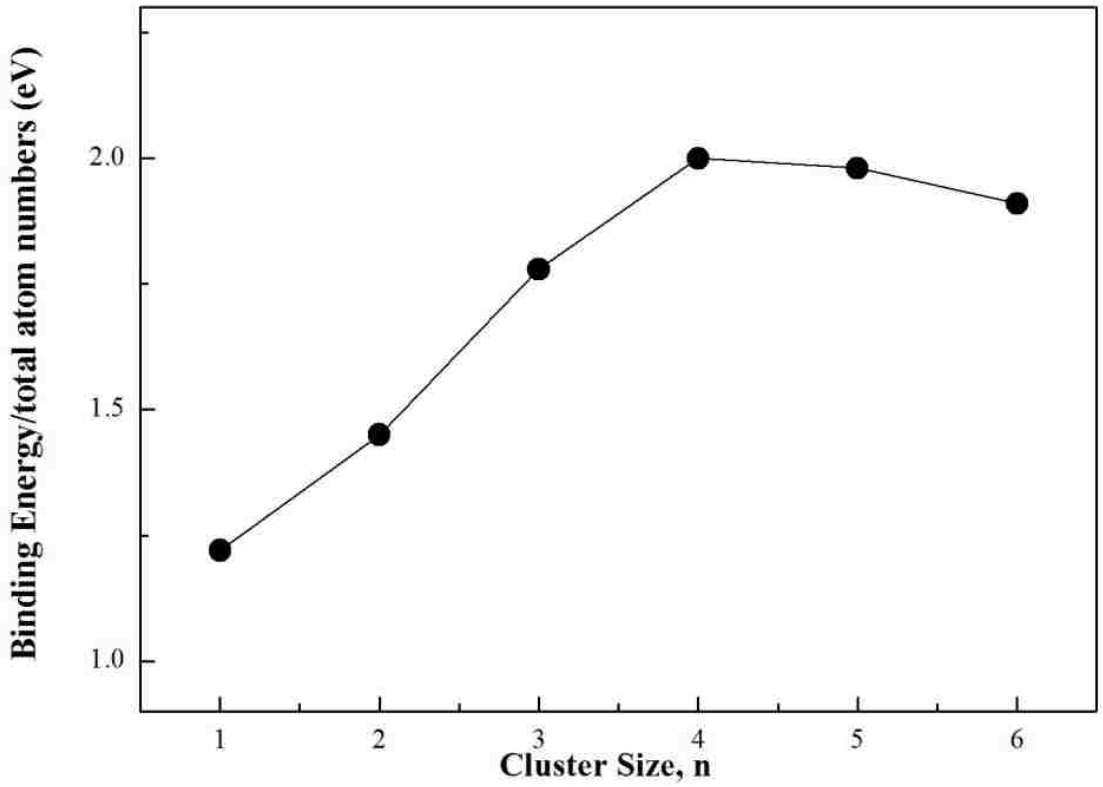

Figure 5.4: Binding energies of neutral CuO_n clusters with n=1-6.

5.2.2 Binding Energies and Second Difference Energies

The binding energies of CuO_n (n=1-6) clusters are shown in Figure 5.4. The definitions of binding energies of single copper oxide clusters are expressed as

$$E_b = [\,E(Cu) + n\,E(O) - E(CuO_n)]/(total\ atom\ number) \quad (1)$$

with the triplet state of an oxygen atom.

The CuO_4 cluster has exhibited local maxima (2.00eV) of binding energies; it has the highest stability and is often used to identify so-called “magic clusters.” We define the energy variation in the formula as $\Delta^2E(n) = [E(n+1) - E(n)] - [E(n) - E(n-1)]$, which is the second difference of total energies for CuO_n (n=1-6) clusters. The special stability of CuO_4 cluster can be seen from the second difference energies of Figure 5.5, which also shows a peak CuO_4 cluster. CuO_5 and CuO_6 clusters in single copper oxide clusters are CuO_4 clusters solvated by O and O_2 molecules.

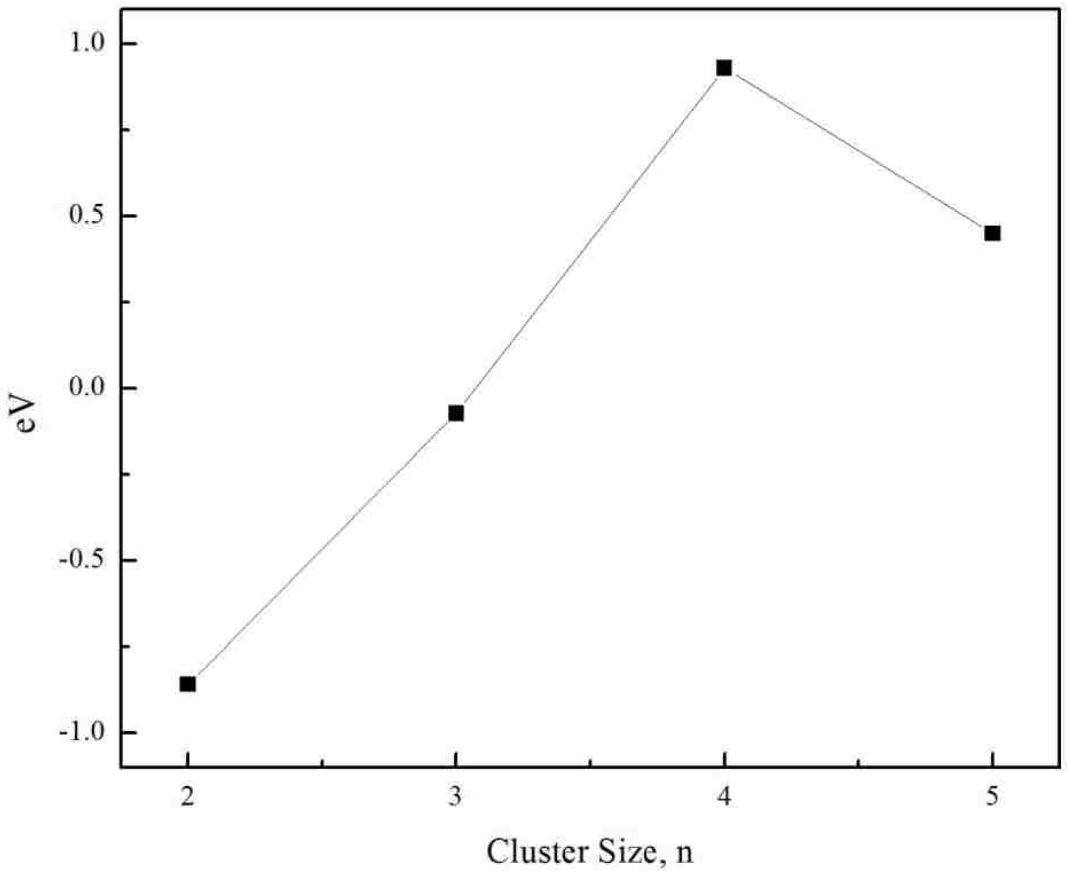

Figure 5.5: Second difference of the energy of CuO_n, clusters with n=1-6

5.2.3 Ionization Potential and Electron Affinities

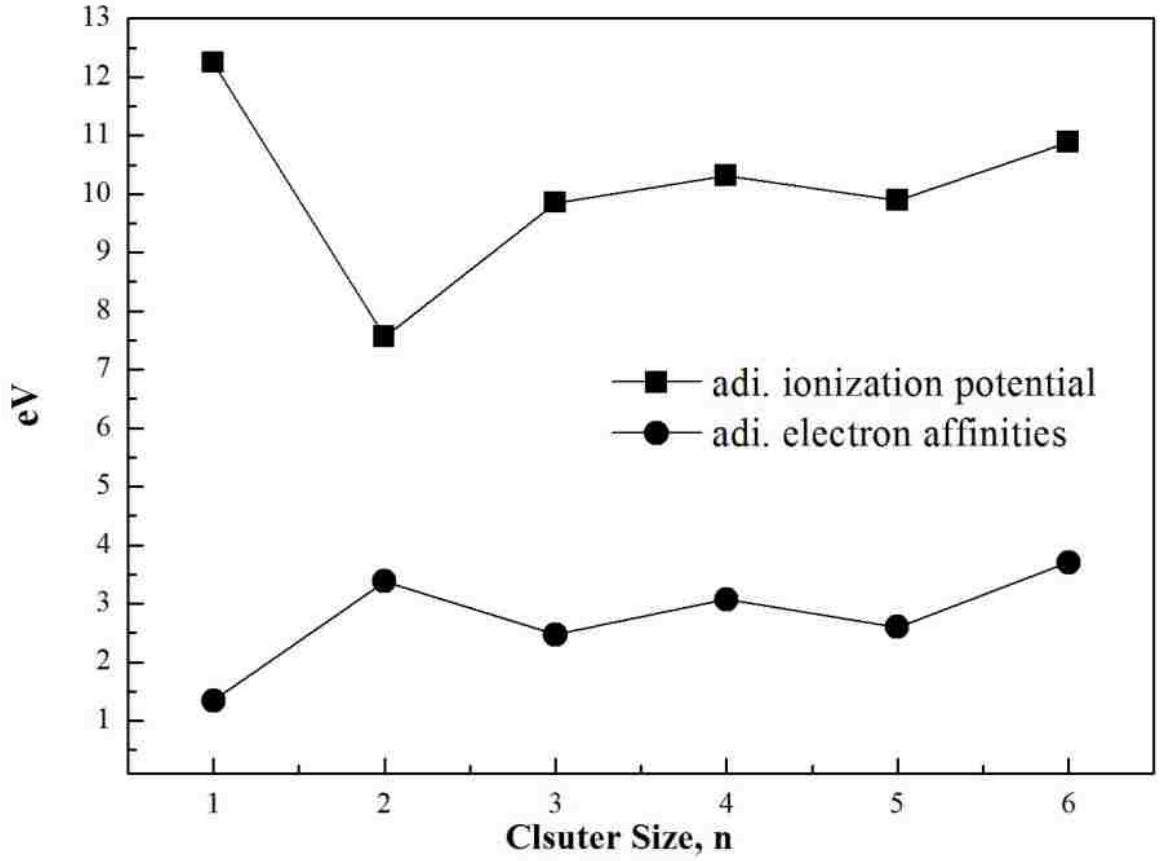

Figure 5.6 Calculated adiabatic ionization potential (IP) and electron affinities (EA) of CuO_n clusters with n=1-6

Figure 5.6 represents adiabatic ionization potential ($IP(X_n)=E(X_n^+)-E(X_n)$) and electron affinities ($EA(X_n)=E(X_n)-E(X_n^-)$. IPs and EAs have been calculated taking the lowest structural energies, which are adiabatic energies. Generally, the IPs and EAs are oscillating for n odd (even); we obtain that IP increases (decreases). In this case, IPs are showing a stabilization for n=3-5 while EAs are oscillating. They had experimented with the magnetic-bottle time-of-flight (MTOF) photoelectron spectrometer for CuO_x (x=0-6).[78] They had investigated the electron affinities, and we can compare their results with ours. It is interesting that the geometries are different for CuO_5 and CuO_6 clusters. They

suggested $(O\text{-}Cu)(O_2)_2$ for CuO_5 cluster and $CuO_2(O_2)_2$ for CuO_6 cluster. Our calculated EAs, are 1.35eV (1.78eV), 3.38eV (3.47eV), 2.47eV (3.53eV), and 3.07eV (3.09eV) for CuO, CuO_2, CuO_3 and CuO_4, respectively. The parentheses show experimental data. The calculated EAs of CuO_2 and CuO_4 clusters are in good agreement with experimental data.

5.2.4 HOMO-LUMO Gaps and Fragmentation Channels

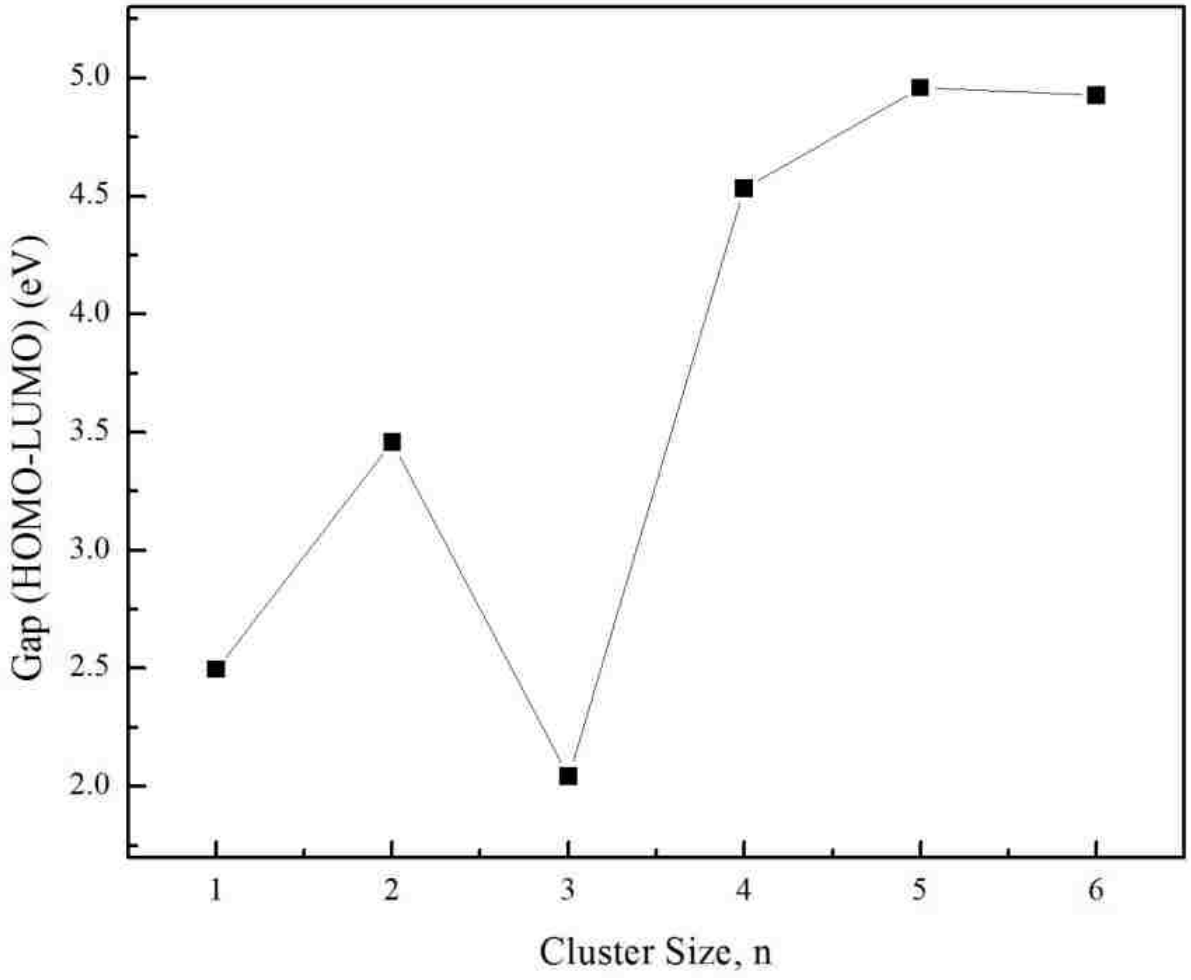

Figure 5.7 Calculated HOMO-LUMO gap of neutral CuO_n clusters with n=1-6

The calculated HOMO-LUMO gaps of neutral CuO_n (n=1-6) clusters are shown in Figure 5.7. The gaps are very sensitive to correlated effects due to the cluster geometry. Among neutral clusters, CuO_3 cluster has the smallest HOMO-LUMO gap of 2.04eV and

CuO_5 cluster has the largest HOMO-LUMO gap, 3.46eV. It is interesting that HOMO-LUMO gaps are increased from CuO_3 to CuO_4 rapidly.

The HOMO-LUMO gap is considered to be an important parameter in terms of the chemical stability of clusters: a large energy gap corresponds to larger reactivity stability. The large HOMO-LUMO gaps are found at n=4, 5, and 6. Therefore, we know CuO_4 cluster has particularly stability from second difference energies and HOMO-LUMO gaps. In fact, the second different energies reflect thermodynamic stability and the HOMO-LUMO gaps show potential chemical reactivity; they have no direct relationship. For example, CuO_4 has large second difference energy; however, it has a relatively small HOMO-LUMO gap. The calculated HOMO-LUMO gaps for neutral CuO_n (n=1-6) clusters are shown in figure 5.7.

Table 5.3: Fragmentation channels of CuO_n clusters with n=1-6

CuO_n (n=1-6)	
$E_{n+m} \rightarrow E_n + E_m$	ΔE (kcal/mol)
$CuO \rightarrow Cu + O$	56.18
$CuO_2 \rightarrow Cu + O_2$	9.80
$\rightarrow CuO + O$	44.25
$CuO_3 \rightarrow Cu + O_2 + O$	73.82
$\rightarrow CuO + O_2$	17.64
$\rightarrow CuO_2 + O$	64.03
$CuO_4 \rightarrow Cu + O_2 + O_2$	48.89
$\rightarrow CuO + O_2 + O$	83.34
$\rightarrow CuO_2 + O_2$	39.09
$\rightarrow CuO_3 + O$	65.70
$CuO_5 \rightarrow Cu + O_2 + O_2 + O$	93.13
$\rightarrow CuO + O_2 + O_2$	36.96
$\rightarrow CuO_2 + O_2 + O$	83.34
$\rightarrow CuO_3 + O_2$	19.31
$\rightarrow CuO_4$ O	44.24
$CuO_6 \rightarrow Cu + O_2 + O_2 + O_2$	36.38
$\rightarrow CuO + O_2 + O_2 + O$	70.83
$\rightarrow CuO_2 + O_2 + O_2$	26.58
$\rightarrow CuO_3 + O_2 + O$	53.19
$\rightarrow CuO_4 + O_2$	-12.51
$\rightarrow CuO_5 + O$	33.87

The fragmentation energy of CuO_6 in becoming $CuO_4 + O_2$ is the lowest value (-12.51 kcal/mol), which we would like to emphasize as the most favorable pathway to break the clusters. CuO_2, CuO_3, CuO_4, CuO_5 and CuO_6 can dissociate into $Cu + O_2$, $CuO + O_2$, $CuO_2 + O_2$, $CuO_3 + O_2$ and $CuO_4 + O_2$, respectively. From CuO_2 to CuO_6 clusters, their fragmentation products contain an O_2 molecule.

5.2.5 Löwdin Charge Distributions

The calculations of Löwdin charge distributions[99] of Cu and O are shown Figure 5.1-5.3

Löwdin charges of the Cu atoms are 0.24 |e| for CuO, -0.0013 |e| for CuO_2, 0.050 |e| for CuO_3, 0.13 |e| for CuO_4, 0.16 |e| for CuO_5, and 0.19 |e| for CuO_6 in neutral clusters. Average Löwdin charges of the O atoms are -0.24 |e| for CuO, 0.0007 |e| for CuO_2, -0.020 |e| for CuO_3, -0.032 |e| for CuO_4, -0.054 |e| for CuO_5, and -0.030 |e| for CuO_6 in neutral clusters.

Löwdin charges of the Cu atoms are 0.95 |e| for CuO, 0.71 |e| for CuO_2, 0.62 |e| for CuO_3, 0.39 |e| for CuO_4, 0.33 |e| for CuO_5, and 0.26 |e| for CuO_6 in positive charged clusters. Average Löwdin charges of the O atoms are 0.048 |e| for CuO, 0.15 |e| for CuO_2, 0.16 |e| for CuO_3, 0.16 |e| for CuO_4, 0.20 |e| for CuO_5, and 0.12 |e| for CuO_6 in positive charged clusters.

Löwdin charges of the Cu atoms are -0.53 |e| for CuO, -0.54 |e| for CuO_2, -0.25 |e| for CuO_3, -0.11 |e| for CuO_4, -0.052 |e| for CuO_5, and -0.12 |e| for CuO_6 in positive charged clusters. Average Löwdin charges of the O atoms are -0.47 |e| for CuO, -0.23 |e| for CuO_2, -0.25 |e| for CuO_3, -0.22 |e| for CuO_4, -0.19 |e| for CuO_5, and -0.15 |e| for CuO_6 in positive charged clusters.

5.2.6 Calculated Single Copper Oxide Reactions

Calculated energies for reactions of single copper with oxygens are shown in Table 5.4. The energy of the Cu + $2O_2$ reaction to form CuO_4 is the lowest value (-48.89 kcal/mol). We have also calculated the fragmentation energies of $(CuO)_n$ n=1-6 clusters for various dissociation pathways in Table 5.3 In single copper oxide clusters, the most favorable pathways of CuO_n, (n=1, 3, and 5) and (n=2, 4, and 6), usually contain pure copper and CuO cluster, respectively.

Table 5.4: Calculated energies (in kcal/mol) for reactions between single copper and oxygen

Reaction	Energy (kcal/mol)
$Cu + 1/2O_2 \rightarrow CuO$	-10.86
$Cu + O_2 \rightarrow CuO_2$	-9.80
$Cu + 3/2O_2 \rightarrow CuO_3$	-28.51
$Cu + 2O_2 \rightarrow CuO_4$	-48.89
$Cu + 5/2O_2 \rightarrow CuO_5$	-47.82
$Cu + 3O_2 \rightarrow CuO_6$	-36.38

5.3 Conclusions

We have investigated the structural and electronic properties of single copper oxide clusters using density functional calculation. We found the lowest energy structures are plane or near plane for all neutral, positive and negative single copper oxide clusters.

We have compared our results with those of Massobrio et al. and concluded that we have similar geometries in neutral single copper oxide clusters, but the spin states of the lowest energy structures are different (neutral CuO, CuO_2, CuO_4 and CuO_6 clusters). The

spin states of our simulations are all quartet spin states except CuO cluster (doublet spin state). The spin states found in the Massobrio et al. results are doublet spin states of even number oxygen clusters and quartet spin states of odd number oxygen clusters.

From binding energies and second difference energies, we confirmed that CuO_4 cluster has the highest stability and is often used to identify so-called “magic clusters.”

The fragmentation energy of CuO_6 in becoming $CuO_4 + O_2$ is the lowest value (-12.51 kcal/mol), which we would like to emphasize as the most favorable pathway to break the clusters.

CHAPTER 6

CONCLUDING REMARKS

Nanoparticles are formed largely by combustion sources as primary PM emissions. Nanoparticles are not efficient captured by air control devices, are transported long distance and penetrate deep into the respiratory system. In combustion systems, nanoparticles are mixtures of organic and inorganic compounds and include a number of transition metals (iron or copper). The production of these transition metal-organic complexes results in lung injury, inflammation, alterations in pulmonary host defense and DNA damage.

Polychlorinated dibenzo-p-dioxins and polychlorinated furans (PCDD/F or dioxin) are the most toxic known environmental pollutants. PCDD/Fs formations can be explained that transition metal oxides and chlorides play a significant role. Therefore, we have performed a detailed study of copper oxide clusters and their reactions with phenol and chlorinated phenols.

We have studied small copper oxide clusters using *ab initio* Monte Carlo simulations. These copper oxide clusters were then optimized using standard *ab initio* methods using GAMESS quantum chemistry package. We used the B3LYP version of DFT in combination with the LANL2DZ basis set. Comparison with existing experimental work demonstrated that the LANL2DZ basis set is in best agreement.

In our studies of copper oxide clusters, we have particularly emphasized several aspects: 1) geometric structures, 2) binding energies and second different energies, 3) ionization potential and electron affinities, 4) HOMO-LUMO gaps, and 5) Löwdin charge distributions.

In Cu_nO_n clusters with n=1-8, a transition from planar to nonplanar geometries occurs at n=4. The negatively charged Cu_4O_4 cluster is a planar structure. Atomization energies and second difference energies show that Cu_5O_5 cluster has highest stability. We find that odd numbered copper oxide clusters have higher stabilities than even numbered copper oxide clusters, which can be explained in two ways. First, the Cu-O-Cu angles are relatively close to tetrahedral values and correlate reasonably well with second difference energy. Second, small rings lead to ring strain and a loss of stability. The even numbered clusters have small rings (3- and 4-membered) and the odd numbered clusters have large rings (6- and 7 membered). Therefore, we expect that odd numbered copper oxide clusters (Cu_9O_9, $Cu_{11}O_{11}$…) will be most stable.

Ionization potentials have some oscillations with cluster size, as these are typical for clusters. The lowest fragmentation energy of Cu_6O_6 cluster (dissociation to Cu_5O_5 + CuO) is, we would like to emphasize, the most favorable pathway to break the cluster. We also expect that bigger copper oxide clusters than Cu_8O_8 cluster would dissociate to contain a CuO cluster as small copper oxide clusters. (From CuO to Cu_8O_8 clusters)

We have investigated the stabilities and reactivities of copper oxide clusters. Reactions of the previously optimized neutral Cu_nO_n clusters with water and organic compounds (phenol, *ortho*-chlorophenol and *para*-chlorophenol) were studied using *ab initio* methods.

The energies, enthalpies, Gibbs free energies of copper oxide, copper oxide-water and copper oxide-organic compounds clusters were calculated to investigate their reaction energetics. We also calculated bond lengths, adsorption energies and Löwdin charge distributions.

We find that organic compounds (phenol and chlorinated phenols) are likely to bind to the copper atom with the largest charge. For Cu_4O_4 to Cu_8O_8 clusters, we can predict

the reaction site from charge distributions of copper oxide clusters.

Our calculations of reaction energies indicate that generally *ortho*-chlorophenol binds less strongly to the surface of copper oxide clusters than phenol and *para*-chlorophenol, which can be explained in two ways. First, H atom of OH group of *ortho*-chlorophenol is displaced to copper oxide cluster. Second, weak Cu-Cl bonds can make stabilization of copper oxide clusters with *ortho*-chlorophenol.

The results can help an understanding the mechanisms of the formation of PCDD/Fs from chlorinated phenols in the copper oxide clusters.

We have also investigated the structural and electronic properties of single copper oxide clusters (CuO_n n=1-6) using density functional calculation. We found the lowest energy structures are plane or near plane for all neutral, positively and negatively single copper oxide clusters.

The spin states of our simulations are all quartet spin states except CuO cluster (doublet spin state). We have compared our results with those of Massobrio et al. and concluded that we have similar geometrics in neutral single copper oxide clusters, but the spin states of the lowest energy structures are different (neutral CuO, CuO_2, CuO_4 and CuO_6 clusters). The spin states of our simulations are all quartet spin states except CuO cluster (doublet spin state). The spin states found by Massobrio et al. are doublet spin states of even number oxygen clusters and quartet spin states of odd number oxygen clusters.

From binding energies and second difference energies, we confirmed that CuO_4 cluster has the highest stability and is often used to identify so-called “magic clusters.”

The fragmentation energy of CuO_6 in becoming $CuO_4 + O_2$ is the lowest value (-12.51 kcal/mol), which we would like to emphasize as the most favorable pathway to break the clusters.

BIBLIOGRAPHY

(1) Pope, C. A., 3rd; Burnett, R. T.; Thun, M. J.; Calle, E. E.; Krewski, D.; Ito, K.; Thurston, G. D. *JAMA* **2002**, *287*, 1132.

(2) Delfino, R. J.; Gong, H.; Linn, W. S.; Pellizzari, E. D.; Hu, Y. *Environ. Health Persp.* **2003**, *111*, 647.

(3) Donaldson, K.; Li, X. Y.; MacNee, W. *J. Aerosol Sci.* **1998**, *29*, 553.

(4) *Air Quality Criteria for Particulate Matter* **1996**, *1-3*, EPA/600/P.

(5) Cahill, T. A.; Cliff, S. S.; Perry, K. D.; Jimenez-Cruz, M.; Bench, G.; Grant, P.; Ueda, D.; Shackelford, J. F.; Dunlap, M.; Meier, M.; Kelly, P. B.; Riddle, S.; Selco, J.; Leifer, R. *Aerosol Sci. Tech.* **2004**, *38*, 165.

(6) Cleveland, C. L.; Landman, U. *Science* **1992**, *257*, 355.

(7) Raz, T.; Levine, R. D. *J. Am. Chem. Soc.* **1994**, *116*, 11167.

(8) Luedtke, W. D.; Landman, U. *Phys. Rev. Lett.* **1994**, *73*, 569.

(9) Haberland, H.; Insepov, Z.; Moseler, M. *Phys. Rev. B* **1995**, *51*, 11061.

(10) Service, R. F. *Science* **1996**, *271*, 920.

(11) Lighty, J. S.; Veranth, J. M.; Sarofim, A. F. *J. Air Waste Manage. Assoc.* **2000**, *50*, 1565.

(12) Linak, W. P.; Wendt, J. O. L. *Fuel Process Technol* **1994**, *39*, 173.

(13) Samet, J. M.; Dominici, F.; Curriero, F. C.; Coursac, I.; Zeger, S. L. *N. Engl. J. Med.* **2000**, *343*, 1742.

(14) Huggins, F. E.; Huffman, G. P.; Linak, W. P.; Miller, C. A. *Environ. Sci. Tech.* **2004**, *38*, 1836.

(15) Oberdörster, G.; Utell, M. J. *Environ. Health Perspect.* **2002**, *110*, A440.

(16) Dockery, D. W.; Pope, C. A.; Xu, X.; Spengler, J. D.; Ware, J. H.; Fay, M. E.; Ferris, B. G.; Speizer, F. E. *N. Engl. J. Med.* **1993**, *329*, 1753.

(17) Pope, C. A., 3rd; Thun, M. J.; Namboodiri, M. M.; Dockery, D. W.; Evans, J. S.; Speizer, F. E.; Heath, C. W., Jr. *Am. J. Respir. Crit. Care Med.* **1995**, *151*, 669.

(18) Chalupa, D. C.; Morrow, P. E.; Oberdörster, G.; Utell, M. J.; Frampton, M. W. *Environ. Health Perspect.* **2004**, *112*, 879.

(19) Pope, C. A., 3rd. *Am. J. Public Health* **1989**, *79*, 623.

(20) Pope, C. A., 3rd. *Arch. Environ. Health* **1991**, *46*, 90.

(21) Schwarz, J. *Arch. Environ. Health* **1994**, *49*, 366.

(22) Schwartz, J.; Morris, R. *Am. J. Epidemiol.* **1995**, *142*, 23.

(23) Pope, C. A., 3rd; Dockery, D. W.; Spengler, J. D.; Raizenne, M. E. *Am. Rev. Respir. Dis.* **1991**, *144*, 668.

(24) Pope, C. A., 3rd; Dockery, D. W. *Am. Rev. Respir. Dis.* **1992**, *145*, 1123.

(25) Roemer, W.; Hoek, G.; Brunekreef, B. *Am. Rev. Respir. Dis.* **1993**, *147*, 118.

(26) Dusseldorp, A.; Kruize, H.; Brunekreef, B.; Hofschreuder, P.; de Meer, G.; van Oudvorst, A. *Am. J. Respir. Crit. Care Med.* **1995**, *152*, 1932.

(27) Pope, C. A., 3rd; Kanner, R. E. *Am. Rev. Respir. Dis.* **1993**, *147*, 1336.

(28) Donaldson, K.; Tran, C. L. *Inhal. Toxicol.* **2002**, *14*, 5.

(29) Lippert, T.; Wokaun, A.; Lenoir, D. *Environ. Sci. Technol.* **1991**, *25*, 1485.

(30) Taylor, P. H.; Tirey, D. A.; Rubey, W. A.; Dellinger, B. *Comb. Sci. Tech.* **1994**, *101*, 75.

(31) Taylor, P. H.; Dellinger, B. *Environ. Sci. Technol.* **2002**, *22*, 438.

(32) Ghorishi, S. B.; Altwicker, E. R. *Hazard. Waste Hazard. Mater.* **1996**, *13*, 11.

(33) Mason, R. P.; Dreher, K. L.; Costa, D. L.; Ghio, A. J. *Chem. Res. Toxicol.* **1997**, *10*, 1104.

(34) Pritchard, R. J.; Ghio, A. J.; Lehmann, J. R.; Winsett, D. W.; Tepper, J. S.; Park, P.; Gilmour, M. I.; Dreher, K. L.; Costa, D. L. *Inhalation Toxicol.* **1996**, *8*, 457.

(35) Huffman, G. P.; Huggins, F. E.; Shah, N.; Huggins, R.; Linak, W. P.; Miller, A.; Pugmire, R. J.; Meuzelaar, H. L. C.; Seehra, M. S.; Manivannan, A. *J. Air & Waste Manage. Assoc.* **2000**, *50*, 1106.

(36) Wehrmeier, A.; Lenoir, D.; Sidhu, S. S.; Taylor, P. H.; Rubey, W. A.; Kettrup, A.; Dellinger, B. *Environ. Sci. Technol.* **1998**, *32*, 2741.

(37) Lomnicki, S.; Dellinger, B. *J. Phys. Chem. A* **2003**, *107*, 4387.

(38) Stieglitz, L. *Environ. Eng. Sci.* **1998**, *15*, 5.

(39) Weber, R.; Hagenmaier, H. *Chemosphere* **1999**, *38*, 2643.

(40) Meyers, J. M.; Gellman, A. J. *Surface Science* **1995**, *337*, 40.

(41) Ritter, E. R.; Bozzelli, J. W. *Combust. Sci. Tech.* **1990**, *74*, 117.

(42) Cormier, S. A.; Lomnicki, S.; Backes, W.; Dellinger, B. *Environ. Health Perspect.* **2006**, *114*, 810.

(43) Lomnicki, S.; Dellinger, B. *Proceedings of the Combustion Institute* **2002**, *29*, 2463.

(44) Altwicker, E. R.; Konduri, R. K. N. V.; Lin, C.; Milligan, M. S. *Chemosphere* **1992**, *25*, 1935.

(45) Mulholland, J. A.; Akki, U.; Yang, Y.; Ryu, J.-Y. *Chemosphere* **2001**, *42*, 719.

(46) Shaub, W. M.; Tsang, W. *Environ. Sci. Technol.* **1983**, *17*, 721.

(47) Tupporainen, K. A.; Ruokojarvi, P. H.; Asikainen, A. H.; Aatamila, M.; Ruuskinen, J. *Environ. Sci. Technol.* **2000**, *34*, 4958.

(48) Weber, R.; Hagenmaier, H. *Chemosphere* **1999**, *38*, 529.

(49) Hell, K.; Stieglitz, L.; Dinjus, E. *Environ. Sci. Technol.* **2001**, *35*, 3892.

(50) Addink, R.; Olie, K. *Environ. Sci. Technol.* **1995**, *29*, 1425.

(51) De Heer, W. A. *Rev. Mod. Phys.* **1993**, *65*, 611.

(52) Morse, M. D. *Chem. Rev.* **1986**, *86*, 1049.

(53) Leopold, D. G.; Ho, J.; Lineberger, W. C. *J. Chem. Phys.* **1987**, *86*, 1715.

(54) Lee, T. H.; Ervin, K. M. *J. Phys. Chem.* **1994**, *98*, 10023.

(55) Shirk, J. S.; Bass, A. M. *J. Chem. Phys.* **1970**, *52*, 1894.

(56) Appelblad, O.; Lagerqvist, A. *Phys. Scr.* **1974**, *10*, 307.

(57) Tevault, D. E.; Mowery, R. L.; Marco, R. A. D.; Smardzewski, R. R. *J. Chem. Phys.* **1981**, *74*, 4342.

(58) Brown, C. E.; Mitchell, S. A.; Hackett, P. A. *J. Phys. Chem.* **1991**, *95*, 1062.

(59) Vinckier, C.; Corthouts, J.; Jaegere, S. D. *J. Chem. Soc., Faraday Trans. 2* **1988**, *84*, 1951.

(60) Sulzle, D.; Schwarz, H.; H. Moock, K.; K. Terlouw, J. *Int. J. Mass Spec. Ion Proc.* **1991**, *108*, 269.

(61) Ozin, G. A.; Mitchell, S. A.; Garcia-Prieto, J. *J. Am. Chem. Soc.* **1983**, *105*, 6399.

(62) Tevault, D. E. *J. Chem. Phys.* **1982**, *76*, 2859.

(63) Bondybey, V. E.; English, J. H. *J. Phys. Chem.* **1984**, *88*, 2247.

(64) Howard, J. A.; Sutcliffe, R.; Mile, B. *J. Phys. Chem.* **1984**, *88*, 4351.

(65) Kasai, P. H.; Jones, P. M. *J. Phys. Chem.* **1986**, *90*, 4239.

(66) Lefebvre, Y.; Pinchemel, B.; Delaval, J. M.; Schamps, J. *Phys. Rev. B* **1988**, *37*, 785.

(67) Mattar, S. M.; Ozin, G. A. *J. Phys. Chem.* **1988**, *92*, 3511.

(68) Langhoff, S. R.; Bauschlicher, C. W. *Chem. Phys. Lett.* **1986**, *124*, 241.

(69) Madhavan, P. V.; Newton, M. D. *J. Chem. Phys.* **1985**, *83*, 2337.

(70) Igel, G.; Wedig, U.; Dolg, M.; Fuentealba, P.; Preuss, H.; Stoll, H.; Frey, R. *J. Chem. Phys.* **1984**, *81*, 2737.

(71) Bagus, P. S.; Nelin, C. J.; Charles W. Bauschlicher, J. *J. Chem. Phys.* **1983**, *79*, 2975.

(72) Merer, A. J. *Ann. Rev. Phys. Chem.* **1989**, *40*, 407.

(73) Hrusak, J.; Koch, W.; Schwarz, H. *J. Chem. Phys.* **1994**, *101*, 3898.

(74) Bauschlicher, C. W.; Langhoff, S. R.; Partridge, H.; Sodupe, M. *J. Phys. Chem.* **1993**, *97*, 856.

(75) Mochizuki, Y.; Nagashima, U.; Yamamoto, S.; Kashiwagi, H. *Chem. Phys. Lett.* **1989**, *164*, 225.

(76) Wu, H.; Desai, S. R.; Wang, L. S. *J. Chem. Phys.* **1995**, *103*, 4363.

(77) Wang, L. S.; Wu, H.; Desai, S. R.; Lou, L. *Phys. Rev. B* **1996**, *53*, 8028.

(78) Wu, H.; Desai, S. R.; Wang, L.-S. *J. Phys. Chem. A* **1997**, *101*, 2103.

(79) Chertihin, G. V.; Andrews, L.; Bauschlicher, C. W. *J. Phys. Chem. A* **1997**, *101*, 4026.

(80) Polak, M. L.; Gilles, M. K.; Ho, J.; Lineberger, W. C. *J. Phys. Chem.* **1991**, *95*, 3460.

(81) Steimle, T. C.; Azuma, Y. *J. of Mol. Spectrosc.* **1986**, *118*, 237.

(82) Brack, M. *Rev. Mod. Phys.* **1993**, *65*, 677.

(83) Aakeby, H.; Panas, I.; Pettersson, L. G. M.; Siegbahn, P.; Wahlgren, U. *J. Phys. Chem.* **1990**, *94*, 5471.

(84) Calaminici, P.; Köster, A. M.; Russo, N.; Salahub, D. R. *J. Chem. Phys* **1996**, *107*, 4066.

(85) Cao, Z.; Wang, Y.; Zhu, J.; Wu, W.; Zhang, Q. *J. Phys. Chem. B* **2003**, *107*, 4066.

(86) Ha, T. K.; Nguyen, M. T. *J. Phys. Chem.* **1985**, *89*, 5569.

(87) Den Boer, D. H. W.; Kaleveld, E. W. *Chem. Phys. Lett.* **1980**, *69*, 389.

(88) Basch, H.; Osman, R. *Chem. Phys. Lett.* **1982**, *93*, 51.

(89) Mochizuki, Y.; Tanaka, K.; Kashiwagi, H. *Chem. Phys.* **1991**, *151*, 11.

(90) Barone, V.; Adamo, C. *J. Phys. Chem.* **1996**, *100*, 2094.

(91) Deng, K.; Yang, J.; Yuan, L.; Zhu, Q. *J. Chem. Phys.* **1999**, *111*, 1477.

(92) Zexing Cao, M. S. H. X., Miquel Duran, Qianer Zhang,. *Intern. J. Quantum Chem.* **2001**, *81*, 162.

(93) Pouillon, Y.; Massobrio, C. *Chem. Phys. Lett.* **2002**, *356*, 469.

(94) Pouillon, Y.; Massobrio, C. *Appl. Surf. Sci.* **2004**, *226*, 306.

(95) Massobrio, C.; Pouillon, Y. *J. Chem. Phys.* **2003**, *119*, 8305.

(96) Cheshnovsky, O.; Yang, S. H.; Pettiette, C. L.; Craycraft, M. J.; Smalley, R. E. *Rev. Sci. Instrum.* **1987**, *58*, 2131.

(97) Wang, L. S.; Cheng, H. S.; Fan, J. *J. Chem. Phys.* **1995**, *102*, 9480.

(98) Dai, B.; Tian, L.; Yang, J. *J. Chem. Phys.* **2004**, *120*, 2746.

(99) Szabo, A.; Ostlund, N. S. *Modern Quantum Chemistry*; Dover, 1996.

(100) Hohenberg, P.; Kohn, W. *Phys. Rev.* **1964**, *136*, B864.

(101) Kohn., W.; Sham., L. *Phys. Rev.* **1965**, *140*, A1133.

(102) Becke, A. D. *J. Chem. Phys.* **1986**, *84*, 4524.

(103) Perdew, J. P.; Yue, W. *Phys. Rev. B* **1986**, *33*, 8800.

(104) Lacks, D. J.; Gordon, R. G. *Phys. Rev. A* **1993**, *47*, 4681.

(105) Perdew, J. P.; Burke, K.; Ernzerhof, M. *Phys. Rev. Lett.* **1996**, *77*, 3865.

(106) Perdew, J. P.; Burke, K.; Ernzerhof, M. *Phys. Rev. Lett.* **1997**, *78*, 1396.

(107) Lee, C.; Yang, W.; Parr, R. G. *Phys. Rev. B* **1988**, *37*, 785.

(108) Perdew, J. P.; Wang, Y. *Phys. Rev. B* **1992**, *45*, 13244.

(109) Becke, A. D. *J. Chem. Phys.* **1996**, *104*, 1040.

(110) Allen, M. P.; Tildesley, D. J. *Computer Simulation of Liquids*; Clarendon Press Oxford, 1987.

(111) Metropolis, N.; Rosenbluth, A.; Rosenbluth, M.; Teller, A.; Teller, E. *J. Chem. Phys.* **1953**, *21*, 1087.

(112) M. J. Frisch, G. W. T., H. B. Schlegel, G. E. Scuseria, M. A. Rob, J. R. Cheeseman, J. A. Montgomery Jr., T. Vreven, K. N. Kudin, J. C. Burant, J. M. Millam, S. S. Iyengar, J. Tomasi, V. Barone, B. Mennucci, M. Cossi, G. Scalmani, N. Rega, G. A. Petersson, H. Nakatsuji, M. Hada, M. Ehara, K. Toyota, R. Fukuda, J. Hasegawa, M. Ishida, T. Nakajima, Y. Honda, O. Kitao, H. Nakai, M. Klene, X. Li, J. E. Knox, H. P. Hratchian, J. B. Cross, V. Bakken, C. Adamo, J. Jaramillo, R. Gomperts, R. E. Stratmann, O. Yazyev, A. J. Austin, R. Cammi, C. Pomelli, J. W. Ochterski, P. Y. Ayala, K. Morokuma, G. A. Voth, P. Salvador, J. J. Dannenberg, V. G. Zakrzewski, S. Dapprich, A. D. Daniels, M. C. Strain, O. Farkas, D. K. Malick, A. D. Rabuck, K. Raghavachari, J. B. Foresman, J. V. Ortiz, Q. Cui, A. G. Baboul, S. Clifford, J. Cioslowski, B. B. Stefanov, G. Liu, A. Liashenko, P. Piskorz, I. Komaromi, R. L. Martin, D. J. Fox, T. Keith, M. A. Al-Laham, C. Y. Peng, A. Nanayakkara, M. Challacombe, P. M. W. Gill, B. Johnson, W. Chen, M. W. Wong, C. Gonzalez, and J. A. Pople, Gaussian 03 (Gaussian, Inc., Wallingford, CT, 2003).

(113) Becke, A. D. *J. Chem. Phys.* **1993**, *98*, 1372.

(114) Stephens, P. J.; Devlin, F. J.; Chabalowski, C. F. *J. Phys. Chem.* **1994**, *98*, 11623.

(115) Curtiss, L. A.; Redfern, P. C.; Raghavachari, K.; Pople, J. A. *J. Chem. Phys.* **2001**, *114*, 108.

(116) Reed, A. E.; Curtiss, L. A.; Weinhold, F. *Chem. Rev.* **1988**, *88*, 899.

(117) GAMESS Version = 24 Mar. 2007 (R3); M.W.Schmidt, K. K. B., J.A.Boatz, S.T.Elbert, M.S.Gordon, J.J.Jensen, S.Koseki, N.Matsunaga, K.A.Nguyen, S.Su, T.L.Windus, M.Dupuis, J.A.Montgomery *J. Comput. Chem.* **1993**, *14*, 1347.

(118) Francl, M. M.; Petro, W. J.; Hehre, W. J.; Binkley, J. S.; Gordon, M. S.; DeFrees, D. J.; Pople, J. A. *J. Chem. Phys.* **1982**, *77*, 3654.

(119) Rassolov, V. A.; Pople, J. A.; Ratner, M. A.; Windus, T. L. *J. Chem. Phys.* **1998**, *109*, 1223.

(120) Hariharan, P. C.; Pople, J. A. *Theo. Chim. Acta.* **1973**, *28*, 213.

(121) Hehre, W. J.; Ditchfield, R.; Pople, J. A. *J. Chem. Phys.* **1972**, *56*, 2257.

(122) Dill, J. D.; Pople, J. A. *J. Chem. Phys.* **1975**, *62*, 2921.

(123) Clark, T.; Chandrasekhar, J.; Schleyer, P. v. R. *J. Comp. Chem.* **1983**, *4*, 294.

(124) Krishnan, R.; Binkley, J. S.; Seeger, R.; Pople, J. A. *J. Chem. Phys.* **1980**, *72*, 650.

(125) Gill, P. M. W.; Johnson, B. G.; Pople, J. A.; Frisch, M. J. *Chem. Phys. Lett.* **1992**, *197*, 499.

(126) Blaudeau, J.-P.; McGrath, M. P.; Curtiss, L. A.; Radom, L. *J. Chem. Phys.* **1997**, *107*, 5016.

(127) Curtiss, L. A.; McGrath, M. P.; Blaudeau, J.-P.; Davis, N. E.; Binning Jr, R. C.; Radom, L. *J. Chem. Phys.* **1995**, *103*, 6104.

(128) Glukhovtsev, M. N.; Pross, A.; McGrath, M. P.; Radom, L. *J. Chem. Phys.* **1995**, *103*, 1878.

(129) Hay, P. J.; Wadt, W. R. *J. Chem. Phys.* **1985**, *82*, 270.

(130) Wadt, W. R.; Hay, P. J. *J. Chem. Phys.* **1985**, *82*, 284.

(131) Hay, P. J.; Wadt, W. R. *J. Chem. Phys.* **1985**, *82*, 299.

(132) Godbout, N.; Salahub, D. R.; Andzelm, J.; Wimmer, E. *Can. J. Chem.* **1992**, *70*, 560.

(133) Sosa, C.; Andzelm, J.; Elkin, B. C.; Wimmer, E.; Dobbs, K. D.; Dixon, D. A. *J. Phys. Chem.* **1992**, *96*, 6630.

(134) Andzelm, J.; Wimmer, E. *J. Chem. Phys.* **1992**, *96*, 1280.

(135) Huang, H.; Buekens, A. *Chemosphere* **2000**, *41*, 943.

(136) Palmisano, L.; Schiavello, M.; Sclafani, A.; Martra, G.; Borello, E.; Coluccia, S. *Appl. Catal. B: Environ.* **1994**, *3*, 117.

(137) Christoskova, S. G.; Stoyanova, M.; Georgieva, M. *Appl. Catal. A* **2001**, *208*, 243.

(138) Bandara, J.; Mielczarski, J. A.; Kiwi, J. *Appl. Catal. B: Environ.* **2001**, *34*, 307.

(139) Russell, J. N.; Leming, A.; Morris, R. E. *Surf. Sci.* **1998**, *399*, 239.

(140) Tyeklar, Z.; Karlin, K. D. *Chem. Res.* **2002**, *22*, 241.

APPENDIX A
LETTERS OF PERMISSION

FW: Academic Permissions Request Form

KENNEDY, Ben <ben.kennedy@oup.com> **Wed, Sep 16, 2009 at 4:02 AM**
To: holybae@gmail.com

Dear Gyun-Tack,
Thank you for your enquiry. You have our permission to use the OUP Material you list in your email below in your thesis for submission to Louisiana State University.

If at some future date your thesis is published it will be necessary to re-clear this permission.
Please also note that if the material to be used is acknowledged to any other source, you will need to clear permission with the rights holder.

Best wishes,

Ben

Ben Kennedy
Permissions Assistant
Academic Rights & Journals
Oxford University Press
Great Clarendon Street
Oxford
OX2 6DP
Direct tel. +44 (0)1865 354728
Direct fax +44 (0)1865 353429
e mail: ben.kennedy@oup.com

Z_TheirTitle	COMPUTATIONAL STUDIES OF THE PROPERTIES OF COPPER OXIDE CLUSTERS AND THE REACTIONS OF PHENOL AND CHLORINATED PHENOLS WITH COPPER OXIDE CLUSTERS
Z_Author	Gyun-Tack Bae
Z_Publisher	
Z_Covers	Unspecified
Z_PrintRunHard	5
Z_pubDate	
Z_Territory	USA
Z_Language	English
Z_Notes	I request this permission for my thesis
Z_Media1	Text
Z_Author1	M. P. Allen and D. J. Tildesley
Z_Title1	Computer Simulation of Liquids
Z_editedby1	
Z_Material1	Chapter 4 figure 4.5 Page 120
Z_ISBN1	0-19-855645-4
Z_OUPpubDate1	01 June 1989
Z_Media2	Text
Z_Author2	
Z_Title2	
Z_editedby2	
Z_Material2	
Z_ISBN2	
Z_OUPpubDate2	
Z_Media3	Text
Z_Author3	
Z_Title3	
Z_editedby3	
Z_ISBN3	
Z_Material3	
Z_OUPpubDate3	
Z_Additional	

AMERICAN INSTITUTE OF PHYSICS LICENSE TERMS AND CONDITIONS

Sep 23, 2009

This is a License Agreement between Gyun-Tack Bae ("You") and American Institute of Physics ("American Institute of Physics") provided by Copyright Clearance Center ("CCC"). The license consists of your order details, the terms and conditions provided by American Institute of Physics, and the payment terms and conditions.

All payments must be made in full to CCC. For payment instructions, please see information listed at the bottom of this form.

License Number	2270340142195
License date	Sep 15, 2009
Licensed content publisher	American Institute of Physics
Licensed content publication	Journal of Chemical Physics
Licensed content title	A theoretical study of small copper oxide clusters: Cu[sub 2]O[sub x] (x = 1--4)
Licensed content author	Bing Dai, Li Tian, Jinlong Yang
Licensed content date	Feb 8, 2004
Volume number	120
Issue number	6
Type of Use	Thesis/Dissertation
Requestor type	Student
Format	Electronic
Portion	Figure/Table
Number of figures/tables	3
Title of your thesis / dissertation	COMPUTATIONAL STUDIES OF THE PROPERTIES OF COPPER OXIDE CLUSTERS AND THE REACTIONS OF PHENOL AND CHLORINATED PHENOLS WITH COPPER OXIDE CLUSTERS
Expected completion date	Sep 2009
Estimated size (number of pages)	87
Total	0.00 USD

Terms and Conditions

American Institute of Physics -- Terms and Conditions: Permissions Uses

American Institute of Physics ("AIP") hereby grants to you the non-exclusive right and license to use and/or distribute the Material according to the use specified in your order, on a one-time basis, for the specified term, with a maximum distribution equal to the number that you have ordered. Any links or other content accompanying the Material are not the subject of this license.

1. You agree to include the following copyright and permission notice with the reproduction of the Material: "Reprinted with permission from [FULL CITATION]. Copyright [PUBLICATION YEAR], American Institute of Physics." For an article, the copyright and permission notice must be printed on the first page of the article or book chapter. For photographs, covers, or tables, the copyright and permission notice may appear with the Material, in a footnote, or in the reference list.
2. If you have licensed reuse of a figure, photograph, cover, or table, it is your responsibility to ensure that the material is original to AIP and does not contain the copyright of another entity, and that the copyright notice of the figure, photograph, cover, or table does not indicate that it was reprinted by AIP, with permission, from another source. Under no circumstances does AIP, purport or intend to grant permission to reuse material to which it does not hold copyright.
3. You may not alter or modify the Material in any manner. You may translate the Material into another language only if you have licensed translation rights. You may not use the Material for promotional purposes. AIP reserves all rights not specifically granted herein.
4. The foregoing license shall not take effect unless and until AIP or its agent, Copyright Clearance Center, receives the Payment in accordance with Copyright Clearance Center Billing and Payment Terms and Conditions, which are incorporated herein by reference.
5. AIP or the Copyright Clearance Center may, within two business days of granting this license, revoke the license for any reason whatsoever, with a full refund payable to you. Should you violate the terms of this license at any time, AIP, American Institute of Physics, or Copyright Clearance Center may revoke the license with no refund to you. Notice of such revocation will be made using the contact information provided by you. Failure to receive such notice will not nullify the revocation.
6. AIP makes no representations or warranties with respect to the Material. You agree to indemnify and hold harmless AIP, American Institute of Physics, and their officers, directors, employees or agents from and against any and all claims arising out of your use of the Material other than as specifically authorized herein.
7. The permission granted herein is personal to you and is not transferable or assignable without the prior written permission of AIP. This license may not be amended except in a writing signed by the party to be charged.
8. If purchase orders, acknowledgments or check endorsements are issued on any forms containing terms and conditions which are inconsistent with these provisions, such inconsistent terms and conditions shall be of no force and effect. This document, including the CCC Billing and Payment Terms and Conditions, shall be the entire agreement between the parties relating to the subject matter hereof.

This Agreement shall be governed by and construed in accordance with the laws of the State of New York. Both parties hereby submit to the jurisdiction of the courts of New York County for purposes of resolving any disputes that may arise hereunder.

AMERICAN INSTITUTE OF PHYSICS LICENSE TERMS AND CONDITIONS

Sep 23, 2009

This is a License Agreement between Gyun-Tack Bae ("You") and American Institute of Physics ("American Institute of Physics") provided by Copyright Clearance Center ("CCC"). The license consists of your order details, the terms and conditions provided by American Institute of Physics, and the payment terms and conditions.

All payments must be made in full to CCC. For payment instructions, please see information listed at the bottom of this form.

License Number	2270320050222
License date	Sep 15, 2009
Licensed content publisher	American Institute of Physics
Licensed content publication	Journal of Chemical Physics
Licensed content title	Photoelectron spectroscopy of size-selected transition metal clusters: Fe[sup -][sub n], n=3--24
Licensed content author	Lai-Sheng WangHan-Song ChengJiawen Fan
Licensed content date	Jun 22, 1995
Volume number	102
Issue number	24
Type of Use	Thesis/Dissertation
Requestor type	Student
Format	Electronic
Portion	Figure/Table
Number of figures/tables	1
Title of your thesis / dissertation	COMPUTATIONAL STUDIES OF THE PROPERTIES OF COPPER OXIDE CLUSTERS AND THE REACTIONS OF PHENOL AND CHLORINATED PHENOLS WITH COPPER OXIDE CLUSTERS
Expected completion date	Sep 2009
Estimated size (number of pages)	87
Total	0.00 USD

Terms and Conditions

American Institute of Physics -- Terms and Conditions: Permissions Uses

American Institute of Physics ("AIP") hereby grants to you the non-exclusive right and license to use and/or distribute the Material according to the use specified in your order, on a one-time basis, for the specified term, with a maximum distribution equal to the number that you have ordered. Any links or other content accompanying the Material are not the subject of this license.

1. You agree to include the following copyright and permission notice with the reproduction of the Material: "Reprinted with permission from [FULL CITATION] Copyright [PUBLICATION YEAR], American Institute of Physics." For an article, the copyright and permission notice must be printed on the first page of the article or book chapter. For photographs, covers, or tables, the copyright and permission notice may appear with the Material, in a footnote, or in the reference list.
2. If you have licensed reuse of a figure, photograph, cover, or table, it is your responsibility to ensure that the material is original to AIP and does not contain the copyright of another entity, and that the copyright notice of the figure, photograph, cover, or table does not indicate that it was reprinted by AIP, with permission, from another source. Under no circumstances does AIP, purport or intend to grant permission to reuse material to which it does not hold copyright.
3. You may not alter or modify the Material in any manner. You may translate the Material into another language only if you have licensed translation rights. You may not use the Material for promotional purposes. AIP reserves all rights not specifically granted herein.
4. The foregoing license shall not take effect unless and until AIP or its agent, Copyright Clearance Center, receives the Payment in accordance with Copyright Clearance Center Billing and Payment Terms and Conditions, which are incorporated herein by reference.
5. AIP or the Copyright Clearance Center may, within two business days of granting this license, revoke the license for any reason whatsoever, with a full refund payable to you. Should you violate the terms of this license at any time, AIP, American Institute of Physics, or Copyright Clearance Center may revoke the license with no refund to you. Notice of such revocation will be made using the contact information provided by you. Failure to receive such notice will not nullify the revocation.
6. AIP makes no representations or warranties with respect to the Material. You agree to indemnify and hold harmless AIP, American Institute of Physics, and their officers, directors, employees or agents from and against any and all claims arising out of your use of the Material other than as specifically authorized herein.
7. The permission granted herein is personal to you and is not transferable or assignable without the prior written permission of AIP. This license may not be amended except in a writing signed by the party to be charged.
8. If purchase orders, acknowledgments or check endorsements are issued on any forms containing terms and conditions which are inconsistent with these provisions, such inconsistent terms and conditions shall be of no force and effect. This document, including the CCC Billing and Payment Terms and Conditions, shall be the entire agreement between the parties relating to the subject matter hereof.

This Agreement shall be governed by and construed in accordance with the laws of the State of New York. Both parties hereby submit to the jurisdiction of the courts of New York County for purposes of resolving any disputes that may arise hereunder.

ELSEVIER LICENSE
TERMS AND CONDITIONS

Sep 23, 2009

This is a License Agreement between Gyun-Tack Bae ("You") and Elsevier ("Elsevier") provided by Copyright Clearance Center ("CCC"). The license consists of your order details, the terms and conditions provided by Elsevier, and the payment terms and conditions.

All payments must be made in full to CCC. For payment instructions, please see information listed at the bottom of this form.

Supplier	Elsevier Limited The Boulevard,Langford Lane Kidlington,Oxford,OX5 1GB,UK
Registered Company Number	1982084
Customer name	Gyun-Tack Bae
Customer address	7410 Bluebonnet Blvd 403 S Baton Rouge, LA 70810
License Number	2270331186458
License date	Sep 15, 2009
Licensed content publisher	Elsevier
Licensed content publication	Applied Surface Science
Licensed content title	Structural and electronic properbes of small CuO_n clusters
Licensed content author	Y. Pouillon and C. Massobrio
Licensed content date	15 March 2004
Volume number	226
Issue number	1-3
Pages	7
Type of Use	Thesis / Dissertation
Portion	Figures/table/illustration/abstracts
Portion Quantity	1
Format	Both print and electronic
You are an author of the Elsevier article	No
Are you translating?	No
Order Reference Number	
Expected publication date	Sep 2009
Elsevier VAT number	GB 494 6272 12
Permissions price	0.00 USD
Value added tax 0.0%	0.00 USD

Total 0.00 USD

Terms and Conditions

INTRODUCTION

1. The publisher for this copyrighted material is Elsevier. By clicking "accept" in connection with completing this licensing transaction, you agree that the following terms and conditions apply to this transaction (along with the Billing and Payment terms and conditions established by Copyright Clearance Center, Inc. ("CCC"), at the time that you opened your Rightslink account and that are available at any time at http://myaccount.copyright.com).

GENERAL TERMS

2. Elsevier hereby grants you permission to reproduce the aforementioned material subject to the terms and conditions indicated.

3. Acknowledgement: If any part of the material to be used (for example, figures) has appeared in our publication with credit or acknowledgement to another source, permission must also be sought from that source. If such permission is not obtained then that material may not be included in your publication/copies. Suitable acknowledgement to the source must be made, either as a footnote or in a reference list at the end of your publication, as follows:

"Reprinted from Publication title, Vol /edition number, Author(s), Title of article / title of chapter, Pages No., Copyright (Year), with permission from Elsevier [OR APPLICABLE SOCIETY COPYRIGHT OWNER]." Also Lancet special credit - "Reprinted from The Lancet, Vol. number, Author(s), Title of article, Pages No., Copyright (Year), with permission from Elsevier."

4. Reproduction of this material is confined to the purpose and/or media for which permission is hereby given.

5. Altering/Modifying Material: Not Permitted. However figures and illustrations may be altered/adapted minimally to serve your work. Any other abbreviations, additions, deletions and/or any other alterations shall be made only with prior written authorization of Elsevier Ltd. (Please contact Elsevier at permissions@elsevier.com)

6. If the permission fee for the requested use of our material is waived in this instance, please be advised that your future requests for Elsevier materials may attract a fee.

7. Reservation of Rights: Publisher reserves all rights not specifically granted in the combination of (i) the license details provided by you and accepted in the course of this licensing transaction, (ii) these terms and conditions and (iii) CCC's Billing and Payment terms and conditions.

8. License Contingent Upon Payment: While you may exercise the rights licensed immediately upon issuance of the license at the end of the licensing process for the transaction, provided that you have disclosed complete and accurate details of your proposed

use, no license is finally effective unless and until full payment is received from you (either by publisher or by CCC) as provided in CCC's Billing and Payment terms and conditions. If full payment is not received on a timely basis, then any license preliminarily granted shall be deemed automatically revoked and shall be void as if never granted. Further, in the event that you breach any of these terms and conditions or any of CCC's Billing and Payment terms and conditions, the license is automatically revoked and shall be void as if never granted. Use of materials as described in a revoked license, as well as any use of the materials beyond the scope of an unrevoked license, may constitute copyright infringement and publisher reserves the right to take any and all action to protect its copyright in the materials.

9. Warranties: Publisher makes no representations or warranties with respect to the licensed material.

10. Indemnity: You hereby indemnify and agree to hold harmless publisher and CCC, and their respective officers, directors, employees and agents, from and against any and all claims arising out of your use of the licensed material other than as specifically authorized pursuant to this license.

11. No Transfer of License: This license is personal to you and may not be sublicensed, assigned, or transferred by you to any other person without publisher's written permission.

12. No Amendment Except in Writing: This license may not be amended except in a writing signed by both parties (or, in the case of publisher, by CCC on publisher's behalf).

13. Objection to Contrary Terms: Publisher hereby objects to any terms contained in any purchase order, acknowledgment, check endorsement or other writing prepared by you, which terms are inconsistent with these terms and conditions or CCC's Billing and Payment terms and conditions. These terms and conditions, together with CCC's Billing and Payment terms and conditions (which are incorporated herein), comprise the entire agreement between you and publisher (and CCC) concerning this licensing transaction. In the event of any conflict between your obligations established by these terms and conditions and those established by CCC's Billing and Payment terms and conditions, these terms and conditions shall control.

14. Revocation: Elsevier or Copyright Clearance Center may deny the permissions described in this License at their sole discretion, for any reason or no reason, with a full refund payable to you. Notice of such denial will be made using the contact information provided by you. Failure to receive such notice will not alter or invalidate the denial. In no event will Elsevier or Copyright Clearance Center be responsible or liable for any costs, expenses or damage incurred by you as a result of a denial of your permission request, other than a refund of the amount(s) paid by you to Elsevier and/or Copyright Clearance Center for denied permissions.

LIMITED LICENSE

The following terms and conditions apply only to specific license types:

15. **Translation**: This permission is granted for non-exclusive world **English** rights only unless your license was granted for translation rights. If you licensed translation rights you

may only translate this content into the languages you requested. A professional translator must perform all translations and reproduce the content word for word preserving the integrity of the article. If this license is to re-use 1 or 2 figures then permission is granted for non-exclusive world rights in all languages.

16. **Website**: The following terms and conditions apply to electronic reserve and author websites:

Electronic reserve: If licensed material is to be posted to website, the web site is to be password-protected and made available only to bona fide students registered on a relevant course if:

This license was made in connection with a course,

This permission is granted for 1 year only. You may obtain a license for future website posting,

All content posted to the web site must maintain the copyright information line on the bottom of each image,

A hyper-text must be included to the Homepage of the journal from which you are licensing at http://www.sciencedirect.com/science/journal/xxxxx or the Elsevier homepage for books at http://www.elsevier.com , and

Central Storage: This license does not include permission for a scanned version of the material to be stored in a central repository such as that provided by Heron/XanEdu.

17. **Author website** for journals with the following additional clauses:

All content posted to the web site must maintain the copyright information line on the bottom of each image, and

he permission granted is limited to the personal version of your paper. You are not allowed to download and post the published electronic version of your article (whether PDF or HTML, proof or final version), nor may you scan the printed edition to create an electronic version,

A hyper-text must be included to the Homepage of the journal from which you are licensing at http://www.sciencedirect.com/science/journal/xxxxx . As part of our normal production process, you will receive an e-mail notice when your article appears on Elsevier's online service ScienceDirect (www.sciencedirect.com). That e-mail will include the article's Digital Object Identifier (DOI). This number provides the electronic link to the published article and should be included in the posting of your personal version. We ask that you wait until you receive this e-mail and have the DOI to do any posting.

Central Storage: This license does not include permission for a scanned version of the material to be stored in a central repository such as that provided by Heron/XanEdu.

18. **Author website** for books with the following additional clauses:

Authors are permitted to place a brief summary of their work online only.

A hyper-text must be included to the Elsevier homepage at http://www.elsevier.com

All content posted to the web site must maintain the copyright information line on the bottom of each image

You are not allowed to download and post the published electronic version of your chapter, nor may you scan the printed edition to create an electronic version.

Central Storage: This license does not include permission for a scanned version of the material to be stored in a central repository such as that provided by Heron/XanEdu.

19. **Website** (regular and for author): A hyper-text must be included to the Homepage of the journal from which you are licensing at http://www.sciencedirect.com/science/journal/xxxxx or for books to the Elsevier homepage at http://www.elsevier.com

20. **Thesis/Dissertation**: If your license is for use in a thesis/dissertation your thesis may be submitted to your institution in either print or electronic form. Should your thesis be published commercially, please reapply for permission. These requirements include permission for the Library and Archives of Canada to supply single copies, on demand, of the complete thesis and include permission for UMI to supply single copies, on demand, of the complete thesis. Should your thesis be published commercially, please reapply for permission.

21. **Other Conditions**:None.

APPENDIX B
MONTE CARLO SIMULATION CODE

#Gaussian Script

```
#!/bin/tcsh
#PBS -A cct_cuo_01
#PBS -q workq
# the queue to be used. "small" is the only queue available at present.
#PBS -l nodes=4:ppn=2
#PBS -l cput=120:00:00
# requested CPU time.
#PBS -l walltime=120:00:00
# requested Wall-clock time.
#PBS -o output-file
# name of the standard out file to be "output-file".
#PBS -j oe
# standard error output merge to the standard output file.
#PBS -N cu6o6_17
# name of the job (that will appear on executing the qstat command) to be "syschk".
#
set NPROCS=`wc -l $PBS_NODEFILE |gawk '//{print $1}'`
setenv g03root /usr/local/packages
setenv GAUSS_SCRDIR /var/scratch/
source  $g03root/g03/bsd/g03.login
set NODELIST = ( -vv -nodelist "" `cat $PBS_NODEFILE` "" -mp 2)
setenv GAUSS_LFLAGS " $NODELIST "
#move to directory with input file
cd ~gbae/mc/
# Change this line to reflect your input file and output file
set NATOMS = 12        #atom number
set NPASSES = 300
set PASS = 0
mc_gaussian_setup_initial
g03l < g03mc.inp > g03mc.out
grep "SCF Done:" g03mc.out>en_initial.out
mc_recover_energy_initial
mv mc_recover_energy.out initial_energy.out
while ($PASS < $NPASSES)
   echo $PASS > npasses
   set ATOM = 0
   while ($ATOM < $NATOMS)
      echo $ATOM > current_atom.pos
      mc_propose_move
      mc_gaussian_setup
      g03l < g03mc.inp > g03mc.out
      grep "SCF Done:" g03mc.out>en.out
      mc_recover_energy
```

```
      mc_decide
      @ ATOM ++
   end
      cat current_coordinates.pos >> trajectory
      cat initial_energy.out >> potential
      cat en.out >> newenergy
      cat tstar >> alltstar
   @ PASS ++
end
#    executes the executable.
rm $GAUSS_SCRDIR/*
#Removes the scratch files
```

```
c       mc_decide

        dimension r(3,1000)
        character*2 atom_name(1000)
        character*8 com
        real*8 newenergy,inienergy,tstar,t1star,t2star
        open(unit=1,file='random',status='old')
        read(1,*) ix
        read(1,*) iy
        read(1,*) iz
        read(1,*) ia
        read(1,*) itrial
        read(1,*) iaccep
        read(1,*) t1star
        read(1,*) t2star
        read(1,*) nmc
        close(1)
        open(unit=1,file='npasses',status='old')
        read(1,*) npasses
        close(1)
        npasses=npasses+1
        tstar=t1star+((npasses-1.d0)/(nmc-1.d0))*(t2star-t1star)
        open(unit=3,file='tstar',status='unknown')
        write(3,*) tstar
        itrial=itrial+1
        open(unit=1,file='mc_recover_energy.out',status='old')
        read(1,22) newenergy
 22     format(e20.10)
        close(1)
        open(unit=2,file='initial_energy.out',status='old')
        read(2,23) inienergy
        pot=inienergy
 23     format(e20.10)
        close(2)
        trans=-(newenergy-inienergy)/tstar
        if(trans .ge. log(unirand(ia))) then
        iaccep=iaccep+1
        open(unit=3,file='new_coordinates.pos',status='old')
        open(unit=4,file='current_coordinates.pos',status='old')
        read(3,*) natoms
        write(4,*) natoms
        read(3,*) com
        write(4,*) com
          do k1=1,natoms
            read(3,*) atom_name(k1),r(1,k1),r(2,k1),r(3,k1)
            write(4,*) atom_name(k1),r(1,k1),r(2,k1),r(3,k1)
          enddo
        close(3)
        close(4)
        pot=newenergy
```

```
      endif
      open(unit=2,file='initial_energy.out',status='unknown')
      write(2,*) pot
      open(unit=1,file='random',status='unknown')
      write(1,*) ix
      write(1,*) iy
      write(1,*) iz
      write(1,*) ia
      write(1,*) itrial
      write(1,*) iaccep
      write(1,*) t1star
      write(1,*) t2star
      write(1,*) nmc
      stop
      end

        real*4 function unirand(ix)
      if(ix .le. 0) ix=1333
      iy=ix*54891
      if(iy) 5,6,6
    5 iy=iy+2147483647+1
    6 y=iy
      ix=iy
      unirand=y*.4656613e-9
      return
      end
```

```
c mc_gaussian_setup

dimension r(3,1000)
character*2 atom_name(1000)
character*8 com
open(unit=1,file='new_coordinates.pos',status='old')
read(1,*) natoms
read(1,*) com
do k1=1,natoms
read(1,*) atom_name(k1),r(1,k1),r(2,k1),r(3,k1)
enddo
close(1)
open(unit=2,file='g03mc.inp',status='unknown')
write(2,*) '%chk=/panasas/scratch/gbae/cu6o6_17.chk'
write(2,*) '%NProcLinda=4'
write(2,*) '%NProcShared=2'
write(2,*) ''
write(2,*) '#b3lyp/6-31g** geom=coord guess=read'
write(2,*) ''
write(2,*) 'title'
write(2,*) ''
write(2,*) '0 1'
do k2=1,natoms
  write(2,*) atom_name(k2),r(1,k2),r(2,k2),r(3,k2)
enddo
write(2,*) ''
stop
end
```

```
c mc_gaussian_setup_initial

      dimension r(3,1000)
      character*2 atom_name(1000)
      character*8 com
      open(unit=1,file='current_coordinates.pos',status='old')
      read(1,*) natoms
      read(1,*) com
      do k1=1,natoms
      read(1,*) atom_name(k1),r(1,k1),r(2,k1),r(3,k1)
      enddo
      close(1)
      open(unit=2,file='g03mc.inp',status='unknown')
      write(2,*) '%chk=/panasas/scratch/gbae/cu6o6_17.chk'
      write(2,*) '%NProcLinda=4'
      write(2,*) '%NProcShared=2'
      write(2,*) ''
      write(2,*) '#b3lyp/6-31g** geom=coord'
      write(2,*) ''
      write(2,*) 'title'
      write(2,*) ''
      write(2,*) '0 1'
      do k2=1,natoms
        write(2,*) atom_name(k2),r(1,k2),r(2,k2),r(3,k2)
      enddo
      write(2,*) ''
      stop
      end
```

```
c       mc_propose_move
          dimension r(3,1000)
          character*2 atom_name(1000)
          character*8 com
          open(unit=1,file='random',status='old')
          read(1,*) ix
          read(1,*) iy
          read(1,*) iz
          read(1,*) ia
          read(1,*) itrial
          read(1,*) iaccep
          read(1,*) t1star
          read(1,*) t2star
          read(1,*) nmc
          close(1)
          open(unit=1,file='current_coordinates.pos',status='old')
          read(1,*) natoms
          read(1,*) com
          do k1=1,natoms
          read(1,*) atom_name(k1),r(1,k1),r(2,k1),r(3,k1)
          enddo
          close(1)
          open(unit=2,file='current_atom.pos',status='old')
          read(2,*) k1
             k1=k1+1
             delr=0.2d0
             dx=2.d0*delr*(unirand(ix)-0.5d0)
             dy=2.d0*delr*(unirand(iy)-0.5d0)
             dz=2.d0*delr*(unirand(iz)-0.5d0)
             r(1,k1)=r(1,k1)+dx
             r(2,k1)=r(2,k1)+dy
             r(3,k1)=r(3,k1)+dz
          open(unit=1,file='random',status='unknown')
          write(1,*) ix
          write(1,*) iy
          write(1,*) iz
          write(1,*) ia
          write(1,*) itrial
          write(1,*) iaccep
          write(1,*) t1star
          write(1,*) t2star
          write(1,*) nmc
          open(unit=3,file='new_coordinates.pos',status='unknown')
          write(3,*) natoms
          write(3,*) com
          do k2=1,natoms
            write(3,*) atom_name(k2),r(1,k2),r(2,k2),r(3,k2)
          enddo
          stop
          end
```

```
      real*4 function unirand(ix)
    if(ix .le. 0) ix=1333
    iy=ix*54891
    if(iy) 5,6,6
5 iy=iy+2147483647+1
6 y=iy
    ix=iy
    unirand=y*.4656613e-9
    return
    end
```

```
c mc_recover_energy

      real*8 b
      character*28 a
      open(unit=1,file='en.out',status='old')
      read (1,22) a,b
 22   format(a27,e20.10)
      close(1)
      open(unit=2,file='mc_recover_energy.out',status='unknown')
      write(2,*) b
      close(2)
      stop
      end
```

```
c mc_recover_energy_initial

      real*8 b
      character*28 a
      open(unit=1,file='en_initial.out',status='old')
      read (1,22) a,b
 22   format(a27,e20.20)
      close(1)
      open(unit=2,file='mc_recover_energy.out',status='unknown')
      write(2,*) b
      close(2)
      stop
      end
```

VITA

Gyun-Tack Bae was born in Seoul, South Korea, in January, 1975. Between 1993 and 1997 he studied chemistry at SoongSil University in Seoul. He received a master of science in chemistry from SoongSil University in June 1997, and a doctorate in chemistry from Louisiana State University in December 2009. His research interests include electronic and structural properties of metal oxide clusters, their reactions and simulations using *ab initio* Monte Carlo.